Motility of bacteria in microfluidics

Monalisha Nayak

Department of Bioengineering

McGill University, Montreal

July 2021

A thesis submitted to McGill University in partial fulfillment of the requirements of the degree of Doctor of Philosophy

Abstract

In nature, as well as in the context of medical applications, bacteria often dwell in highly complex environments such as soil, waste matter, plant and animal tissues. Consequently, bacteria have developed numerous movement patterns for their growth and survival across a broad spectrum of habitats. Understanding bacterial movements through human-engineered micro confinements can be important for medical and industrial applications, for bacteria-based biocomputation, as well as for biosensors and industrial fermentation controls. A majority of the studies focused on bacterial movement patterns through open spaces, bulk fluids, larger confinements, but to address specific knowledge gaps within this field our study focuses on studying the motility of five bacterial species of various sizes and different flagellar architectures (*Vibrio natriegens*, *Magnetococcus marinus*, *Pseudomonas putida*, *Vibrio fischeri*, and *Escherichia coli)* through micro confinements. Using micro confined environments of different complexity, we aim to find the ideal bacterial candidate for solving a small instance of non-polynomial time complete (NP-complete) problems. The first chapter discusses the hydrodynamics-based interactions of bacteria with the surrounding walls in open spaces, the steric interactions through tighter confined environments, and finally the overlapping of both interactions through mesoscale regions. Classifying the bacterial candidates (theoretically and experimentally) into different categories based on their movement patterns, such as movement parallel to the wall, stable movement along the wall, and wall escapers. The following chapter evaluates the bacterial efficiency for space searching and partitioning through or by using maze networks of different complexity. We presented how bacterial motility during space searching is strongly influenced by the surroundings and the presence of obstacles found in the micro confinements. The efficiency for finding all possible valid paths through the network, as well as finding the shortest paths were evaluated. Our observations suggested that *Vibrio natriegens* and *Escherichia coli* explored the possible paths more efficiently despite having lower velocity compared to other bacterial species with minimum energy expenditure, making them ideal candidates for network-based biocomputational approach. In the last chapter, bacteria-based network- biocomputation has been proposed for a highly compact SSP (Subset Sum Problems) network – Pascal's unit series network. This study also demonstrated the scalability and possible solutions for use of microscopy for biocomputation applications.

These ensembles of bacterial motility observations in microfluidic networks of different special complexity can be used as a methodological template for designing microdevices for biosensing, drug delivery, bacterial cell sorting (according to their movement pattern classification), and more importantly, the selection of bacterial candidates for network-based biocomputation approaches.

Résumé

Dans la nature, ainsi que dans le contexte des applications médicales, les bactéries vivent souvent dans des environnements très complexes tels que le sol, les déchets, les tissus végétaux et animaux. Par conséquent, les bactéries ont développé de nombreux modèles de mouvement pour leur croissance et leur survie dans un large éventail d'habitats. La compréhension des mouvements bactériens à travers des micro-confinements créés par l'homme peut être importante pour les applications médicales et industrielles, pour le biocalcul basé sur les bactéries, ainsi que pour les biocapteurs et les contrôles industriels de la fermentation. La majorité des études se sont concentrées sur les modèles de mouvement des bactéries à travers les espaces ouverts, les fluides en vrac, les confinements plus importants, mais pour combler les lacunes de connaissances spécifiques dans ce domaine, notre étude se concentre sur l'étude de la motilité de cinq espèces bactériennes de différentes tailles et différentes architectures flagellaires (*Vibrio natriegens* , *Magnetococcus marinus*, *Pseudomonas putida*, *Vibrio fischeri* et *Escherichia coli*) par micro confinement. En utilisant des environnements micro-confinés de complexité différente, nous visons à trouver le candidat bactérien idéal pour résoudre une petite instance de problèmes non polynomiaux complets (NP-complet). Le premier chapitre traite des interactions basées sur l'hydrodynamique des bactéries avec les murs environnants dans les espaces ouverts, les interactions stériques à travers des environnements confinés plus serrés, et enfin le chevauchement des deux interactions à travers des régions à mésoéchelle. Classer les candidats bactériens (théoriquement et expérimentalement) en différentes catégories en fonction de leurs schémas de mouvement, tels que le mouvement parallèle à la paroi, le mouvement stable le long de la paroi et les échappements muraux. Le chapitre suivant évalue l'efficacité bactérienne pour la recherche et le partitionnement de l'espace à travers ou en utilisant des réseaux de labyrinthe de complexité différente. Nous avons présenté comment la motilité bactérienne lors de la recherche spatiale est fortement influencée par l'environnement et la présence d'obstacles trouvés dans les micro-confinements. L'efficacité pour trouver tous les chemins valides possibles à travers le réseau, ainsi que pour trouver les chemins les plus courts ont été évaluées. Nos observations suggèrent que *Vibrio natriegens* et *Escherichia coli* ont exploré les chemins possibles plus efficacement malgré une vitesse inférieure à celle d'autres espèces bactériennes avec une dépense énergétique minimale, ce qui en fait des candidats idéaux pour une approche bioinformatique basée sur le réseau. Dans le dernier chapitre, le biocalcul en réseau basé sur les bactéries a été proposé pour un réseau SSP

(Subset Sum Problems) très compact – le réseau de séries unitaires de Pascal. Cette étude a également démontré l'évolutivité et les solutions possibles pour l'utilisation de la microscopie pour les applications de biocalcul.

Ces ensembles d'observations de la motilité bactérienne dans des réseaux microfluidiques de complexité particulière différente peuvent être utilisés comme modèle méthodologique pour la conception de microdispositifs pour la biodétection, l'administration de médicaments, le tri des cellules bactériennes (selon leur classification des modèles de mouvement) et, plus important encore, la sélection de candidats bactériens. pour les approches de biocalcul en réseau.

Acknowledgement

First and foremost, I would like to thank my supervisor **Prof. Dan V. Nicolau** for providing me with this great research opportunity as a PhD candidate. His insight and knowledge into the subject steered me through this research. During rough times, his help and support guided me to be in the right path and disciplined throughout. My gratitude extends to my Ph.D. committee members for their precious guidance on my work and future steps. I would also like to express my sincere gratitude to the Faculty of Engineering for awarding me the McGill Engineering Doctoral Award **(MEDA)**, which helped fund my stipend for the duration of my studies.

I would also like to thank the biomedical engineering department; **Pina Sorrini** and **Sabrina Teoli**, and bioengineering department; **Antonella Fratino**, **Aimée Jabour**, **Luisa Seidl**, **Dr. Horia Roman**, **Xavier Elisseeff**, and **Andy Catalano** for all administrative help and wonderful support.

I would like to thank other members of my team members for their kind help and co-operations throughout my research period. I owe a deep sense of gratitude to **Dr. Ayyappasamy Sudalaiyadum Perumal** for his timely suggestions for my experiments with kindness, enthusiasm, and dynamism. I would like to also thank my teammate **Giulia** for all the support.

I am very thankful to my friends for their love and care during tough times and support me during sleepless nights. My first year of Ph.D. in a different continent was very difficult for me. **Sara** and **JuanJuan,** you girls made it easy for me with countless coffee and tea sessions. Thank you so much guys for comforting me whenever I was frustrated, sad, and anxious, also through skype during lockdown. I owe you girls a lot. Without you guys, I could not imagine my life in the initial years of lab and also in Canada. **Kavya,** I sincerely thank you for bringing so much happiness into my life. I am really grateful for our post group meeting discussions, lunch breaks, tea breaks, and also endless phone calls. Life would have been so difficult without you in the lab and also in my life. I would like to thank **Pooja, Prasad**, **Preeti,** and **Prabh** for our much-needed weekend get togethers and photo sessions. I would also thank **Jackie, Mahsa, Linda**, and **Mira** for motivating me during the lab and for the brunch sessions for much needed break from work.

Kirti Snigdha, my best friend, thank you for always motivating me for everything in life. Its you, who forced me to apply for PhD, when I was very doubtful about me. You are a good researcher and I really admire you. Thank you so much for your support.

Prerna Ma'am and Divvy , thank you for being in my life and this Ph.D. journey was incomplete without you. Ma'am, you inspire me the way, anyone could ever think of. Your research ethics, presentation skills, intelligence, and mentorship always motivated me to think and work like a true researcher during my Ph.D. Thank you for listening to me and motivating me whenever I needed you, specifically during my progress meetings. **Ankur Sir**, thank you for being an intelligent senior and mentor and helping me through out my research life. You motivated me to apply for PhD, which was a long path for me back then. I always look up to you.

I am lucky to have wonderful flatmates to share my life with. I would like to thank **Arpit, Abhisek**, **Baishali, Rahul** and **Arghya** for being my family here. **Arpit** and **Abhisek**, thank you guys for treating me with amazing tea, whenever I needed it and listening to me whenever I was anxious about my work.

I will dedicate my thesis to my family, who knows nothing about my PhD work. I am dedicating my thesis to my father and grandfather, who is not there in my life anymore but still blessing me and protecting me from all negative energies during the tough times. I would like to thank my siblings **Sona Lisha, Sujit, Shubhashis,** and **Ritu parna** for unlimited phone calls, entertainments, specifically just being online to support me while I work, cry and laugh during late night work sessions. Of course, My mom and Rina Dei, Tutu mamu for always praying for me, for my work and for my wellbeing.

Last but not the least, I would stop here with a quote

"If the facts don't fit the theory, change the facts." - Albert Einstein"

Contribution to original knowledge

During my Ph.D. studies, I have first authored two original communications (contributed towards my Ph.D. thesis), co-authored two original communications, contributed on one book chapter and one conference proceedings. More details about each work are presented below.

The motility of five bacterial species with various sizes and flagellar architectures, namely *Vibrio natriegens, Magnetococcus marinus*, *Pseudomonas putida*, *Vibrio fischeri*, and *Escherichia coli*, were studied in microfluidic environments presenting various levels of confinement and geometrical complexity. Microfluidic devices are commonly used for the manipulation of individual, or small populations of cells in micrometre sized channels, for medical diagnostics, drug screening, cell separation, detection and sorting, and single-cell genomics. Microfluidic structures are used for motility studies on mammalian cells and microorganisms, e.g., fungi, algae, or bacteria, they are typically focused on a single species. On the contrary, the present study investigates the motility of five different bacterial species. The study also provides a methodological template for the development of microfluidic devices for single-cell genomic screening, bacterial entrapment for diagnostics, biocomputation, and biosimulation. ***(https://doi.org/10.1073/pnas.2013925118)***

Further studies demonstrated the ability of the previously studied bacterial species to explore maze environments as individual navigators. Additionally, different performance parameters such as average time required for finding solutions to maze, number of vertices explored during navigation, success rate for maze solving cand their energy expenditure during their navigation, have been evaluated. These experimental characterizations are advantageous in finding the best candidate for maze exploration, allowing a practical, straight forward space searching and partitioning algorithm which can be used for the analysis of more complex geometrics relevant to real-world applications such as transportation system planning, development of urban transportation, vehicle routing problems, and in the food and biomedical industries etc.

(*Ready to be submitted to Biosensors & Bioelectronics; accepted as oral presentation to the World Biosensors Congress, July, 2021*)

Contribution of authors

1. **Patterns of bacterial motility in microfluidics-confined environments, https://doi.org/10.1073/pnas.2013925118, First co-author with V. T, A.S.P, and H.S.**

   Authors: Viola Tokárová[1], Ayyappasamy Sudalaiyadum Perumal[1], **Monalisha Nayak[1]**, Henry Shum[1], Ondrej Kašpar, Kavya Rajendran, Mahmood Mohammadi, Charles Tremblay, Eamonn A. Gaffney, Sylvain Martel, Dan V. Nicolau Jr, and Dan V. Nicolau.

   D.V.N. designed research; V.T., A.S.P., **M.N**., H.S., O.K., M.M., C.T., and D.V.N. Jr. performed research; S.M. contributed new reagents/analytic tools; V.T., A.S.P., **M.N**., H.S., O.K., K.R., E.A.G., D.V.N. Jr., and D.V.N. analyzed data; and V.T., A.S.P., **M.N**., H.S., O.K., and D.V.N. wrote the paper.

2. **Bacterial navigation through uniform/non-uniform maze, ready to be submitted to Biosensors & Bioelectronics; accepted as oral presentation to the World Biosensors Congress, July, 2021, Primary author.**

   Authors: **Monalisha Nayak**, Ayyappasamy Sudalaiyadum Perumal, Viola Tokárová, Ondej Kašpar Dan V. Nicolau

   D.V.N. designed research; **M.N**, A.S.P., V.T., O.K., performed research; **M.N,** A.S.P., V.T., analyzed the data, **M.**N, A.S.P., contributed towards data interpretation; and **M.N,** A.S.P., V.T., D.V.N. wrote the paper.

3. **Agents-based network bio-computing solutions to high-density, compact NP-complete Subset Sum Problems**; **accepted as oral presentation to the NANO 2021, July, 2021, First co-author with A.S.P.**

   Authors: Ayyappasamy Sudalaiyadum Perumal[1], **Monalisha Nayak[1],** Falco C.M.J.M. van Delft and Dan V. Nicolau

D.V.N. designed research; A.S.P and **M.N**., performed research; **M.N,** analyzed the data, A.S.P, **M.N** and FCMJMvD., contributed towards data interpretation; A.S.P, **M.N,** FCMJMvD, and D.V.N. wrote the paper.

4. **Self-propelled, dividing bacteria solve NP-complete problems by space searching of an encoded physical network (under review, Science advances), Co-author.**

   Authors: Ayyappasamy Sudalaiyadum Perumal, Falco C.M.J.M. van Delft, Giulia Ippoliti, Ondřej Kašpar, Viola Tokárová, Jessica Li, **Monalisha Nayak**, Anja van Langen-Suurling, Charles de Boer, Frank Dirne, Dan V. Nicolau Jr. and Dan V. Nicolau.

   ASP, FCMJMvD, DVNJr, DVN contributed towards Conceptualization, ASP, FCMJMvD, GI, OK, VT, JL, **MN**, AvLS, CdB, FD established the methodology, ASP, FCMJMvD, GI, JL, **MN**, AvLS, CdB, FD performed the Investigation and data visualization, ASP, FCMJMvD, GI, OK, DVNJr, DVN wrote the original draft, and ASP, FCMJMvD, GI, OK, DVNJr, DVN performed the review & editing of the manuscript.

5. **A True Random Number Generator using Bacterial Motility in Microfluidic Networks (ready to be submitted**), **Co-author.**

   Author: Giulia Ippoliti, Ayyappasamy Sudalaiyadum Perumal, Falco C.M.J.M. van Delft, Dan V. Nicolau Jr., **Monalisha Nayak**, Dan V. Nicolau.

   GI conceived the random number generator design and the object recognition algorithm, developed the full code base of the model, performed image processing, derived statistics, tested the full output and wrote the manuscript, ASP ran the experimental session required to generate stochastic behaviour and performed image processing, **MN** helped in data analysis, GI, ASP, DVN wrote and reviewed the manuscript.

Table of Contents

1. Introduction 1
1.1 Microbial motility in natural environments 1
1.1.1 Bacterial survival strategies and insights into bacterial motility 1
1.1.2 Bacterial flagellum 3
1.2 Methods for understanding the microbial motility 5
1.2.1 Traditional methods; prior to the advent of microfluidics 5
1.2.2 Advanced motility research 5
1.3 Microfluidics for studying bacterial motility 6
1.3.1 Microfluidics for controlling the microbial environment 7
1.4 Evaluation of decision-making behavior and path-finding abilities 13
1.4.1 Nonconventional approaches for solving mazes 14
1.5 Unconventional computing 17
2. Patterns of bacterial motility in microfluidics-confining environments 20
Significance 21
Abstract 22
2.1 Introduction 22
2. 2 Results and Discussion 24
2.2.1 Motility in large chambers 25
2.2.2 Motility in tightly confining geometries 32
2.2.2.1 Motility in linear channels 32
2.2.2.2 Motility in channels with angled exits 35
2.2.2.3 Motility in meandered channels 38
2.3. Perspectives and future work 41
2.4. Conclusion 43
2.5. Materials and Methods 43
2.6. Acknowledgement 43
Reference 44
3. Navigation through uniform and non-uniform maze 51
Abstract 52

3.1. Introduction 53
3.2. Materials and Methods 56
3.3. Results 58
3.3.1 Navigation through uniform maze 58
3.3.1.1 Overall motility pattern 58
3.3.1.2 Ability to find the shortest route 60
3.3.1.3 Ability to find all possible routes 61
3.3.2 Navigation through non-uniform maze 63
3.3.2.1 Overall motility pattern 63
3.3.2.2 Ability to find the shortest route 64
3.3.2.3 Ability to find all possible valid routes 65
3.4 Discussion 67
3.5 Conclusion 71
3.6 Perspective of future work 72
Reference 72
4. Agents-based network bio-computing solutions to high-density, compact NP-complete Subset Sum Problems 78
Abstract 78
4.1 INTRODUTION 79
4.2 METHODS 80
4.3 RESULTS AND DISCUSSION 80
4.4 FIGURES 82
4.5 CONCLUSION 83
REFERENCES 84
5. Discussion 85
6. Conclusion 91
References 93
Appendix A 100
SUPPORTING INFORMATION 100
1. Detailed Experimental Section 100
1.1. Experimental protocols 100
1.2. Bacterial species 105
1.3. Microfluidics structures and their characteristic dimensions 106

2. Results and Discussion..... 107
2.1. Motility in large chambers 107
2.2. Motility in tightly confining geometries 117
2.3. Motility in channels with angled exits 124
2.4 Motility in meandered channels 126
2.4. Velocity distribution for bacterial species in different motility structures..... 129
2.5 Tight geometrical like confinements from nature 130
References..... 136

List of Figures and Tables

Figure 1. Various modes of bacterial motility. Swarming is the movement across a surface and powered by rotating the helical flagella; Swimming is the movement in the liquid and powdered by rotating the flagella; Twitching is the surface movement that powered by the extension of pilli, which then attach to the surface and retract by pulling the cell closer to the attachment; Gliding is surface that does not require flagella or pilli and has focal adhesion complexes; Sliding is powered by growth; Darting is passive motility facilitated by growth and movement occur by cell aggregates. The direction of cell movement is indicated by black arrows. 2

Figure 2. Structure of flagellum of gram-negative bacteria 4

Figure 3. Motility in plazas with 6 μm high ceilings**.** (A) Density maps of bacterial locations. Color code (bottom): "min" and "max" represent no and the highest presence of bacteria, respectively. (B) Spatial distribution of bacteria obtained by superimposing and averaging the data from all four quarters of the density maps in A. Color code (bottom): frequency of bacterial presence, with red for the highest and dark green for the minimum probability. (C) Characteristic long 2D projections of bacterial trajectories. (D) 3D bacterial trajectories. By rows, from top to bottom, are the following: V. natriegens (average count of bacterial positions in each frame, n = 14/frame); M. marinus (n = 12/frame); P. putida (n = 15/frame); V. fischeri (n = 15/frame); and E. coli (n = 13/frame). 28

Figure 4. Prediction of motility behavior. (A) Bacterial positions, according to their dimensions, on a motility "map" [32], derived from hydrodynamic principles, for monotrichous bacteria. *V. natriegens, V. fischeri*, and *E. coli*, "swim parallel to walls" (confirmed experimentally, Fig. 2B and SI Appendix, Fig. S9). *M. marinus* is placed at the boundary between "wall accumulators" and "wall escapers" regions (confirmed experimentally by its wall-bouncing behavior). *P. putida*, with the largest variability of sizes, straddles the extreme "swimming parallel to wall" and "wall escaper" regions (confirmed by spatial distribution in Fig. 2B and SI Appendix, Fig. S9). The legend (updated from ref. 32, SI Appendix, Table S2) is as follows: a1 = polar radius of cell body (half the cell length); a2 = equatorial radius of cell body (half of the diameter diameter); [a1/a2] = aspect ratio of the cell body; L = curvilinear length of the flagellum (approximated by the axial length of the flagellum); _a = radius of sphere with volume of cell body; L/_a = nondimensional length of the flagellum/a; h* = optimal distance from wall (for swimmers parallel to walls); and h*/_a = nondimensional stable distance from wall. The colors of bacterial coordinates approximately replicate the color equivalent to h*/_a (determined from z-stack analysis). (B) Example of a bacterium moving stable parallel to the walls: *E. coli* (also exhibiting "escape from wall" jumps). (C) Example of a "wall escaper" bacterium: *M. marinus*. 31

Figure 5. Bacterial motility in linear channels. (A, Left) Density maps of the movement patterns of bacteria in channels with different widths. (A, Right) Bacterial trajectories in 8 μm wide channels, moving from one direction (green) or from an opposite one (red). (B) Double histograms of velocity (y-axis) versus normalized distance from the center of the linear channel (channel wall on the extreme right) for 6 μm × 6 μm channels (the full analysis is presented in SI Appendix, Fig. S14). E. coli and V. natriegens present a specific bimodal distribution of velocities near the wall. (C) Influence of the channel width on the fraction of U-turns. By rows, from top to bottom, are the following: V. natriegens (average count of bacteria each frame, n = 20/frame); M. marinus (n = 10/ frame); P. putida (n = 19/frame); V. fischeri (n = 18/frame); and E. coli (n = 22/frame). (D) Graphical representation of the top view of a bacterium with their average dimensions, in linear channels. The thick and dotted lines represent the minimum and maximum channel widths. 33

Figure 6. Bacterial motility in channels with angled exits. (A) Density maps of the movement patterns of bacteria in straight parallel channels, connected by side channels at angles ranging from 0° to 150°. All

channels are nominally 4 μm wide. (B) Bacterial trajectories, either from top (green) or from the opposite direction (red). (C) Frequencies of bacteria moving at different exit angles. By rows, from top to bottom, are the following: V. natriegens (average count of bacteria each frame, n = 10/frame); M. marinus (n = 8/frame); P. putida (n = 10/frame); V. fischeri (n = 13/frame); and E. coli (n = 11/frame). (D) Graphical representation of the top view of bacterium with average dimensions in the angled channels (few representative angles). The areas in light brown representspaces that exceed the dimensions of the respective bacteria in the respective position. 36
Figure 7. Bacterial motility in meandered channels. (A) Density maps of the bacterial movement patterns. (B) Representative tracks of the bacterial motility (trajectories in red are for bacteria that took U-turns or got trapped). (C) Frequency of bacteria making successful exits, relative to those that are trapped, or performed U-turns (unsuccessful tracks) for each meandered channel. By rows, from top to bottom, are the following: V. natriegens (average count of bacteria each frame, n = 18/frame); M. marinus (n = 12/frame); P. putida (n = 22/frame); V. fischeri (n = 25/frame); and E. coli (n = 19/frame). (D) Graphical representation of the top view of bacteria in the mesoscale-sized channel. 39
Figure 8. Experimental setup for bacterial navigation through microfluidic mazes B and C. PDMS microfluidic structures Uniform and Non-uniform strutures respectively. 56
Figure 9. A. Density maps of movement for five bacterial strains through diamond like structure (uniform-MAZE), B. Few of the representative successful trajectories, that correspond to the bacteria movement through the structure, C. Probability of number of vertices traveled to complete a trajectory and their distribution in an individual experiment. 62
Figure 10. Bacterial Motility in non-uniform maze A. Density maps of movement for five bacterial strains through nonuniform-maze, B. Few of the representative successful trajectories, that correspond to the bacteria movement through the structure, C. Probability of number of vertices traveled to complete a trajectory and their distribution in an individual experiment. 66
Figure 11. Comparison between multiple parameters (exploring the shortest path). Radar chart A. (Uniform maze), B. (Non-uniform maze) shows how the studied bacterial candidate behaves for different parameters like success rate, average time, energy demand, vertices travelled once and vertices travelled/sec. For each parameter larger area of the polygon represents a better candidate for solving the maze. 68
Figure 12. Comparison between multiple parameters (exploring all possible paths). Radar chart A. (Uniform maze), B. (Non-uniform maze) shows how the studied bacterial candidate behaves for different parameters like success rate, average time, energy demand, vertices travelled once and vertices travelled/sec. For each parameter larger area of the polygon represents a better candidate for solving the maze 68
Figure 13. Demonstration of solutions for bacteria operated Pascal series of N+1 set (N=5, Pascal SSP@5 {1,1,1,1,1}). A and B represent the density maps, bar graphs (answering Q1), and individual trajectories (answering Q2) to each solution by NBC approach (different routes to one exit, i.e., target sum (highlighted with yellow) by E. coli. 82
Figure 14. Demonstration of solutions for bacteria operated Pascal series of N+1 set (N=9, Pascal SSP@9 {1,1,1,1,11,1,1,1}). A represents the density map derived solutions to the SSP problem of N=9 explored by *E. coli*. B. Four bar graphs show the computation time for different cardinalities. 83

Chapter 1

1. Introduction

1.1 Microbial motility in natural environments

1.1.1 Bacterial survival strategies and insights into bacterial motility

Microorganisms are challenged through various stresses for their survival due to constantly changing environments in their natural habitats [1]. These environmental changes include nutrient limitation, temperature, radiation, pH and osmolarity changes, as well as the presence of excessive amounts of superoxides and metals. To cope with these stressful conditions, microorganisms employ numerous survival strategies, such as the formation of cysts and spores, modification in their cell membrane, changes in gene expression, etc. [1]. Alternative survival strategies that biological cells exhibit is directional motility in response to various environmental stimulus, also known as taxis, e.g., formation of biofilms by phytoplankton [2, 3], migration of bacteria towards plants rhizosphere for obtaining organic nutrients in soil [4], and motility of spermatozoa for fertilization [5], etc.

Bacteria, a large group of micrometres sized organisms, constitute a significant proportion of biomass of Earth. They are able to swim in water and crawl on surfaces and come in different shape and sizes [6]. Six different categories of bacterial motility patterns have been identified: swimming, swarming, gliding, twitching, sliding, and darting [7]. Swimming is the most apparent behavior of bacteria, and it is dependent on flagella along with swarming [8, 9]. Gliding and twitching are correlated with type IV pili [10, 11].

Flagella, one or several cellular appendages, are the key structures responsible for bacterial swimming. Bacteria rotate one or several passive, helically shaped filaments, which are connected to a rotary motor in the cell wall, to propel themselves forward using the asymmetric drag force exerted by the surrounding fluid on the individual segments of the helix [12]. Flagella are categorized based on their position on a cell: monotrichous (single polar (at one or both the poles) flagellum), amphitrichous (single flagellum on both sides), lophotrichous (tufts of flagella at one or both sides), and peritrichous (arranged randomly on the cell body) flagella. The finding that intestinal *Escherichia coli* has left-handed helical flagella [13, 14] laid the foundation for the better insight of the interaction between bacterial motility and Brownian motion.

The most known bacterial motility mechanism is the 'run-and-tumble' mechanism (Figure 1) [15]. Counterclockwise rotation of all flagella motors wraps the filaments in the helical bundle to initiate swimming, also known as "run", which is mostly observed in peritrichous species such as *E. coli*. The alternative mechanism is a clockwise rotation that untangles the bundle making it "tumble", reorienting the bacterial cells and producing a new swimming direction [16, 17]. Additionally, the sudden change in the rotation of filaments can have a polymorphic transition due to a viscous drag that changes the pitch, radius, and helix from left to right [18].

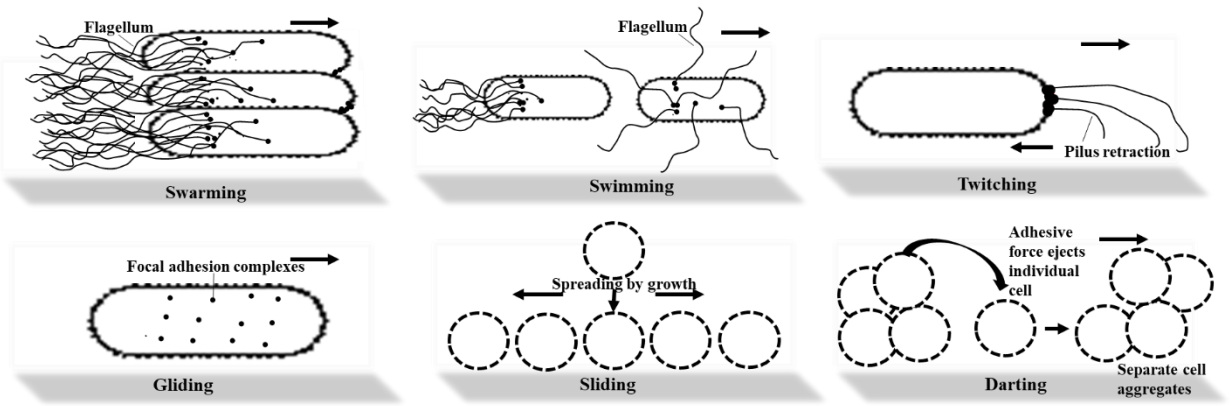

Figure 1. Various modes of bacterial motility. Swarming is the movement across a surface and powered by rotating the helical flagella; Swimming is the movement in the liquid and powdered by rotating the flagella; Twitching is the surface movement that powered by the extension of pilli, which then attach to the surface and retract by pulling the cell closer to the attachment; Gliding is surface that does not require flagella or pilli and has focal adhesion complexes; Sliding is powered by growth; Darting is passive motility facilitated by growth and movement occur by cell aggregates. The direction of cell movement is indicated by black arrows.

In monotrichous bacterial species, the swimming behavior is completely different from those of peritrichous bacteria. Approximately 90% of motile marine bacterial species are found to be monotrichous and lack a tumbling pattern like *E. coli* [19]. Instead of the tumbling pattern, monotrichous marine bacteria, namely, *Vibrio alginolyticus*, *Shewanella putrefaciens*, and *Pseudoalteromonas haloplanktis* reorient their swimming direction by rotating their single motor

[20]. The swimming patterns of the above-mentioned bacterial cells are different from those of *E. coli* as they alternate between forward swimming (when the flagellum pushes the cell head) and backward swimming (when the flagellum pulls the cell head). However, *E. coli* always swims forward with its flagella pushing the cell. Swimming for monotrichous bacterial cells occur back and forth in the same direction and they do not change their swimming direction. The ability to change the direction in the absence of multiple flagella for monotrichous bacteria was difficult to explain until the discovery of another motility adaptation, known as 'flick'. This motility adaptation is prevalent in marine bacteria [21, 22]. The flick is completely mechanically driven [22], and it results in the deformation of the flagellum, which reorients the swimming direction. This discovery also demonstrated that microbial cells are dependent on the forward-backward swimming intervals during chemotaxis [22]. The 'run reverse flick' motility enables microbial cells to reorient themselves using only one flagellum and can also complement their chemotactic performance [20, 23, 24].

Classical studies have qualitatively emphasized on bacterial motility and have conferred them as the first chemical gradients microsensors [25]. In a non-uniform environment, the presence of an external stimuli, e.g., gradients in the concentration of oxygen, pH, nutrients, or the intensity of light, influence bacterial motility and make it biased towards one direction [17]. A majority of studies have focused to study the modeling of free-swimming cells motility in bulk fluid, which presents both random and biased movement. Extensive experiments have investigated power generation with the flagellar motor unit during swimming [26], the effect of cell geometry and flagellation on the motility patterns [21], the shape transitions of flagella during the run and tumble motility [27], and the effect of viscosity on different motility patterns [28].

1.1.2 Bacterial flagellum

The flagellum is a gigantic protein complex necessary for bacterial motility [29]. It consists of three major parts: the filament, hook, and basal body. (Figure 2)

The filament is the largest part of the flagellum, with a thickness of 20–40 nm. Each individual bacterial filament is a helical tube connected to a single motor unit. The filament consists of thousands of subunits of one or multiple kinds of a protein called flagellin FliC [30].

The hook is flexible and is connected to the filament. It is also coupled to a rigid rod, which is attached to four rings. The rings are made of different proteins, namely, FlgB, FlgC, FlgF, and FlgG. The outer pair of the rings are called L (lipopolysaccharide) and P (peptidoglycan) ring and (cytoplasmic) ring [22].

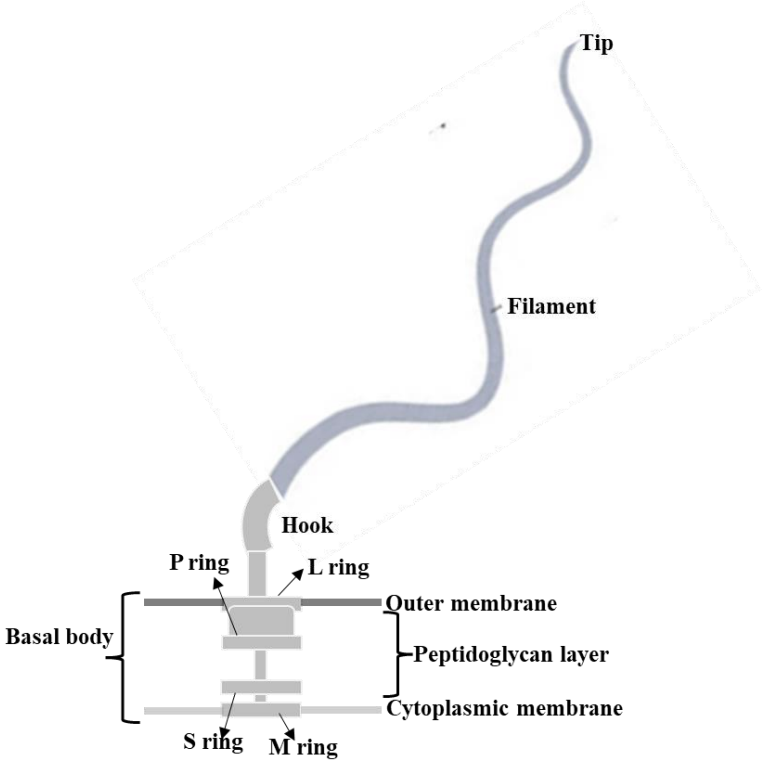

Figure 2. Structure of flagellum of gram-negative bacteria

The basal body has an active rotary unit called a flagellar motor that is rigidly attached to the cell wall. The flagellar motor unit found in the basal body, is composed of stator components called MotA and MotB. A proton gradient across the membrane drives a flux of H^+ ions through the stator complex binding to the MotB protein. The binding creates a conformational change in the MotA protein and results in a power stroke on the MS ring causing the rotor to rotate incrementally. The H^+ ions are released from the MotB protein at the end of the power stroke, which generates another conformational change [30].

1.2 Methods for understanding the microbial motility

1.2.1 Traditional methods; prior to the advent of microfluidics

In the past, research on bacterial motility was performed using microbiological assays like the swim plate, agar-plug, and chemical-in-plug assays [31, 32].

1.2.1.1 Microbiological assays

Swim plate assay. A gradient of nutrients and bacterial media is created on an agar plate, inoculating the bacterial colony at the center of the low concentration gradient. Bacteria use the chemotaxis mechanism as they consume the nutrients locally, and swim towards the areas of higher nutrient concentration [32]. However, the results obtained from these traditional assays get affected by various factors simultaneously such as the swimming speed of bacteria, their chemo sensing capacities, and their growth rate.

Chemical-in-plug and agar plug assays. This simple and quick assay was employed to monitor bacterial motility behavior by studying the effect of repellent stimuli [33]. In this method, an agar plug containing a chemo effector is placed at the center of a turbid suspension of bacterial cells on soft agar. If the chemical within the plug is a repellent, then a clear zone around the hard agar plugs appears due to bacteria swimming away from it. The distance of the cleared zone was solely dependent on the concentration of the repellent. However, this assay was prone to false-positive results when lacking suitable controls [34].

Microcapillary assays. The capillary-based motility assay was a well-known method for investigating bacterial motility. In this method bacteria were placed at one end of a capillary tube and an attractant at the other end, causing bacteria to migrate along the gradients [32].

1.2.2 Advanced motility research

Fluorescence microscopy. More sophisticated techniques were introduced for studying motility, such as fluorescence microscopy, wherein different microcompartments with varying ionic concentrations were fabricated to describe the motility near surfaces through bulk fluid and constrained fluid [35]. This study also demonstrated the link between cell shape and surface dependent motility. Hydrodynamic entrapment was not observed in spherical-shaped cells, on the other hand rod-shaped cells swam parallel to the surface [35].

Magnetotaxis. Another remarkable research was conducted by Chemla et al. to study bacterial magnetotaxis using a superinduction quantum interface device [36]. In their experiment a microscope of magnetic fields with similar strengths to Earth, was designed. In this study, different performance parameters were measured such as flagellar rotation rate, cell rotation rate, rotational drag coefficient, and cell size. This study also claimed that motility of non-magnetic cells can also be investigated by attaching magnetic particles to them.

Flagellar control. Flagellar shape and bundle stress gets influenced by environmental changes [37]. Scharf et al. studied the flagellar confirmational changes of *Rhizobium lupuni*, which has flagellar filaments with three flagellin subunits locked in a right-handed helical conformation [38]. These filaments were affected by higher viscosities and pH levels causing the flagella to tumble. Theoretical modeling also suggested that turbulence disrupts the swimming speed leading to occasional stops [39].

1.3 Microfluidics for studying bacterial motility

Ongoing technological developments provide the opportunity to use microfluidic platforms for studying bacterial motility. Considering bacterial behavior gets easily altered by environmental conditions such as, chemical gradients, magnetic fields, and physical constraints, it is difficult to simultaneously analyze all the factors involved in the above-mentioned assays. Because of this, microfluidics has become one of the most promising technologies for studying bacterial motility.

Why microfluidics?

Microfluidics is an appealing technology to study microbial motility for the following reasons.

- The environment of study can be manipulated in miniature channels with nano to micrometer level accuracy [40].
- The ability and flexibility to control fluid flow by mimicking the salient features of the microbial environment [41].
- Microfluidic devices can enable the use of stimuli gradients allowing more promising studies in bacterial taxis [42].
- Microfluidics allow single-cell analysis [43].
- Seamless fabrication of funnels, obstacles, and barriers can be used to study microbial interactions and understand their adaptation and evolution.

1.3.1 Microfluidics for controlling the microbial environment

The use of microfluidics has expanded dramatically in the last decade mainly due to the introduction of a seamless fabrication technique, i.e., soft lithography [40]. Soft lithography includes various techniques like printing, molding, and embossing using elastomeric polymers as mask and a stamp or cast to pattern. The most frequently used polymer is polydimethylsiloxane (PDMS) given its transparency, flexibility, gas permeability, chemical inertness, and biocompatibility [40]. Microfluidics have transformed basic and applied research in different areas such as chemical engineering, soft matter physics, and disease diagnostics. The application of microfluidics in microbial studies, specifically studies with controlled physical and chemical environments, shows the great potential of this technology.

Controlling the fluid flow. Microfluidics have received considerable attention for studying microbial motility and understanding their response to the surrounding environment simultaneously. To mimic the salient features of the microbial environment, microfluidic channels can be fabricated to control the fluid flow [41]. The flow inside the microchannel is deep laminar. A microfluidic channel is fabricated to generate non-uniform flow velocity for achieving a velocity gradient. The flow velocity at the top, bottom, and sidewalls is essentially zero and maximum at the center [44]. This above-mentioned study reveals the surface attachment of cells in certain regions of the flow.

Establishing chemical gradients. Microfluidic devices are designed to create chemical gradients (steady, unsteady, linear, and non-linear) of small molecules or gases that mimic the chemical ecology of microorganisms [45-47]. Microfluidic devices consisting of hydrogels or membranes facilitate the creation of a steady chemical gradient. These devices enable the study of microbial behavior or physiology in a chemically controlled environment [48]. Simultaneous quantification and migration of cells based on chemotaxis were studied by establishing a chemical gradient. Additionally, chemical gradients also allowed surface attachment of microbial cells [49].

Modifying the surface chemistry. Microfluidic devices can be used for controlling surface chemistry. Traditional studies use bovine serum albumin (BSA) for preventing surface attachment during chemotaxis-based studies [50, 51]. On the other hand, microstamping techniques are used for biofilm studies [52].

1.3.2 Microfluidic devices for studying bacterial motility

Motility with information. Different biological cells can react to the same kind of stimulus in different ways. Biological cells present directional motility known as taxis, which can be classified as active or passive taxis. In active taxis, the bacterium adapts a new motility pattern by getting influenced by an attractant such as chemotaxis [53] and thermotaxis [54]. On the other hand, in passive taxis, bacterial motility is influenced by an imposed force such as magnetotaxis [55] and gyrotaxis [2].

Chemotaxis and static/flow conditions. Microbial chemotaxis is one of the most extensively studied biological sensory systems. Microfluidic approaches are well suited for studying the microbial response to the chemical landscape that mimics the microbial environment. Microbial chemotaxis has essential roles in various processes, including nutrient consumption, pathogenesis, and surface colonization [56, 57]. Most microbial survival strategies are influenced by chemical gradients in the environment resulting in a biased movement towards the most favorable condition. Bacteria use transmembrane receptors (kinase complexes) for sensing the chemical stimuli. After sensing, these receptors initiate a series of molecular signals for regulating the intracellular levels of phosphorylated CheY. These molecules bind to the rotor of the biological flagellar motor to bias the rotational direction/switching event [53]. The chemotaxis machinery helps bacteria to either migrate towards the higher concentration of chemo attractants or away from chemorepellents. Chemotaxis has been explored for sorting or separating bacterial cells subpopulations as well as to study bacterial motility [58]. To separate subpopulations, microchannels are fabricated to establish a chemical gradient inside and across the channels either in static conditions or flow conditions which are described below.

Static condition assays. Static condition assays are very similar to the traditional swim-plate assay, where a stable and linear chemical gradient is established across the membrane through the diffusion of chemo attractants. For example, in [59] two different cell types, *P. aeruginosa* and *E. coli*, were physically separated through a porous membrane using two-layered microfluidic devices and a weak chemoattractant (lysine) to initiate the chemotaxis process. An in situ chemotaxis assay (ISCA) was performed in a marine ecosystem using a 3D printed microfluidic device containing various cylindrical chambers containing specific chemo attractants to attract specific microbes [60]. The device was presented to the marine microbes to initiate the chemotaxis process which was quantified using flow cytometry. A microstructure designed with T junctions

in a three inlet and twenty two outlet device was used to sort bacterial cells based on chemotactic sensitivity [61]. A chemotactic gradient was created across the hydrogel-filled microstructure causing bacterial cells to migrate through the channels by sensing the chemical stimuli. The technique was observed to be very sensitive, as it linked the concentration of chemo effectors with chemo attractants/repellents. Another study presented a microfluidic device with a steady gradient to introduce chemotaxis with *E. coli* [62]. The response of *E. coli* was not found to be significantly altered over a wide range of concentration gradients. And were able to continue their chemotactic performance by modifying their motility behavior not in response to the concentration but to the normalized gradient, also known as logarithm sensing. This mechanism helps bacterial cells maintain high sensitivity towards a wide range of environmental conditions, similar to the human vision and hearing [63, 64]. Microfluidic devices having multiple chemical gradients offered the possibility of getting a better understanding of microbial motility as they can have the common features of the natural environment. For instance, a microfluidic device having chemical gradients of two different amino acids such as aspartame and serine were presented to *E. coli* cells [48]. *E. coli* has five types of chemoreceptors, of which Tar and Tsr are the most abundant [65]. Tar and Tsr have the highest affinity towards aspartame and serine respectively. The result provides insights about the decision-making mechanism of chemotactic bacteria, when subjected to multiple stimuli.

Rheotaxis; response to fluid currents. Swimming patterns of microorganisms can be influenced by the current of the fluid. This behavioral orientation is called rheotaxis and was observed with fish [66] and sperm [67], where they sense the water current and swim against the flow direction. Various studies used a microfluidic approach to study bacterial rheotaxis. Microchannels were fabricated and presented to bacteria for studying their response to flowing fluid [68]. In this study, changes in swimming pattern of *E. coli* under different conditions of flow were observed. The bacteria presented circular and random trajectories under no flow conditions, positive rheotaxis under moderate flow, and sideways trajectories at high shear rates. The study deduce that the bacteria exhibit positive rheotaxis when the surface is smooth and maintain a laminar flow within the first few microns over it. Any sidewalls, imperfections and scratches within the bounding surface led to upstream motility.

Another study observed hydrodynamic interactions between the bacterial flagella and the flowing fluid when swimming [69]. Based on this approach, a series of microchannels were fabricated and

bacterial motility was studied and classified based on the microchannel height of the microchannel and flow rate [70].

Aerotaxis; response to oxygen concentration. Oxygen concentration, or aerotaxis, influences the motility patterns of aerobic bacteria such as *E. coli* and *B. subtilis.* Various studies employed microfluidics to study motility pattern modifications due to aerotaxis [47, 71]. Microfluidic devices were fabricated with a stable oxygen gradient throughout the microchannel and presented to the bacteria. Bacterial motility was oriented towards the higher oxygen concentration. Another approach used a hydrogel-based microfluidic device to study the motility of *Shewanella oneidensis* through the interplay of chemotaxis and aerotaxis [72].

Thermotaxis; response to temperature. Temperature gradients were created inside microchannels, allowing bacteria to navigate towards the most favorable temperature. This type of directional navigation approach is known as thermotaxis. Salman et al. used thermotaxis to study bacterial motility with a microfluidic device, demonstrating an interplay between thermotaxis, chemotaxis, and metabolism of *E. coli*, where they noticed that, when the established nutrient gradient was opposed to the temperature gradient, bacteria migrates towards lower temperatures [73]. Another approach used the interplay between thermotaxis and chemotaxis to understand bacterial motility, where the bacterial motility was influenced by the optimal temperature [74].

pH taxis. pH taxis demonstrate the directional motility towards favorable pH conditions. A hydrogel-based microfluidic device was fabricated to study bacterial motility under the influence of pH taxis [75]. Gradients of different pH values were created using hydrogel, and bacterial motility was analyzed under higher and lower pH conditions [75]. Another study investigated bacterial motility using microfluidic-based pH taxis approach coupled with hydrodynamics [76]. The diffusion across laminar flow enables to test the flow conditions and the study of how hydrodynamics under flow correlate with the pH taxis.

Magnetotaxis and other taxes. Bacterial motility influenced by a magnetic field is known as magnetotaxis. Bacteria that respond to magnetic fields are known as magnetotactic bacteria, which found applications in drug delivery applications [77]. Microfluidic approaches have been used along with magnetic fields to investigate bacterial motility and to sorting cells [78]. Bacterial cells also exhibit directional motility towards light (phototaxis) [79] and osmolarity (osmotaxis) [80].

Apart from cues such as chemicals, temperature, pH etc., bacterial motility is often affected by physical environmental cues.

Motility near and on surfaces; Effect on speed, curvature, and cell orientation. The interaction of microbes with surfaces and boundaries is a prime question in microbial ecology. The motility of microorganisms is considerably influenced by surfaces since they act as physical barriers. Hydrodynamic forces can trap swimming bacterial cells adjacent to the surfaces and alter their swimming patterns [81]. Furthermore, surfaces in microbial habitats can enable biofilm formation. The attachment of cells to surfaces, by encasing themselves to form biofilms, increases their resistance to antibiotics and mechanical stress [82, 83]. As a result of an exquisite control over geometry, microfluidic devices were used to study bacterial motility by directing their directionality or collecting microbes near surfaces. Microbes near boundaries can attach to surfaces because of various complex processes, such as electrostatic, van der Walls, and hydrophobic interactions by appendages, e.g., pili, fimbriae, and flagella. Various features that affect the rate of attachment or biofilm formation have been analyzed. For instance, *E. coli* gets trapped to the surface independently of the distance from the surface while swimming [81]. The flagella of *E. coli* push the cell head forward, causing the fluid to move away from the cell along the swimming direction. This fluid flow generates a force that attracts them to the surfaces. On the other hand, mono-flagellated bacteria, which can adapt the flick motility pattern, are pulled into the fluid [84]. Another striking feature was that trajectories were circular near the boundaries. This phenomenon is the result of a reactive force coming from the surface and acting on the cell head and flagellar bundle, making it rotate in opposite directions [85]. The reactive force generates stress on the bacteria making them curve and causing the swimming pattern to appear circular. While *E. coli* cells were allowed to navigate through microchannels slightly taller than their width, they preferred to swim along the right-side wall [86].

Trapping near the surfaces can also be highly dependent on the behavior of pili. *Vibrio cholerae* uses their pili along with their flagella to sense the physical surface before it gets attached to them [87]. Depending on the frictional forces between the surface and the pili, the pattern of trajectories changes. Low frictional forces lead to meandering trajectories, while high frictional forces generate high curvature trajectories. The different appendages on microorganisms also contribute to their ability of having distinct surface motility patterns. *Pseudomonas aeruginosa* can attach and detach the pili to have two different patterns of motility, such as moving in a vertical or horizontal orientation, respectively [88].

Motility in moving fluids. Microbial habitats are characterized by the fluid flow from lakes and oceans to soils, and the human body. Microfluidics have been used as an ideal approach for studying motility patterns of microorganisms in fluids and to understand their interactions. Marcos "et al." used microfluidic channels to study the correlation between shear rate and velocity of non-motile, helically shaped bacteria *(Leptospira biflexa)* [89]. By precisely imaging the bacteria at various depth of the channel and with theoretical prediction, the result deduce that the drift velocity is directly proportional to shear rate. A different effect of flow was observed with motile bacteria *(Bacillus subtilis)* [90]. Here, the swimming direction of bacteria is biased by the coupling between shear and the chirality of the bacterial flagellum.

In another study with motile flagella driven microorganisms, the rotation rate is faster when cells are traversing parallel to the flow and slower when they are aligned with the fluid flow [44]. Additional observations revealed the consequences of different swimming patterns with different fluid flows on chemotaxis and surface trapping [44]. Other studies with *E. coli* swimming near surfaces suggested upstream migration in the presence of flow [91]. Thus, fast fluid flows can be assumed to have important implications for colonization processes where upstream migration may cause bacterial transport into unexpected regions of the flow system.

Motility in groups. The collective motion of microorganisms received attention in the last decades. Studies have proved that physical interactions between densely packed cells are responsible for collective behavior [92, 93]. However, it remains uncertain whether these interactions are based on a simple physical contact, or they are the results of a more complex hydrodynamic interaction. Understanding collective motility can contribute towards some fundamental insights on bacterial dispersion and collective bacterial resistance to antibiotics [94].

Motility through tightly confined geometries and obstacles. Several theoretical [85, 95] and experimental [96, 97] studies investigated the effect of constricted geometries on the motility patterns of microorganisms. Studies with *E. coli* have been performed with narrow to wider microfluidic channels to understand how motility patterns are related to tight confinements [97]. The dimension of microchannels can be tuned for either channel height or channel width such that *E. coli* cells are able to grow and move through very narrow channels [98]. However, for very small width channels (smaller than the cell's diameter), cells were not able to move, but their growth remained unaffected. When motility was studied with narrow confinements, the motility patterns were observed to be less random and distinct [97]. Peritrichous bacteria, like *E. coli*,

presented a run-and-tumble mechanism in bulk media, while the motility pattern was circular through a constrained two-dimensional network [99, 100]. Additionally, they were able to swim in narrow channels with a smaller turn angle. *Serratia marcescens* presented straight motility patterns along the wall through narrow strip channels [99].

Bacterial motility can be altered with the transition of microchannels from linear to other shapes. Various studied have shown that bacterial cells switched their motility pattern from a straight line to a zig-zag pattern with changing structures [99, 101]. Various shapes of microstructures have been used for sorting bacteria based on their motility, for instance a ratchet-shaped microstructure was used as a rectifier to collect bacteria [102]. Alternative strategies, such as presenting obstacles to bacteria during motility, was investigated. A microchannel with several wall aligned pillars was designed and fabricated to study bacterial motility, which was found to be hindered due to obstacles that makes bacteria change their path repetitively after collision [102, 103]. Different obstacles, such as symmetric funnels, were used to direct bacterial motility and to establish well-defined motility patterns through interactions with the channel's boundaries [103, 104].

This extensive information on motility makes bacteria an attractive model candidate for studying and evaluating their decision-making behavior and path finding/space searching abilities in a maze or labyrinth.

1.4 Evaluation of decision-making behavior and path-finding abilities

Mazes – sometimes also called labyrinths are a type of graphical puzzles that consist of a series of nodes, junctions, and connectors arranged to form a network of interconnected paths. They are used as prototype models in graph theory, robotics [105, 106], experimental psychology [107], and urban transportation [108]. The simplest maze problem involves determining the shortest distance from the entrance to the exit and can be solved using digital computation in polynomial time [109]. Solving a maze problem with increasing complexity that incorporates non-linear behavior can be very challenging to solve, if at all, by a computational algorithm. With the advent of computers, several automated maze solving algorithms were developed. The "wall follower" algorithm [110] is the simplest and the best-known algorithm to find a solution to mazes, but it is not the most efficient for achieving multiple solutions in parallel. Other mathematical algorithms for maze-solving and path planning are Dijkstra's algorithm, which is used to find the shortest routes by connecting the nodes. A* (A star) search algorithm [111] uses graph traversal and pathfinding

processes for computer games. Rapidly exploring random tree algorithm uses the sampling based algorithm approach to find optimal solutions through the complex environments with many iterations [112]. The maze problems with increasing complexity are non-trivial exercises such as simultaneous maze problems are NP-Complete problems [113, 114]. These algorithms operate in a sequential fashion and are extremely slow when the complexity of the maze increases. Moreover, various chemical and biological systems have been explored by researchers to solve maze problems as a non-conventional approach.

1.4.1 Nonconventional approaches for solving mazes

Abiotic approaches.

Chemical based maze solving techniques. Using chemical waves to solve mazes was one of the earliest chemical based techniques [115]. A 2D maze was created with polymer membranes saturated with the Belousov-Zhabotinsky (BZ) reaction precursor, a family of oscillating chemical reactions. In this method, chemical waves were initiated through the maze, and their dispersion was recorded and analyzed using an image processing system. The direction of wave propagation was derived from the recorded image based on the velocity field while the shortest path was calculated using this vector field. However, the main drawback of this method was the requirement of a computer-based algorithm for post analysis.

Another chemical system designed for maze-solving used a droplet of organic solvent (2-hexyldecanoic acid/ pure 2-hexyldecanoic acid) [105]. In this experiment, complex mazes were designed and fabricated photolithographically, and a pH gradient was created throughout the structure. The surfactants or droplets were dyed with Calco Oil Red to increase the optical constant and the movement through the pH gradient, to be recorded. The droplet was found to move towards the regions of lower pH by finding the shortest path to the exit.

An alternative chemical-based pathfinding process was demonstrated using the Marangoni flow induced by a pH gradient [116]. The pH gradient through the network induced the Marangoni flow towards the region of lower pH. These experiments predicted the shortest path in a few seconds. In another study, the chemotactic motion of a decanol droplet towards a salt source was analyzed to explore the shortest path in a topologically complex environment [117].

Temperature induced method. After the study of pH-induced Marangoni flow for exploring the path finding process, temperature-induced Marangoni flow was investigated for finding the

shortest path in a maze [118]. Temperature gradients can be easily generated for solving maze problems. Marangoni flows are not limited to liquid–air interfaces. Microfluidic mazes have been presented with Marangoni flows to solve mazes effectively [119]. However, the major drawback in this case was that the temperature-induced Marangoni flow was relatively weak and could only be used for topologically simple mazes.

Using liquid metals. A gallium droplet was used to navigate along the highest electrical current density through a maze structure to explore the path finding process. Gallium droplets navigated through the shortest path as the intensity of the electric current was strongest through the shortest path [120].

Biotic approaches; exploring biological agents

DNA. Pathfinding operations with DNA molecules were studied by Chao "et al." [121]. A DNA nano device was designed, and each single-molecule navigator autonomously explores any of the possible paths through the maze. The DNA molecules explore the paths by connecting a given pair of start and end vertices in the maze. However, the study focused on the solutions of a simply connected maze without cyclic paths.

Slime mold. The slime mold *Physarum polycephalum* is famous as a computing biological agent because of its ability to find the minimum length distance through a maze [122]. The amoeboid forms a dynamic tubular network by connecting the food sources from entry to exit during foraging. Various algorithms were designed based on the path finding patterns of slime mold, but many of the *Physarum* inspired algorithms remained inefficient due to the low growth rate.

Fungi. Hanson "et al.", investigated the growth of filamentous fungi, which used long-term directional memory and collision-induced branching for space searching in a micro-confined maze network [123]. Directional memory is a tendency to extend in an initial direction, yet in the presence of an obstacle, the hyphae will stop. Directional memory was also observed to vary with different fungal species. The efficiency of the fungal (*Pycnoporus Cinnabarinus*) space searching algorithm outperforms a number of classical space searching algorithms such as Breadth-First-Search, A*, and Dijkstra algorithm studied by Asenova "et al." [124]. Held "et al." [125] studied the fungal growth through microfluidic mazes to understand the space searching strategies. This study suggests that the intracellular processes such as fungal hyphal extension and branching are involved in directional memory, which contributes towards the fungal space searching processes.

Mammalian cells. Moving cells such as neutrophils [122], leukocytes [123], and epithelial cancer cells [124] were investigated as biological candidates for navigating through mazes. Neutrophils and lymphocytes implemented their navigation process, guided by chemoattractant gradients. In contrast, epithelial cancer cells established the shortest distance from entry to exit in the absence of any external attractants, guided by self-generated gradients.

Worms. Caenorhabditis elegans was used as model candidate for exploring complex networks with [126] or without [127] any external cues. *C. elegans* associates the cues from food and information on the surrounding structures to explore the maze networks [126].

Bacteria. A classical microfluidic T-maze was designed and fabricated to study the chemotactic decision-making ability as well as the chemotactic sensitivity coefficient of bacterial populations. [128]. The study presented both experimental and theoretical observation, which reveals the heterogenicity in chemotactic sensitivity within bacterial populations. The study by Weber "et al." explained that the dispersal of the bacteria through the maze gets greatly influenced by the underlying geometry of the structure. The narrower channels and obstacles guide the movement of bacteria. They also compared the experimental data with a theoretical model and numerical simulations [129]. Park "et al." also studied the behavior of bacteria in the context of their spatial environment. *E. coli* cells traversed towards the dead ends of the maze under nutrient-deprived conditions. The study reveals that the topology of complex structures influences the movement of bacteria when there are no external cues [130].

Advancement in maze solving; exploring all possible paths to the maze

Although finding the shortest path in a maze network is the scientific goal, all possible valid and unique routes to the maze network need to be analyzed for important real-world applications. Computing the shortest route benefits emergency services such as; ambulances, fire engines [131], board game designers [132], and food and commodities transportation[133]. However, for the computer game industry, exploring unique paths is always a crucial task [134]. Even navigating in a new city to find simple multiple paths to the destination is always challenging. Nonetheless, few studies have investigated the navigation through mazes to explore and identify all valid paths, regardless of being the shortest ones.

In the pressure-driven flow was demonstrated by Fuerstman "et al." [135] to compute all possible solutions in a parallel manner. The maze was fabricated in the form of a network of microchannels with multiple paths. The study was conducted by changing the channels' shapes and dimensions,

and by using different tracing fluids to target multiple paths. In another study, networks of memristors performed calculations simultaneously to find all the possible solutions in a complex maze based on their length [136]. Lovas "et al." introduced temperature-induced Marangoni flow to find all possible paths in a maze network of different complexities [118]. The major issue with this method was that temperature-induced Marangoni flow is relatively weak and therefore, it can only be used for simple maze networks.

1.5 Unconventional computing

Unconventional computation deals with computing implemented in physical, chemical, and biological system. Light, fluid, microorganisms [137], or DNA [138], protein [139], and other molecules can be used as a computational medium for unconventional computation.
*Computation inspired by nature**;** Nature inspired computation is beneficial in many ways; when*,

- The problem is complex and nonlinear, such as combinatorial mathematical problems that involves many possible/potential variables/solutions. The time increases exponentially with the problem size and becomes intractable for sequential electronic computers.
- Finding an optimal solution using a conventional approach is difficult, and impossible to obtain.
- Modeling the problem cannot be possibly obtained by conventional approaches such as identifying complex pattern and classifying them.

Population based computation. This is mainly inspired by a wide range of biological systems, such as group of organisms or cells that work together or compete to search or find a solution [140]. The population and the overall search process benefit us to design evolutionary algorithms. Competition between a population of antibodies to target an intruder leads to the development of immune algorithms [141]. Kennedy and Eberhart designed particle swam optimization algorithms by studying the pattern of birds cooperation for finding food [137]. One of the most notable population algorithms is known as the ant colony optimization (ACO) algorithm, which is based on a nest of ants cooperating to target the shortest path to and from a food source [142].
DNA computation. DNA computation occurs in solutions [143] or on surfaces [144], which consists of a reaction between the four DNA bases. The initial implementation of DNA computation was by Adleman “et al.” to solve the Travel Salesman Problem (TSP) [143], which

requires to find the shortest complete route The cities and the paths between the cities were represented by the sequence of individual DNA strands. When strands hybridize, it represents a sequence of visited nodes by a path. DNA computing requires unreasonable amount of DNA for medium size problems [145]. The necessary number of oligonucleotides for a larger problem would be just slightly less than the number of the particle in the universe [138] Also, DNA computation is prone to errors and redundancy in ligation and PCR amplification at each computational step.

Network based computation. Network-based computation draws on a rich suite of biological processes. A network comprises a collection of nodes joined by edges. The network is more often abstract: the nodes are typically physical objects, but the edges are abstractions of different kinds of interactions. Examples include genetic regulation networks (the regulatory interaction between genes via their expressed proteins) [146], metabolic networks (the interactions between metabolic molecules, mediated by enzymes) [147], signaling networks (interaction pathways as signal molecules that propagate from the outside to the interior of a cell, mediated by proteins) [148], food webs (who eats whom), and social networks [149].

Network-based computation for solving combinatorial problems. Combinatorial mathematical problems require exploring many candidate solutions by brute-force, making the number of solutions to raise exponentially with the problem size. These problems are relevant to molecular biology [150, 151], information management [152], and cryptography [153]. Network-based computation processes include a) formulation of specific NP-complete problems into graphs, b) translation of graphs into physical networks, which contain microfluidic channels, nodes, entries, and exits, and c) massively parallel exploration of the network by many agents.

The proof of concept for solving Subset Sum Problem (SSP) using network-based computation with self-propelled cytoskeletal filaments, i.e., actin filaments, or microtubules has been proposed recently [154]. The major drawback of this approach is related to scalability, and it is also prone to errors. In this case the requirement of ATP restoration for the filaments and computational errors due to unexpected addition or loss of filaments restrict its practicality. Alternative proof of principles was reported for network-based computing such as microscopic beads for Clique problem using 3D microfluidics network [150] and photons for SSP [151]. Nevertheless, there are several drawbacks associated with fabrication as well as for visualizing techniques.

Scaling and imaging. One of the significant problem for all these above mentioned biocomputational approaches are scalability [155]. The limiting factor in the scaling up is the Field-of-View (FoV) of the network that encodes for the combinatorial problems with larger size [155]. The FoV is needed to monitor the networks that are of high density, but low compactness. With the increasing problem set size, the network's overall computing area explodes exponentially, too large to be recorded in one FoV. There are also advancements for imaging such as; lens-less microscopy and mobile phone-based microscopy [156], but it appears that the scaling of networks for solving SSP is problematic, and the FoV for larger networks is not achievable easily.

Accordingly, in the course of this dissertation, my first objective is to understand the motility behaviour of bacteria in confined microenvironments starting with quasi-open spaces like plazas, different widths linear channels, channels presenting lateral exits at various angles, and meandered confinements in comb-like structures. The second objective is the navigation of bacteria through mazes which are a class of NP-Complete problem, to study the space searching efficiencies to compute maximum possible paths in mazes of different complexity. With the studied knowledge on bacterial motility, the last objective is to perform Agent-based Network BioComputation with compact SSP series – (Pascal's series).

Chapter 2

2. Patterns of bacterial motility in microfluidics-confining environments

For an advancement in understanding of the motility of individual bacterial cells in confining microenvironments, and to assess the extent by which the behavior of bacteria with complex architectures can be assimilated with that of the more predictable monotrichous bacteria, the present chapter presents the investigation of the movement of five species, i.e., *Vibrio natriegens*, *Magnetococcus marinus*, *Pseudomonas putida*, *Vibrio fischeri*, and *Escherichia coli* in microfluidic geometries with various levels of confinement and geometrical complexity.

Patterns of bacterial motility in microfluidics-confining environments

Viola Tokárová[a,b,1], Ayyappasamy Sudalaiyadum Perumal[a,1], Monalisha Nayak[a,1], Henry Shum[c,1], Ondrej Kašpar[a,b,] Kavya Rajendran[a], Mahmood Mohammadi[d], Charles Tremblay[d], Eamonn A. Gaffney[e], Sylvain Martel[d], Dan V. Nicolau Jr[e], and Dan V. Nicolau[a,2]

[a]Faculty of Engineering, Department of Bioengineering, McGill University, Montreal, QC H3A 0C3, Canada; [b]Department of Chemical Engineering, University of Chemistry and Technology, Prague, 166 28 Prague, Czech Republic; [c]Department of Applied Mathematics, University of Waterloo, Waterloo, ON N2L 3G1, Canada; [d]Department of Computer Engineering, École Polytechnique de Montréal, Montreal, QC H3T 1J4, Canada; and [e]School of Mathematical Sciences, Queensland University of Technology, Brisbane, QLD 4000 Australia

Edited by Robert H. Austin, Princeton University, Princeton, NJ, and approved March 19, 2021 (received for review July 5, 2020)

Author contributions: D.V.N. designed research; V.T., A.S.P., M.N., H.S., O.K., M.M., C.T., and D.V.N. Jr. performed research; S.M. contributed new reagents/analytic tools; V.T., A.S.P., M.N., H.S., O.K., K.R., E.A.G., D.V.N. Jr., and D.V.N. analyzed data; and V.T., A.S.P., M.N., H.S., O.K., and D.V.N. wrote the paper.
The authors declare no competing interest.
This article is a PNAS Direct Submission.

1V.T., A.S.P., M.N., and H.S. contributed equally to this work.
2To whom correspondence may be addressed. Email: dan.nicolau@mcgill.ca.

Significance

Understanding bacterial movement is crucial for health, agriculture, environment, and industry. Studying the motility of five bacterial species in microfluidic environments showed that bacterial motility behavior is the result of a “tug-of-war” between hydrodynamics and local nanomechanics. In less confining spaces, bacterial motility is governed by hydrodynamics and can be approximately predicted by modeling developed for the simplest species. Conversely, in tightly confining environments, movement is mainly controlled by the steric interactions between flagella and the surrounding walls. Intriguingly, in mesoscale-sized geometries, hydrodynamics and bacterium– wall interactions overlap, either “constructively,” leading to smooth movement in straight channels, or “destructively,” leading to trapping. Our study provides a methodological

template for the development of devices for single-cell genomics, diagnostics, or biocomputation.

Abstract

Understanding the motility behavior of bacteria in confining microenvironments, in which they search for available physical space and move in response to stimuli, is important for environmental, food industry, and biomedical applications. We studied the motility of five bacterial species with various sizes and flagellar architectures (*Vibrio natriegens*, *Magnetococcus marinus*, *Pseudomonas putida*, *Vibrio fischeri*, and *Escherichia coli*) in microfluidic environments presenting various levels of confinement and geometrical complexity, in the absence of external flow and concentration gradients. When the confinement is moderate, such as in quasi-open spaces with only one limiting wall, and in wide channels, the motility behavior of bacteria with complex flagellar architectures approximately follows the hydrodynamics-based predictions developed for simple monotrichous bacteria. Specifically, *V. natriegens* and *V. fischeri* moved parallel to the wall and *P. putida* and *E. coli* presented a stable movement parallel to the wall but with incidental wall escape events, while *M. marinus* exhibited frequent flipping between wall accumulator and wall escaper regimes. Conversely, in tighter confining environments, the motility is governed by the steric interactions between bacteria and the surrounding walls. In mesoscale regions, where the impacts of hydrodynamics and steric interactions overlap, these mechanisms can either push bacteria in the same directions in linear channels, leading to smooth bacterial movement, or they could be oppositional (e.g., in mesoscale-sized meandered channels), leading to chaotic movement and subsequent bacterial trapping. The study provides a methodological template for the design of microfluidic devices for single-cell genomic screening, bacterial entrapment for diagnostics, or biocomputation.

Keywords: bacterial motility, microfluidic devices, space partitioning, wall escaper, wall accumulator

2.1 Introduction

Many motile bacteria live in confining microenvironments (e.g., animal or plant tissue, soil, waste, granulated, and porous materials) and consequently are important to many applications like health [infectious diseases [1, 2], pharmaceuticals [3], and nutrition [4]], agriculture [veterinary [5] and

crops [6]], environmental science [photosynthesis (7), biodegradation (8), and bioremediation (9)], and industrial activities [mining [10] and biofouling [11]]. Bacterial motility is essential in the search for available physical space as well as for enabling bacterial taxis in response to external stimuli, such as temperature [12], chemical gradients [13, 14], mechanical cues [15], or magnetic fields [16]. To thrive in environments with diverse geometrical and physical characteristics, from open spaces to constraining environments, motile bacteria have evolved a multitude of propelling mechanisms [17], with flagellum-driven being the most common [18,19]. Flagellum-based machinery features various numbers of flagella [20] and designs: monotrichous, lophotrichous, amphitrichous, or peritrichous. The mechanics of this machinery, coupled with cell morphology [21] (e.g., coccus, rod-like, or curved) translates into several motility modes (e.g., turn angle, run-and-tumble, or run-and-flick) [22], and various motility behaviors (e.g., swimming, tumbling, and swarming) [17, 23]. Environmental factors [24,25] (e.g., chemical composition, viscosity, temperature, pH, and the chemistry and the roughness of adjacent surfaces) also influence bacterial motility.

"Pure" bacterial motility, unbiased by chemotaxis or fluid flow, was reported near simple flat surfaces [26, 27] and in channels [28–30]. Simulations of model bacteria in analogous conditions were also undertaken [31–37] but owing to the complexity of bacterial mechanics [38], modeling from first principles did not provide sufficient understanding to accurately predict movement patterns of different species in complex, confined environments. Consequently, studies of the effects of bacterial geometry in confined geometries were limited to models of simple, monotrichous bacteria with an assumed rigid flagellum [32, 39].

Microfluidic devices [40, 41] are commonly used for the manipulation of individual or small populations of cells in micrometer-sized channels for medical diagnostics [42], drug screening [43], cell separation [44, 45], detection and sorting [46], and single-cell genomics [47]. While microfluidic structures are used for the study of the motility of mammalian cells (48, 49), and microorganisms [e.g., fungi [50, 51], algae (52), or bacteria (29, 53–56)], these studies typically focus on a single species.

To make progress toward a more general understanding of the motility of individual bacterial cells in confining microenvironments, as well as to assess the extent to which the behavior of bacteria with complex architectures can be assimilated with that of the more predictable monotrichous bacteria, the present work investigated the movement of five species (i.e., *Vibrio natriegens*,

Magnetococcus marinus, *Pseudomonas putida*, *Vibrio fischeri*, and *Escherichia coli*) in microfluidic geometries with various levels of confinement and geometrical complexity.

2. 2 Results and Discussion

The modulation of motility behavior by confinement was assessed by observing, by three-dimensional (3D) imaging, the movement of individual bacteria, presenting various characteristics (Fig. 3A and SI Appendix, Fig. S1) in microfluidic structures with high (6 μm) or low (4 μm) ceilings (Fig. 1B) and with various geometries (Fig. 3C and SI Appendix, Fig. S2) as follows: 1) large chambers with quasi-open spaces ("plazas"), 2) linear channels with various widths, 3) channels presenting lateral exits at various angles, and 4) meandered channels with various widths. In the absence of pressure and concentration gradients, this approach allowed the study of the interaction between hydrodynamics and the steric interactions of bacteria with the walls, unobscured by other external factors (e.g., rheo- and chemotaxis). Experimental, image analysis, and simulation protocols are fully described in SI Appendix.

2.2.1 Motility in large chambers

Impact of the distance between horizontal planes. To minimize the possible coupling of the impact of horizontal planes, the designs of microfluidic chambers, made of polydimethylsiloxane (PDMS), had to find a compromise between their height and fabrication and operation issues. From the design perspective, it was found that a height of 6 μm (Fig. 3A and SI Appendix, Table S1) allows, conservatively, the unencumbered bacterial motility. Furthermore, preliminary experiments comparing motility in both types of microfluidic structures presented evidence (Movie S1) of the coupling of the impact on both horizontal planes on bacterial motility for those with 4 μm heights. Consequently, 6 μm–tall microfluidic structures were used for all further experiments. A detailed discussion is presented in SI Appendix.

Spatial distribution of bacteria. The bacterial species studied presented different motility behaviors with respect to proximity of vertical walls and corners (Fig. 4 A–C). First, *V. fischeri*, *V. natriegens*, and *E. coli* moved at small distances from vertical walls. Second, *M. marinus* presented an uneven, broken density near vertical walls, due to the frequent "ping-pong"–like collisions and reflections (Movie S1). Third, *P. putida* presented an even spatial distribution throughout the chamber.

The 3D imaging and z-stack sectioning of bacterial trajectories in 6 μm–tall plazas (Fig. 4D and SI Appendix, Figs. S6–S8) revealed a similar behavior in the central area close to the horizonal walls (i.e., free of the possible edge effects from the vertical walls). *V. natriegens*, *V. fischeri*, and *E. coli* presented trajectories in proximity to and parallel with the horizontal walls. This was not the case for *P. putida* and *M. marinus*, which frequently fluctuated between z-planes (SI Appendix, Figs. S7 and S8). Statistical analysis of the bacterial positions (SI Appendix, Fig. S9) showed that *V. natriegens*, *V. fischeri*, and *E. coli* moved preferentially in a parallel plane to the horizontal walls and that *P. putida* and *M. marinus* presented a rather uniform distribution of positions on the vertical axis.

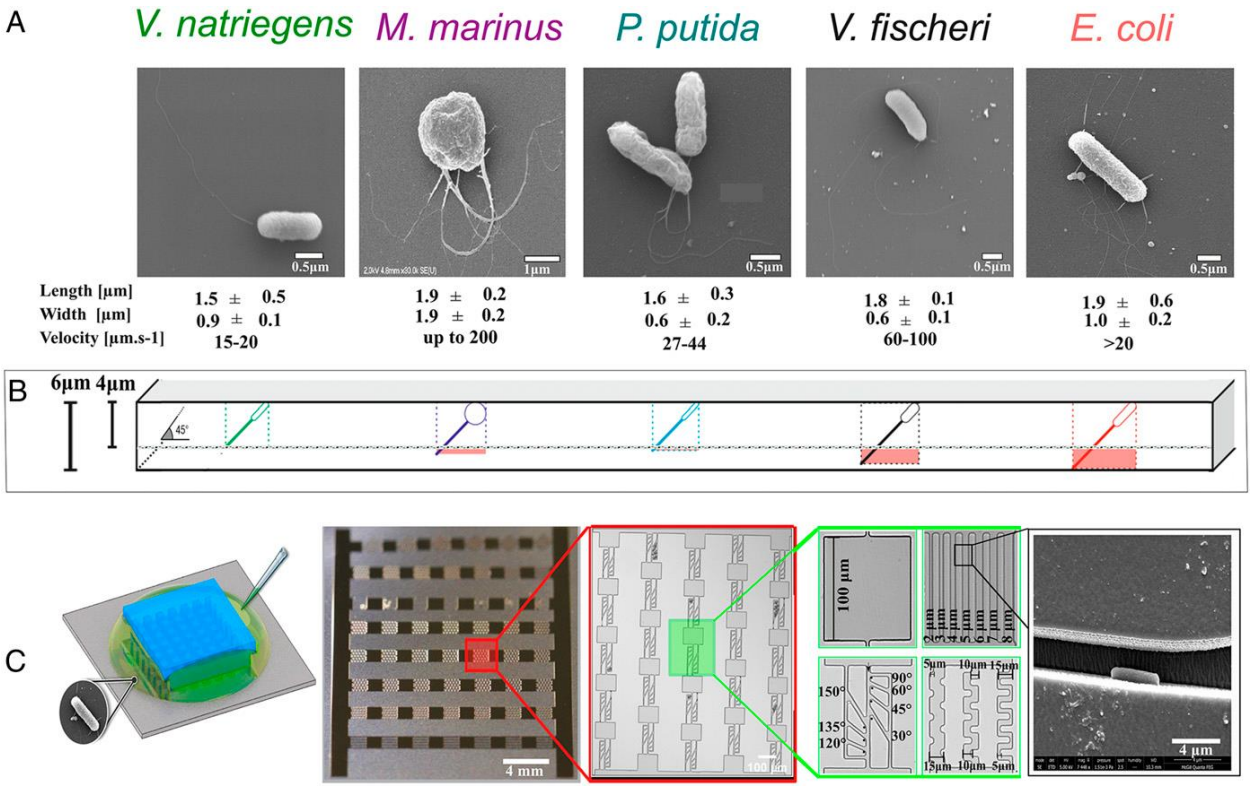

Figure 3. Microfluidics chip for testing microbial motility. (A) Scanning electron micrographs (SEM) images of bacteria studied with various architectures and dimensions (full details in SI Appendix, Table S1). (B) Graphical projection of the fit of the total bacterial length (body plus flagella) positioned at 45° versus the height of the microfluidic structures for 6 µm and 4 µm heights. (C) Sequential, from left to right, zoom-in images of the experimental device: 1) the bacterial suspension is introduced from the side of the chip attached to the cover slide; 2) the overall architecture of the chip; 3) zoom-in of one lane of experimental structures (sequence of angled channels separated by plazas); 4) detailed image of the experimental structures used in this study (i.e., plazas) and linear channels (top row), angled, and meandered channels (bottom row); and 5) SEM image of a bacterium (here, *E. coli*) in a channel.

Theoretical classification of bacterial motility behavior. For bacteria that are propelled by a flagellum or flagellar bundle behind the cell, the fluid flow generated by swimming has a dipolar structure: the fluid is pushed backward by the flagellum and pulled forward by the cell body. This flow has been shown to attract swimmers to solid walls, causing them to remain close to the wall for long time periods despite rotational Brownian motion [57]. A separate effect of swimming near surfaces is that hydrodynamic interactions between the wall and rotating flagellum and between the wall and counter-rotating cell body, respectively, lead to bacteria swimming in circular orbits when they are close to a wall [58].

Detailed hydrodynamic modeling of monotrichous bacteria showed that the geometrical parameters of the cell (length and width) and of the helical flagellum (length, helical amplitude, and wavelength) determine the motility behavior near a single flat surface [32]. Based on this modeling framework, correlated with the experimental observations from the present study, three classes of behavior were observed, depending on the geometry of the bacterium. “Wall accumulators” descend to the walls and exhibit a strong propensity for swimming in the closest vicinity to the wall (with a separation of tens of nanometres between the bacterium and the surface), where steric interactions are likely, thus making difficult the precise prediction of motility behavior even for the simplest monotrichous bacteria. When bacteria swim at distances further than this from the wall but at a nearly constant separation, exhibiting the characteristic circular orbits predicted by simpler analysis, they are classified as “stable swimmers parallel to the wall.” It was observed [26] those dynamical interactions are negligible before collisions with the walls, but once bacteria swim on parallel planes a few micrometers away from surfaces, hydrodynamic forces maintain long residence times in this region. Finally, when hydrodynamic interactions result in bacterial movement away from surfaces, they are classified as “wall escapers.” The demarcation between these classes is approximate, due to the inherent stochasticity of bacterial motility.

Two key geometrical parameters determining whether a particular bacterium is an accumulator, escaper, or moving parallel to the wall are 1) the cell body aspect ratio and 2) the length of the flagellum. Higher aspect ratios (more rod-like) and shorter flagella encourage escape from walls (Fig. 5). For geometries at the boundary between parallel motion and escapers, it is possible for a bacterium to exhibit either stable motion close to the wall or escape depending on the angle of approach to the wall. It is useful to first determine the behavior of bacteria near a single wall because this is indicative of motility in more complex environments. For example, simulations showed that parallel–stable swimmers and escapers had different characteristics when placed between parallel walls [35] and in corners of rectangular channels [39]. However, the variability of characteristic bacterial dimensions adds to the inherent stochasticity of movement. This in turn makes the demarcation between motility classes approximate. Details of the modeling used in Fig. 5 are given in SI Appendix, and the characteristic dimensions of bacteria are presented in SI Appendix, Table S2.

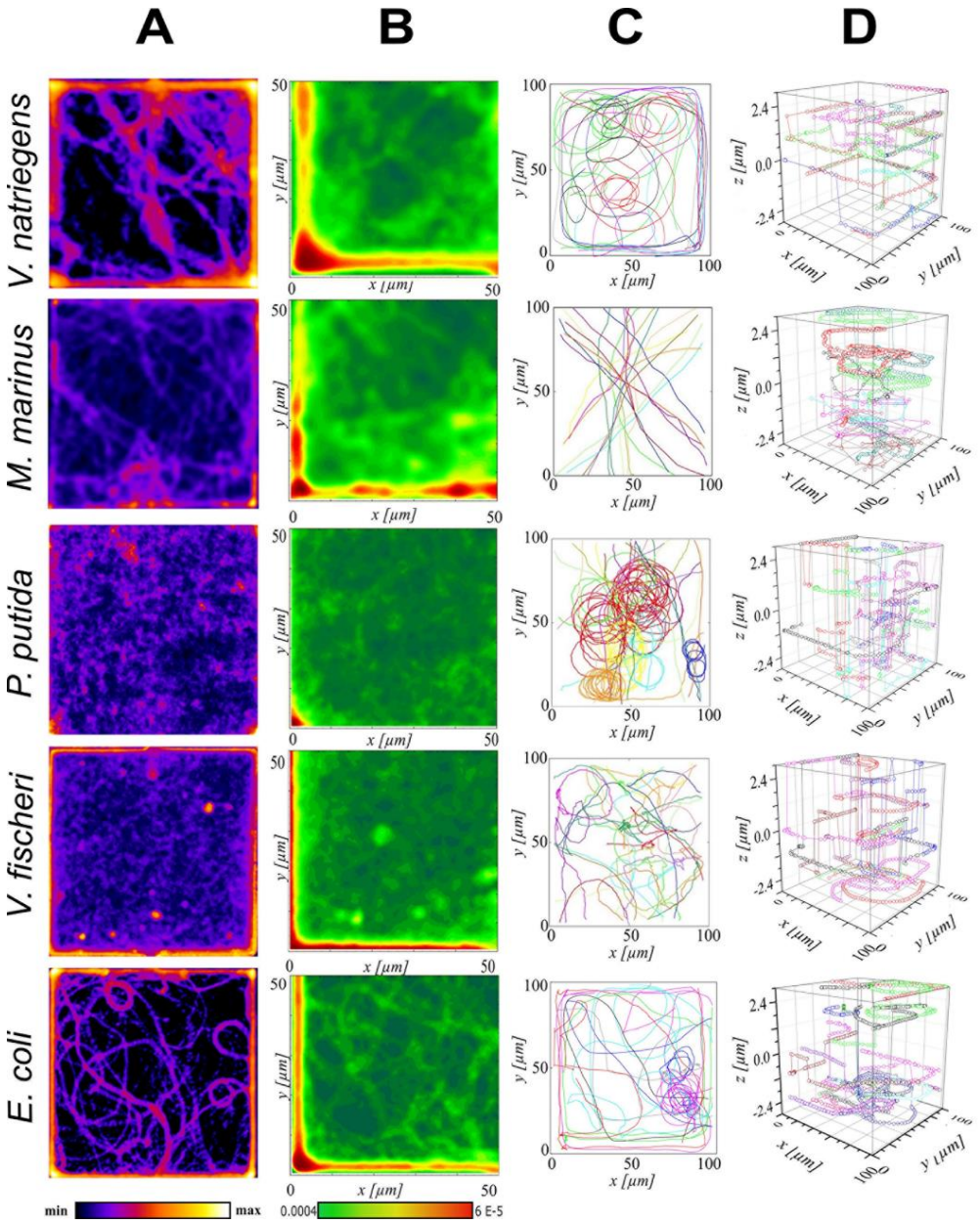

Figure 4. Motility in plazas with 6 μm high ceilings**.** (A) Density maps of bacterial locations. Color code (bottom): "min" and "max" represent no and the highest presence of bacteria, respectively. (B) Spatial distribution of bacteria obtained by superimposing and averaging the data from all four quarters of the density maps in A. Color code (bottom): frequency of bacterial presence, with red for the highest and dark green for the minimum probability. (C) Characteristic long 2D projections of bacterial trajectories. (D) 3D bacterial trajectories. By rows, from top to bottom, are the following: *V. natriegens* (average count of bacterial positions in each frame, n = 14/frame); *M. marinus* (n = 12/frame); *P. putida* (n = 15/frame); *V. fischeri* (n = 15/frame); and *E. coli* (n = 13/frame).

While these theoretical studies were based on a model with a single, polar flagellum, it was demonstrated that such models accurately reproduce the experimentally observed radius of curvature

of near-wall tracks for *E. coli*, which swim with several flagella [31]. Therefore, it is expected that this classification serves as a useful conceptual background for the characterization of motility behavior in relation to a solid surface, even though most of the species in the current study are architecturally more complex than the monotrichous model (here, *V. natriegens*). Indeed, the propensity to move near surfaces was observed experimentally for several non monotrichous bacterial species, for instance (extensively) for *E. coli* [26, 27, 30, 31, 57, 59], but also for *Serratia marcescens* [29] and *Pseudomonas aeruginosa* [60].

Comparison of experimental and theoretically predicted behavior. By comparison with monotrichous model bacteria of equivalent dimensions, *M. marinus* is predicted to be a wall accumulator, but it is near the boundary between accumulators and escapers (Fig. 5). All other species are expected to maintain stable motion parallel to and near the walls (Fig. 5), although variability within populations is sufficient for some individuals to be classified as escapers. There are elements that correlate well with the predicted motility behavior of simple bacteria with that of the more complex geometries studied as well as explanations for the deviations from this general "motility landscape" (Fig. 5):

1) Our experiments showed that *M. marinus* did not exhibit stable motion parallel to the wall but rather a "ping-pong"–like movement, with abrupt approaches to the walls alternating with equally abrupt breakouts. Recently, a model of the movement of a polar biflagellate bacterium [61], based on *M. marinus*, showed that such wall escaping (scattering) behavior could occur for certain arrangements of the two flagella. Additionally, it was recently reported that *M. marinus* swims with one flagellar bundle in front of the cell body and one behind [62], a mode of motility that is fundamentally different from the monotrichous model.

2) The density maps, probability maps, long trajectories, represented as two-dimensional (2D) projections and in 3D (Fig. 4 A– D, respectively) for *P. putida* and *E. coli*, showed characteristics of both escapers, more apparent for P. putida, and movement parallel to the wall, more apparent for *E. coli*. The persistent circular orbits indicate motion close to the horizontal walls, and for *E. coli*, the long trajectories along the vertical walls also highlight boundary accumulation. In contrast, the long, relatively straight trajectories through the middle of the chamber and frequent transitions between z-planes represent wall escaping behaviors. These seemingly contradictory observations are, in fact, consistent with the variability found in the measured cell shapes and flagella lengths. While the average values for both *P. putida* and *E. coli* lie within the movement parallel to the wall regime (Fig. 3), the spread of parameters extends considerably into the wall escaper region.

3) Density and probability maps, as well as 2D projections and 3D bacterial trajectories (Fig. 4 A–D, respectively), are consistent with the placement of *V. natriegens* and *V. fischeri* deep in the

movement parallel to the walls, according to the theoretical predictions in Fig. 5. Both species showed circular trajectories (more prominent in *V. natriegens*) and high densities around the perimeter of the chamber. Interestingly, *V. natriegens* was often observed swimming parallel to the vertical walls but at distances of around 3.5 μm from the wall (Fig. 4B) rather than keeping almost in contact with the wall. This type of parallel motion was found in simulations of boundary accumulators in corners of channels [39].

Motility patterns. The longest trajectories of bacterial motility in plazas had characteristics that were the most species specific (Fig. 4C and Movie S1, top row). *V. natriegens*, *E. coli*, and *V. fischeri* presented, to various degrees, two classes of trajectories: 1) movement along the vertical and horizontal walls and, when detached, 2) circular motions, until again attaching to the walls. *M. marinus* exhibited a "ping-pong"–like motility pattern, generally following relatively straight paths until it approached and scattered off a vertical wall, resulting in a statistically higher density localized near the walls (due to frequent collisions). There was little discernible movement along the vertical or horizontal walls of the plaza, and no complete circular orbits were observed. Two classes of behavior were present in the longest trajectories of *P. putida*. Some were relatively straight, spanning from one side of the chamber to the other, whereas other trajectories were circular and persisted for many overlapping cycles. Long trajectories around the perimeter of the chamber, as observed for *V. natriegens*, *E. coli*, and even *V. fischeri*, were uncommon for *P. putida*.

Circular motion. The circular motion of bacteria near surfaces was previously reported for *E. coli* both at air–liquid [27] and solid–liquid interfaces [58, 63] and for *P. putida* at solid–liquid interfaces [33, 64]. Counterintuitively, despite their very different flagellar arrangements (Fig. 3A and SI Appendix, Fig. S1 and Table S1), circular patterns were also observed here for *P. putida*, to a lesser extent for *E. coli*, and for *V. natriegens* (Fig. 4 C and D). Theoretically, the hydrodynamic interactions between a flat surface and a bacterium swimming on a parallel plane to it are indeed able to explain this curved pattern of trajectories [58, 60].

In summary, in quasi-open spaces, such as plazas, when the movement is limited only by parallel vertical or horizontal walls placed at distances considerably larger than the size of bacteria, their motility can be approximately characterized as stable movement parallel to the wall, wall escapers, or rarely as wall accumulators, as derived from bacterial geometric parameters and hydrodynamics-based modeling of the movement near surfaces of monotrichous bacteria.

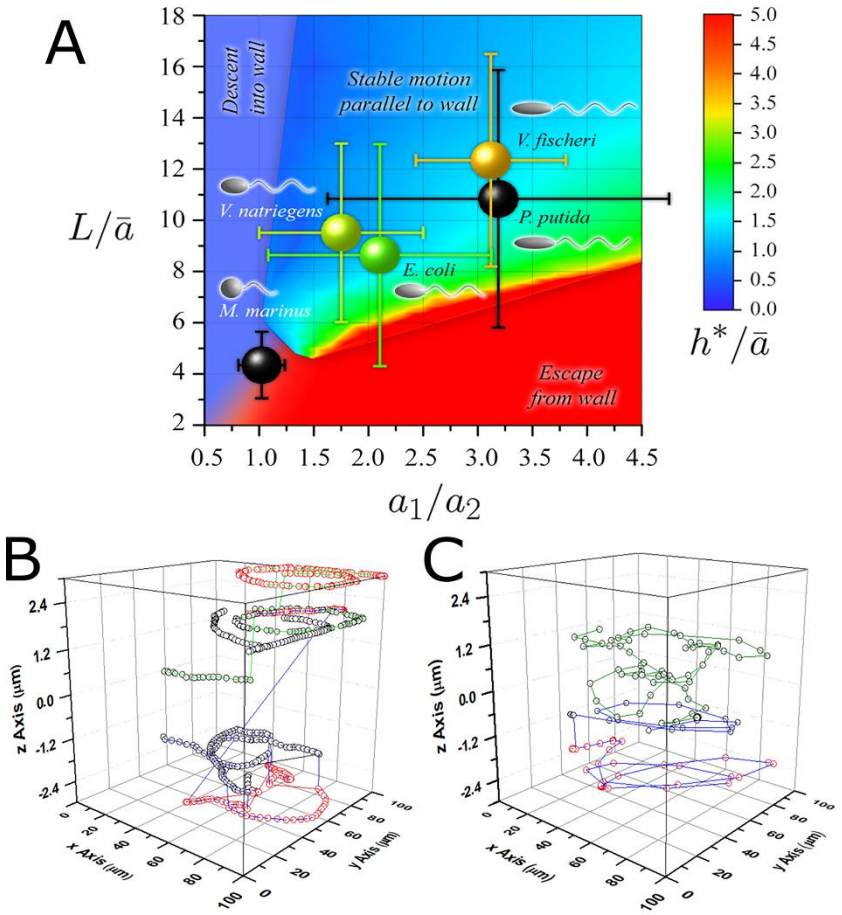

Figure 5. Prediction of motility behavior. (A) Bacterial positions, according to their dimensions, on a motility "map" [32], derived from hydrodynamic principles, for monotrichous bacteria. *V. natriegens*, *V. fischeri*, and *E. coli*, "swim parallel to walls" (confirmed experimentally, Fig. 2B and SI Appendix, Fig. S9). *M. marinus* is placed at the boundary between "wall accumulators" and "wall escapers" regions (confirmed experimentally by its wall-bouncing behavior). *P. putida*, with the largest variability of sizes, straddles the extreme "swimming parallel to wall" and "wall escaper" regions (confirmed by spatial distribution in Fig. 2B and SI Appendix, Fig. S9). The legend (updated from ref. 32, SI Appendix, Table S2) is as follows: a1 = polar radius of cell body (half the cell length); a2 = equatorial radius of cell body (half of the diameter diameter); [a1/a2] = aspect ratio of the cell body; L = curvilinear length of the flagellum (approximated by the axial length of the flagellum); _a = radius of sphere with volume of cell body; L/_a = nondimensional length of the flagellum/a; h* = optimal distance from wall (for swimmers parallel to walls); and h*/_a = nondimensional stable distance from wall. The colors of bacterial coordinates approximately replicate the color equivalent to h*/_a (determined from z-stack analysis). (B) Example of a bacterium moving stable parallel to the walls: *E. coli* (also exhibiting "escape from wall" jumps). (C) Example of a "wall escaper" bacterium: *M. marinus*.

2.2.2 Motility in tightly confining geometries

2.2.2.1 Motility in linear channels

Following the experiments in plazas with high and low ceilings and to avoid (to the extent possible) the impact on motility from more than two vertical walls, further experiments used only microfluidic channels with a 6 μm distance between the horizontal planes.

Overall motility characteristics; sinusoidal movement. When laterally confined in wider channels (e.g., 6 to 8 μm), *V. natriegens* and *E. coli* showed the strongest propensity for moving along walls (Fig. 6A and SI Appendix, Fig. S10 for 3D trajectories), correlating well with their motility behavior in plazas (Fig. 4A and B) and their movement parallel to the vertical (Fig. 4C and D) and horizontal walls (SI Appendix, Fig. S9).

P. putida exhibited an apparent sinusoidal movement, especially in larger channels (Fig. 6A). A Fast Fourier Transform (FFT) analysis of the trajectories (SI Appendix, Figs. S11 and S12B) indicated that *V. natriegens*, *V. fischeri*, and, to a much lesser extent, *E. coli* also present sinusoidal movement characteristics, with wavelengths increasing roughly proportionally with an increase in channel widths (SI Appendix, Fig. S12B). It was demonstrated [39,65] that monotrichous wall escapers (with this behavior being predicted, partially, for *P. putida* in Fig. 5) move in distorted helical paths in channels of large rectangular transversal section. This upwards correlation between motility wavelengths and available volume for movement is like the larger radii of the circular movement in plazas with higher ceilings than in those with low ceilings (Fig. 4C and SI Appendix, Fig. S5C). *M. marinus* also exhibited sinusoidal-like behavior, but the FFT analysis showed that this movement is only the result of frequent collisions to, and bouncing from, the walls.

In narrower channels (i.e., 3 to 6 μm), the tighter confinement increasingly forced bacteria to move along the channel axis (except for *M. marinus*) rather than exhibited their motility behavior observed in open spaces (plazas). Moreover, in tighter (but still larger than the lateral size of the cell) channels, bacterial movement appeared to benefit from both hydrodynamics and steric interaction with the walls, which synergistically push bacteria in the same direction due to the lateral-only confinement of straight channels [66].

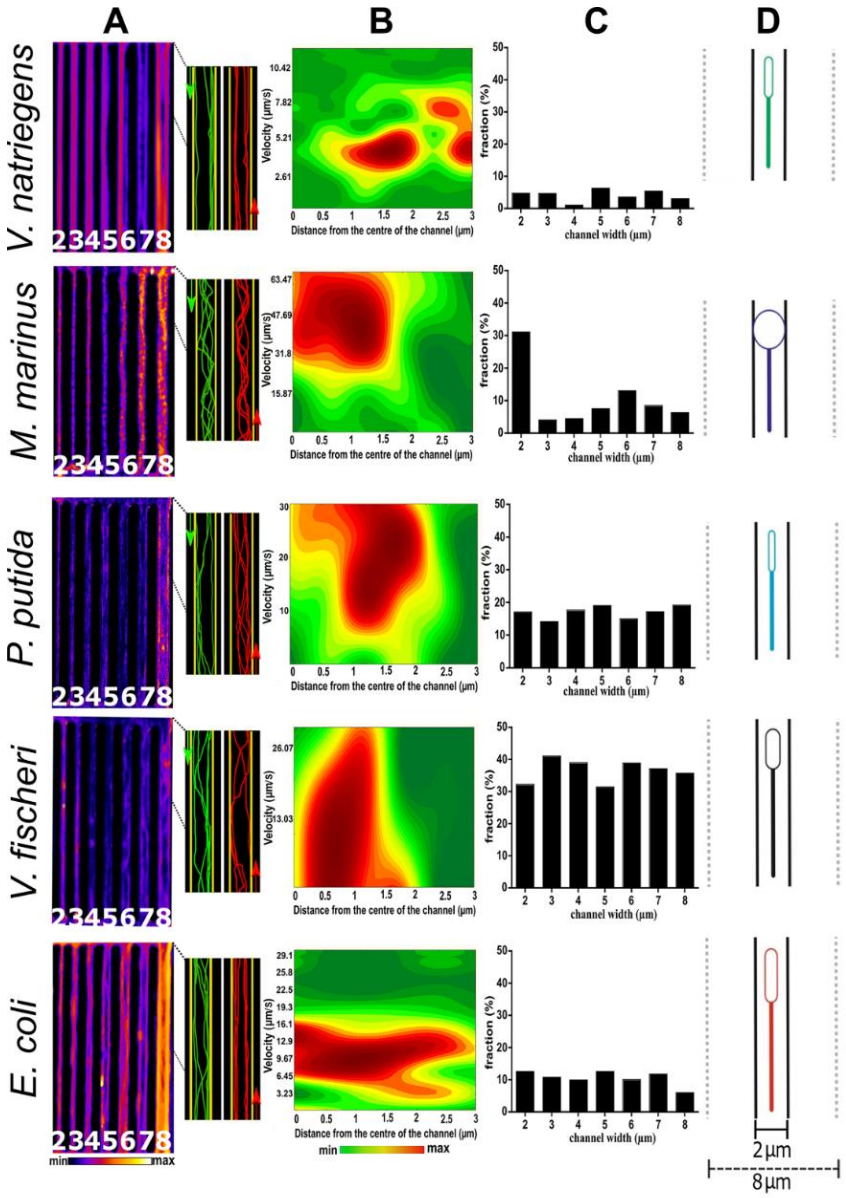

Figure 6. Bacterial motility in linear channels. (A, Left) Density maps of the movement patterns of bacteria in channels with different widths. (A, Right) Bacterial trajectories in 8 μm wide channels, moving from one direction (green) or from an opposite one (red). (B) Double histograms of velocity (y-axis) versus normalized distance from the center of the linear channel (channel wall on the extreme right) for 6 μm × 6 μm channels (the full analysis is presented in SI Appendix, Fig. S14). *E. coli* and *V. natriegens* present a specific bimodal distribution of velocities near the wall. (C) Influence of the channel width on the fraction of U-turns. By rows, from top to bottom, are the following: *V. natriegens* (average count of bacteria each frame, n = 20/frame); *M. marinus* (n = 10/ frame); P. *putida* (n = 19/frame); *V. fischeri* (n = 18/frame); and *E. coli* (n = 22/frame). (D) Graphical representation of the top view of a bacterium with their average dimensions, in linear channels. The thick and dotted lines represent the minimum and maximum channel widths.

Velocities in channels. Analysis of the velocities in straight channels appeared to further substantiate the synergy between hydrodynamics-driven and steric interactions–driven motility mechanisms. Indeed, while *M. marinus* exhibited a moderate decrease in average velocity with the decrease of the width of the channel, including compared with that in the plazas, due to an increase in collisions with the walls, all other species did not show any notable and systemic velocity variation with channel widths (SI Appendix, Fig. S13). Furthermore, the double histograms of the velocity in channels (Fig. 6B, for rectangular 6 × 6 μm channels; full analysis in SI Appendix, Fig. S14) revealed that *V. natriegens* and *E. coli* presented a distinctive bimodal distribution of velocities at the walls, with one velocity higher and one lower than the overall velocity. This bimodal distribution, for the species with the lowest ratios of the cell body and of the flagella (a1/a2 and L/_a, respectively, Fig. 5 and SI Appendix, Table S2), could be the result of separate instances of short-term cell adhesion to the wall and movement acceleration due to the steric interaction of flagella with the walls. In this context, it was reported [67] that the interaction between the walls and the flagella of *E. coli* translates into a "thrusting aid" for those bacteria running smoothly along solid surfaces. It was also reported, for *E. coli* [30, 68], *B. subtilis* [69], and *S. marcescens* [29], that bacteria exhibited higher velocities in narrower channels (which eventually decreases significantly in even narrower channels, due to the severe mechanical constraints applied to the cells), which is supported by the bimodal distribution of velocities observed for *E. coli* (and *V. natriegens*) here.

Straight versus U-turn movements. In straight channels, bacterial motility was expected to be increasingly driven by steric interactions, to the detriment of hydrodynamics, with a decrease in channel widths. This increased impact of the steric interactions can explain the species-specific proportion of U-turns (Fig. 6C). First, the species with the lowest ratio of flagellum/length/cell body (i.e., *V. natriegens* and *E. coli*) (Fig. 5) had the lowest overall proportion of U-turns, with an apparent decrease of U-turns with the channel width for the larger *E. coli* (Fig. 6C, Bottom). Conversely, the species clustered at higher characteristic values of L/_a and a1/a2 ratios (i.e., *P. putida* and *V. fischeri*) (Fig. 5) have a considerably higher proportion of U-turns than *V. natriegens* and *E. coli*, and there was even a considerably higher proportion for *V. fischeri* (Fig. 4D, fourth from the top). Second, *M. marinus*, with its characteristic frequent collisions and rebounds from the walls, had a low ratio of U-turns, with the notable exception of the 2 μm– wide channels. This unique behavior can be explained by the extreme steric interactions of *M. marinus* with both walls in channels with 2 μm widths, (i.e., as large as the cell body) (Fig. 6D, second from the top), resulting in the bacterial cell being "pinned" by both vertical walls then "flipped" in the 6 μm–tall vertical plane of the

channel, followed by the movement in the opposite direction. Third, *P. putida*, experiencing intermittent wall contact, exhibited a similar ratio of U-turns as *V. natriegens* and *E. coli.* Fourth, *V. fischeri*, which swim the closest to the wall (Fig. 4B), had the highest ratio of U-turns.

In summary, these results demonstrate that, when a strong and complex coupling exists between the interaction by parallel walls placed at distances like the dimensions of bacteria, their motility is primarily governed by the local steric interactions between the walls and the flagella and, in extreme confinement, the cell body. Consequently, the increase in confinement with narrower channels leads to a decrease in hydrodynamics-based propulsion, and the dilution, or outright disappearance of the classes of motility behavior observed in open spaces.

2.2.2.2 Motility in channels with angled exits

Motility in channels with angled exits. In the structures with angled exits (Fig. 3C, lower right of the fourth image from the left), all bacterial species had a large preference for moving in straight trajectories along the middle axis of the channel, as qualitatively suggested by the density maps (Fig. 7A), by representative trajectories (Fig. 7B and Movie S3), and by representative bacterial 3D trajectories (SI Appendix, Fig. S15). Even for the smallest exit angle (i.e., 30°), the probability of movement in a straight line instead of exiting laterally (estimated as the ratio between bacteria moving straight and the total number that arrived at that intersection) ranges from 72% (for *P. putida*) to 58% (for *M. marinus*). While the general trend for all bacteria was that the exiting probability decreased with increasing exit angle, there were some species-specific details (Fig. 7C). First, *V. natriegens*, *E. coli*, and *P. putida* had a clearly decreasing exiting probability with an increase in exit angle, while for *V. fischeri* this trend was less visible, and *M. marinus* exhibited a rather indifferent relationship between exit probabilities and exit angles, following an abrupt drop at angles higher than 30°. Second, all species other than *M. marinus* had a relatively higher exiting probability at 90° angles.

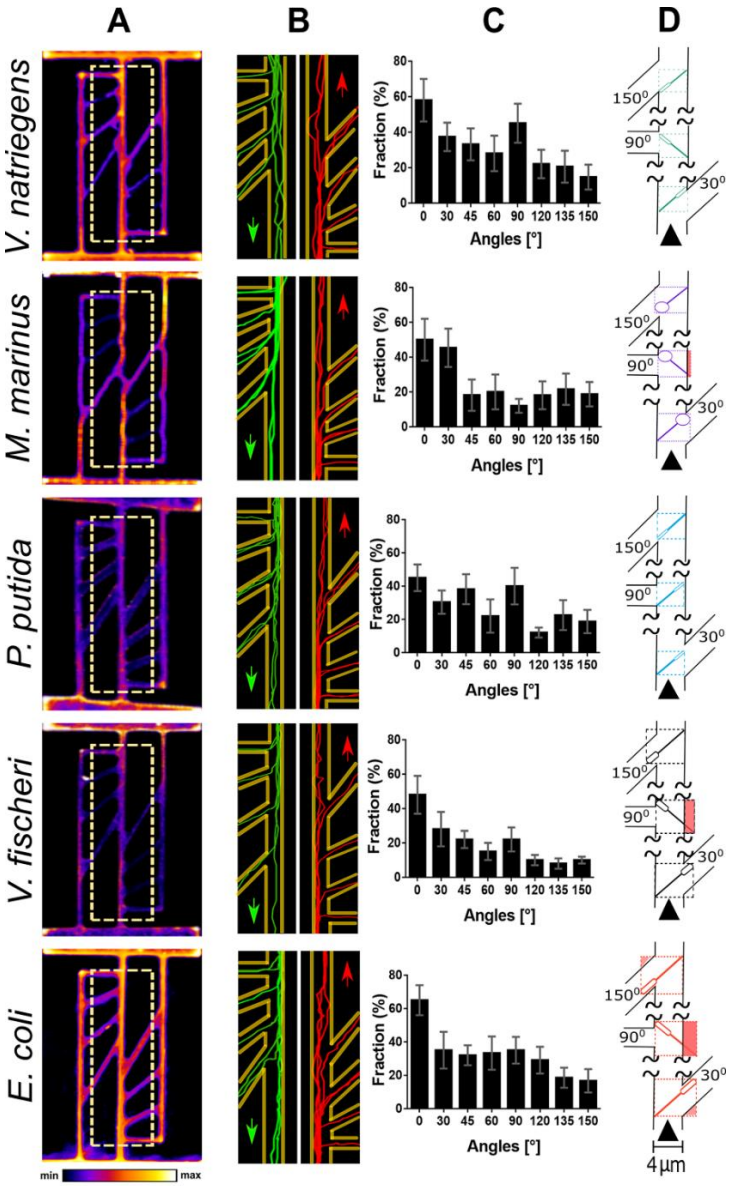

Figure 7. Bacterial motility in channels with angled exits. (A) Density maps of the movement patterns of bacteria in straight parallel channels, connected by side channels at angles ranging from 0° to 150°. All channels are nominally 4 µm wide. (B) Bacterial trajectories, either from top (green) or from the opposite direction (red). (C) Frequencies of bacteria moving at different exit angles. By rows, from top to bottom, are the following: *V. natriegens* (average count of bacteria each frame, n = 10/frame); *M. marinus* (n = 8/frame); *P. putida* (n = 10/frame); *V. fischeri* (n = 13/frame); and *E. coli* (n = 11/frame). (D) Graphical representation of the top view of bacterium with average dimensions in the angled channels (few representative angles). The areas in light brown representspaces that exceed the dimensions of the respective bacteria in the respective position.

This species-specific motility behavior in angled channels appeared to be the result of bacterial movement being driven by both local hydrodynamics and by steric interactions with the walls. First, the decrease of exit probabilities with exit angles for all species, but especially for *V. natriegens* and *E. coli*, resembles the lower frequency of turning by large angles in open spaces (SI Appendix, Fig. S3). The deflection angles in open spaces (SI Appendix, Figs. S3 and S4) are near-instantaneous measurements, and while longer integration times would lead to larger apparent values, this could also incorporate other sudden changes of direction, thus obscuring the inherent propensity of bacteria for sideways movement. With this qualification, it is reasonable to expect a connection between the propensity to escape laterally at set angles in angled channels (Fig. 7C) and the deflection angles in open spaces. However, this similarity had notable limitations (e.g., all species studied had negligible probabilities of deflection angles at much lower angles than those for bacteria in the angled channels). Second, while the wide spread of deflection angles in plazas (SI Appendix, Figs. S3 and S16) for *P. putida* could justify its relatively wide spread of exit probabilities in angled channels, *E. coli*, which had a narrow distribution of deflection angles, had a considerably larger and wider distribution of exit probabilities in angled channels than *P. putida*. Similarly, while both *V. natriegens* and *V. fischeri* exhibited a monotone decrease of frequency with increasing deflection angles in plazas (SI Appendix, Figs. S3 and S16), this behavior translated into a monotone decrease of exit probabilities in angled channels only for the former, whereas the latter did not show any obvious correlation between exit probabilities and respective escape angles. Finally, *M. marinus* had a monotone decrease of frequency with increasing deflection angles (after 10°) but an approximately flat relationship between the exit probabilities and escape angles (after 30°).

These observations suggest that, in addition to species-specific hydrodynamics-driven spread of deflection angles in open spaces (plazas), another mechanism was also responsible for determining the exit probabilities in angled channels. Indeed, the species that exhibited a notable departure from the expected extrapolation of behavior in open spaces is also the species whose dimensions exceed the clearance in the angled channels (i.e., *E. coli* and *V. fischeri*) (Fig. 7D). Conversely, the species whose dimensions did not surpass the clearance in the angled channels (i.e., *V. natriegens* and *P. putida*) are also those which exhibited a reasonable extrapolation of deflection angles in open spaces to a monotonical decrease of exit probabilities with escape angles. The frequent collisions and bouncing of *M. marinus* had the effect of levelling the exit probabilities regardless of the escape angles (except for 30°, for which there is enough turning space and therefore a higher exit probability, Fig. 7D).

It must be also noted that the confinement at the intersection between central and lateral channels did not fully correlate with the respective exit angle. For instance, the 150° exit offered the largest volume available for movement at the intersection between the axial and lateral channels (highlighted in SI Appendix, Fig. S2), thus making the comparison with U-turns (at 180°) in tight linear channels, with no variation of widths, inconsistent. Finally, the relatively higher escape probabilities for 90° angles could be the result of smaller free volume at the intersection of the axial channel, with steric interactions biasing bacteria toward lateral exits.

In conclusion, bacterial motility studies in angled channels revealed that when the level of confinement is low, due to the large volume at cross-intersection in relation to smaller bacterial sizes, the movement is mostly driven by hydrodynamics, as an extension of the behavior observed in open spaces. Conversely, when the confinement is tight, due to larger bacterial sizes, the local steric interactions between flagella and the walls contribute substantially to the motility behavior.

2.2.2.3 Motility in meandered channels

The trapping of bacteria in purposefully designed microfluidics structures is of special interest to various applications [e.g., single-cell genomics [70] and accelerated evolution [71]], and therefore, the responsible mechanisms were studied [72, 73].

The meandered system comprised three channels, each with a different gap between the edge of the "teeth" (i.e., 5 μm [left], 10 μm [middle], and 15 μm [right]) (Fig. 3C, lower right, fourth image from left). The tightly confined, 5 μm–wide meandered channels made the motility of all species more complex (Fig. 8 and SI Appendix, Fig. S17 and Movie S4). The elastic-like collisions of *M. marinus* resulted in frequent trappings and, consequently, a considerably lower overall "success rate" (defined as the ratio of bacterial entries versus exits, at steady state) than the rest of the bacterial species (Fig. 8C). In addition, the 90°-angled corners appeared to operate as traps for *E. coli* and to a lesser extent for *V. natriegens* (bright spots in the density maps in Fig. 8A; the higher retention time for *E. coli*, SI Appendix, Tables S3 and S4).

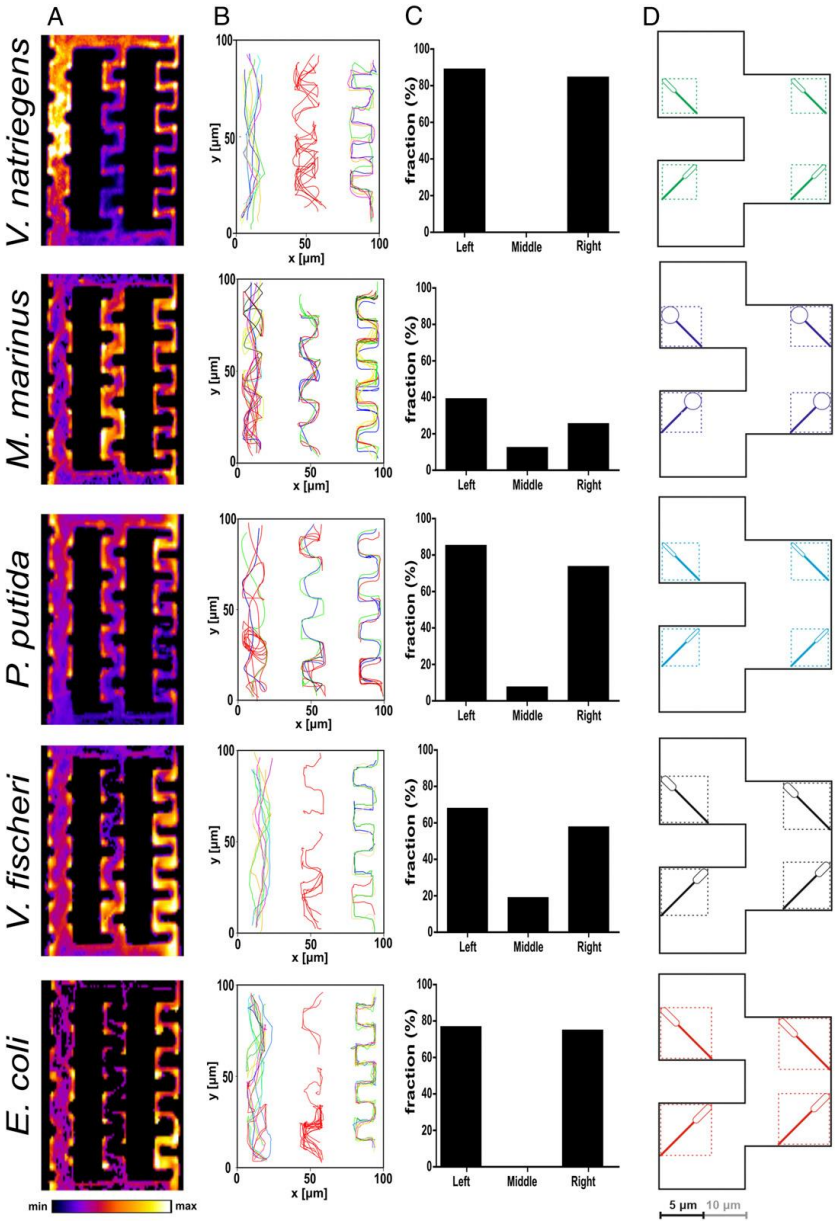

Figure 8. Bacterial motility in meandered channels. (A) Density maps of the bacterial movement patterns. (B) Representative tracks of the bacterial motility (trajectories in red are for bacteria that took U-turns or got trapped). (C) Frequency of bacteria making successful exits, relative to those that are trapped, or performed U-turns (unsuccessful tracks) for each meandered channel. By rows, from top to bottom, are the following: *V. natriegens* (average count of bacteria each frame, n = 18/frame); *M. marinus* (n = 12/frame); *P. putida* (n = 22/frame); *V. fischeri* (n = 25/frame); and *E. coli* (n = 19/frame). (D) Graphical representation of the top view of bacteria in the mesoscale-sized channel.

Intriguingly, all species appeared to have difficulty in passing the middle, 10 μm–wide channels (Fig. 8C). All species made U-turns or carried out repeated deflection at different angles, as well as being trapped (SI Appendix, Fig. S18). Intuitively, the overall bacterial velocity in meandered channels is the lowest when compared with those in plazas and straight channels (SI Appendix, Fig. S19). However, perhaps counterintuitively, the larger-than–5 μm distance between the walls made the trapping effect of the 90°-angled corners more effective, to a near-total extent for *V. natriegens* and *E. coli* and to a lower relative extent for *V. fischeri*, *M. marinus*, and *P. putida*. As expected, the highest passage "success rate" was provided by the meandered channels with the largest distance between walls (Fig. 8C). Again, *M. marinus* and *P. putida* executed more zigzagged trajectories than *V. natriegens*, *V. fischeri*, and *E. coli* (Fig. 8B).

This complex and species-specific behavior can be explained in view of previous findings as follows. In channels with large gaps between comb teeth, all bacteria can negotiate the passage, their movement being driven mostly by hydrodynamics, with only occasional interference of the local steric interactions between the flagella and the walls. Conversely, in channels with tight confinement, bacteria are also capable of successfully negotiating the channels, this time "channelled" by the local steric interaction between flagella and the 90°-angled walls. Finally, in the channels in the mesoscale region (i.e., 10 μm distance between the "comb teeth"), the mechanism based on hydrodynamics and that based on the local steric interaction do not operate synergistically, increasing the chaotic character of motility and making the overall forward advancement difficult. This is particularly obvious for *V. natriegens* and *E. coli*, which swim parallel to walls (Fig. 5) at a ∼2 μm distance from the walls (Fig. 4B), thus leading to frequent U-turns. Additionally, these two species are those with the lowest ratios of the cell body and of the flagella (Fig. 5 and SI Appendix, Table S2). The more compact architectures of *V. natriegens* and *E. co*li could explain the near-perfect trapping by frequent circular movements in very confined spaces leading to long retention times. Conversely, but for different reasons, *V. fischeri* (a species swimming the closest to the walls, Fig. 4B) and *P. putida* (a species with opportunistic distribution in free volumes) can avoid, to a larger extent than *V. natriegens* and *E. coli*, being trapped in the meandered channels. Tellingly, these two species are also those with the highest ratios of the cell body and of the whole bacterium (Fig. 5 and SI Appendix, Table S2). This dichotomy of behavior for species swimming parallel to the walls suggests that the steric interactions–driven movement in tight confinement is also modulated by bacterial shape and not only by size (presented schematically in Fig. 8D). Indeed, *V. natriegens* and *E. coli* are both very effectively trapped in mesoscale-sized meandered channels, and while *P. putida*, a much shorter species (SI Appendix, Table S2), appeared to have some success, *V. fischeri*, the largest of the species swimming parallel to the walls, had the best success rate. Finally, *M. marinus* was also found

to exit mesoscale meandered channels more, but its frequent collision-and-rebound on the walls led to slightly lower trapping efficiencies.

To elucidate whether the trapping effect is permanent or transient, the average duration for successfully traversing the meandered channels was quantified (SI Appendix, Table S3). Within the experimental time window (4 to 5 min), *V. natriegens* and *E. coli* were unable to successfully traverse the middle-meandered channels. Although *M. marinus* had a shorter retention time due to its high velocity, the distance that it needed to travel to be able to exit the meandered channel was longer. Representative 3D trajectories in meandered channels are presented in SI Appendix, Fig. S17. The color-coded trajectories for U-turns, successful passages, and trapped bacteria are presented in SI Appendix, Fig. S18.

To conclude, in complex geometries, such as meandered channels, hydrodynamics-driven motility is prevalent in wider channels, and the local steric interactions–based mechanism governs bacterial motility in narrow channels. However, in the mesoscale region, these two mechanisms do not act in synergy, resulting in trapping bacteria, with high efficiency for species swimming parallel to the walls, finely modulated by their characteristic shape ratios.

2.3. Perspectives and future work

The present study, in which we studied a wide range of bacterial motility behavior, provides insights in several areas of applications, as well as suggesting further research.

Fundamentals of bacterial motility mechanics in microenvironments. It was previously shown that a fundamental understanding of the mechanics of the movement of monoflagellated [32, 33, 39] and even bi-flagellated [61] bacteria in simple geometries, such as the proximity to a surface, can accurately predict motility patterns of bacteria. However, the current study, which described motility patterns of more complex bacterial architectures and in more complex geometries, revealed the limits of this understanding, which would be critical for designing microdevices manipulating bacteria for biosensing, drug delivery, cell sorting, or biocomputation. Further theoretical directions suggested by our study, perhaps coupled with long-term monitoring [74], include analyzing the impact of population variation on cell behavior, investigating the extent to which more complicated bacterial geometries and flagellar arrangements can be represented by more advanced mechanical models, and the need to conduct systematic validation studies. Studies of this type, using artificial microfluidics systems mimicking their natural counterparts, recently carried out for bacteria [75] and fungi [76] or for specifically investigating stochastic processes in bacteria [77], are motivated by the abundance of microbial habitats comprising linear and meandered channels and spaces with different angled turns (SI Appendix, Fig. S20).

Motility of magnetic bacteria in biological networks. Chemically or magnetically guided self-propelled bacteria were used for non-systemic delivery of drugs and cargoes in tumour therapy [78–81]. The targeted physiological regions (e.g., deep enteric tissues, hypoxic tumors, tissue granules, and arterioles) [78, 82] are essentially impenetrable to probing devices, but they can be accessed, in principle, by robust bacteria operating as autonomous microrobots moving in the natural microfluidic vascular system [78]. The description of bacterial motility, that of *M. marinus*, in PDMS microfluidic channels mimicking the microvascular system surrounding the tumor (e.g., micrometer-range sizes and relevant mechanical elasticity) can lead to the optimization of the operation of these microrobots outside clinical settings, which are expensive to operate and unable to provide reproducible observations at the microscale and in real time.

Bacterial cell sorting. The efficient characterization, sorting, or selection of individual bacterial cells in small volumes are achieved in various microfluidics-based applications, such as those derived from the classical flow cytometry [83–85] to the more recent single-cell analysis [70]. In fact, microfluidic devices have been increasingly used for assessing bacterial chemotaxis [86–89], motility [29, 30, 90, 91], and for bacterial cell sorting [46, 72, 91–93], and our results can offer insights for the design of these devices. For instance, the characterization of bacteria as wall accumulators, or wall escapers, can suggest entirely different geometries for microfluidic structures for bacterial cell sorting. Similarly, microfluidic channels can be designed to increase retention time (e.g., by having helical profiles) or to amplify the differences in mechanical responses to flow in microfluidics-based flow cytometry.

Network-based biocomputation. Microfluidics-based approaches to computation of problems intractable to electronic computers have been proposed for clique problem (94) and subset sum problem [95]. These biological computers require the independent exploration of microfluidic networks encoding a mathematical problem by autonomous agents such as beads [94], cytoskeletal filaments [95], or microorganisms [96]. The precision of the microfluidics-based computation is determined by the capacity of biological agents, such as bacteria, to faithfully follow the movement rules embedded in the logic junctions they visit [97]. Consequently, the selection of bacterial candidates and the designs of computational microfluidic networks will require the removal or at least minimization of errors, such as U-turns in narrow channels, as well as optimization of the angles of logic gates channels.

2.4. Conclusion

We here provided a comprehensive account of the motility of individual bacterial cells, belonging to five species with considerably varied dimensions and morphologies, in microfluidic networks and with various levels of confinement and complexity. For lesser confining geometries, such as facing one limiting wall, the motility behavior of the five species studied can be assimilated, with qualifications, to that of monotrichous bacteria with similar dimensions. However, when increasing confinement complexity, as for instance in straight channels with various widths, in networks with exits at various angles, and meandered channels, the classification as swimming parallel to the walls for *V. natriegens*, *E. coli*, *V. fischeri*, and *P. putida* and as escapers, partially, for *E. coli*, *P. putida*, and *M. marinus* is increasingly inaccurate, as a result of the increase of the impact of local steric interaction of species-specific morphology with the tightly confining geometry. The study can be also used as a methodological template for the optimization of the design of microfluidic devices with specific functions (e.g., motility-based cell selection for single-cell genomic screening, detection of rare cells, bacterial entrapment devices for diagnostics, or biocomputation).

2.5. Materials and Methods

All experimental, modeling, and simulation data analysis protocols are presented in SI Appendix.
Data Availability. All study data are included in the article and/or supporting information.

2.6. Acknowledgement

This work was financially supported by the Defense Advanced Research Projects Agency under grant agreements HR0011-16-2- 0028 and N66001-03-1-8913, by the Natural Sciences and Engineering Research Council of Canada under grant agreements RGPIN-2016-05019 and RGPIN-2018-04418, by the New Frontiers Research Fund of Canada under grant agreement NFRFE-2019-00129, by the Czech Science Foundation under grant agreement GACR, project 17-11851Y, and by Australian Research Council Future Fellowship FT180100698. We thank the researchers from the Facility for Electron Microscopy Research at McGill University, from the Faculty of Dental Medicine at the University of Montreal, and from the Department of Geology of the University of Quebec at Montreal, for help in electron microscopy characterization of bacteria.

Reference

1. A. A. Salyers, D. D. Whitt, Bacterial Pathogenesis: A Molecular Approach (ASM Press, Washington, DC, 1994), vol. 3.
2. N. Woodford, D. M. Livermore, Infections caused by gram-positive bacteria: A review of the global challenge. J. Infect. 59 (suppl. 1), S4–S16 (2009).
3. P. P. Nagarkar, S. D. Ravetkar, M. G. Watve, Oligophilic bacteria as tools to monitor aseptic pharmaceutical production units. Appl. Environ. Microbiol. 67, 1371–1374 (2001).
4. M. G. Gareau, P. M. Sherman, W. A. Walker, Probiotics and the gut microbiota in intestinal health and disease. Nat. Rev. Gastroenterol. Hepatol. 7, 503–514 (2010).
5. T. A. Harper et al., Bioaerosol sampling for airborne bacteria in a small animal veterinary teaching hospital. Infect. Ecol. Epidemiol. 3 (2013).
6. S. L. Kandel, N. Herschberger, S. H. Kim, S. L. Doty, Diazotrophic endophytes of poplar and willow for growth promotion of rice plants in nitrogen-limited conditions. Crop Sci. 55, 1765–1772 (2015).
7. Y. Asada, J. Miyake, Photobiological hydrogen production. J. Biosci. Bioeng. 88, 1–6 (1999).
8. A. Esmaeili, A. A. Pourbabaee, H. A. Alikhani, F. Shabani, E. Esmaeili, Biodegradation of low-density polyethylene (LDPE) by mixed culture of Lysinibacillus xylanilyticus and Aspergillus Niger in soil. PLoS One 8, e71720 (2013).
9. M. Höckenreiner, H. Neugebauer, L. Elango, Ex situ bioremediation method for the treatment of groundwater contaminated with PAHs. Int. J. Environ. Sci. Technol. 12, 285–296 (2015).
10. F. Reith, C. M. Zammit, S. L. Rogers, D. C. McPhail, J. Brugger, Potential utilisation of micro-organisms in gold processing: A review. Miner. Process. Extr. Metall. 121, 251–260 (2012).
11. O. Habimana, A. Semião, E. Casey, The role of cell-surface interactions in bacterial initial adhesion and consequent biofilm formation on nanofiltration/reverse osmosis membranes. J. Membrane Sci. 454, 82–96 (2014).
12. C. Verde, D. Giordano, C. M. Bellas, G. di Prisco, A. M. Anesio, “Polar marine microorganisms and climate change” in Advances in Microbial Physiology, R. K. Poole, Ed. (Elsevier, 2016), 69, pp. 187–215.
13. G. H. Wadhams, J. P. Armitage, Making sense of it all: Bacterial chemotaxis. Nat. Rev. Mol. Cell Biol. 5, 1024–1037 (2004).

14. A. Z. Komaromy et al., Arrays of nano-structured surfaces to probe the adhesion and viability of bacteria. Microelectron. Eng. 91, 39–43 (2012).
15. A. Persat et al., The mechanical world of bacteria. Cell 161, 988–997 (2015).
16. O. Felfoul, S. Martel, Assessment of navigation control strategy for magnetotactic bacteria in microchannel: Toward targeting solid tumors. Biomed. Microdevices 15, 1015–1024 (2013).
17. K. F. Jarrell, M. J. McBride, The surprisingly diverse ways that prokaryotes move. Nat. Rev. Microbiol. 6, 466–476 (2008).
18. M. E. J. Holwill, R. E. Burge, A hydrodynamic study of the motility of flagellated bacteria. Arch. Biochem. Biophys. 101, 249–260 (1963).
19. F. Bai et al., Conformational spread as a mechanism for cooperativity in the bacterial flagellar switch. Science 327, 685–689 (2010).
20. F. F. Chevance, K. T. Hughes, Coordinating assembly of a bacterial macromolecular machine. Nat. Rev. Microbiol. 6, 455–465 (2008).
21. K. D. Young, Bacterial morphology: Why have different shapes? Curr. Opin. Microbiol. 10, 596–600 (2007).
22. A. Bren, M. Eisenbach, How signals are heard during bacterial chemotaxis: Proteinprotein interactions in sensory signal propagation. J. Bacteriol. 182, 6865–6873 (2000).
23. R. M. Harshey, Bacterial motility on a surface: Many ways to a common goal. Annu. Rev. Microbiol. 57, 249–273 (2003).
24. J. G. Mitchell, K. Kogure, Bacterial motility: Links to the environment and a driving force for microbial physics. FEMS Microbiol. Ecol. 55, 3–16 (2006).
25. P. Denissenko, V. Kantsler, D. J. Smith, J. Kirkman-Brown, Human spermatozoa migration in microchannels reveals boundary-following navigation. Proc. Natl. Acad. Sci. U.S.A. 109, 8007–8010 (2012).
26. K. Drescher, J. Dunkel, L. H. Cisneros, S. Ganguly, R. E. Goldstein, Fluid dynamics and noise in bacterial cell-cell and cell-surface scattering. Proc. Natl. Acad. Sci. U.S.A. 108, 10940–10945 (2011).
27. L. Lemelle, J. F. Palierne, E. Chatre, C. Place, Counterclockwise circular motion of bacteria swimming at the air-liquid interface. J. Bacteriol. 192, 6307–6308 (2010).
28. H. C. Berg, L. Turner, Chemotaxis of bacteria in glass capillary arrays. Escherichia coli, motility, microchannel plate, and light scattering. Biophys. J. 58, 919–930 (1990).
29. M. Binz, A. P. Lee, C. Edwards, D. V. Nicolau, Motility of bacteria in microfluidic structures. Microelectron. Eng. 87, 810–813 (2010).

30. B. Libberton, M. Binz, H. van Zalinge, D. V. Nicolau, Efficiency of the flagellar propulsion of Escherichia coli in confined microfluidic geometries. Phys. Rev. E 99, 012408 (2019).
31. D. Giacché, T. Ishikawa, T. Yamaguchi, Hydrodynamic entrapment of bacteria swimming near a solid surface. Phys. Rev. E Stat. Nonlin. Soft Matter Phys. 82, 056309 (2010).
32. H. Shum, E. A. Gaffney, D. J. Smith, Modelling bacterial behaviour close to a no-slip plane boundary: The influence of bacterial geometry. Proc. Royal Soc. Math. Phys. Eng. Sci. 466, 1725–1748 (2010).
33. H. Shum, E. A. Gaffney, The effects of flagellar hook compliance on motility of monotrichous bacteria: A modeling study. Phys. Fluids 24, 061901 (2012).
34. A. Acemoglu, S. Yesilyurt, Effects of geometric parameters on swimming of microorganisms with single helical flagellum in circular channels. Biophys. J. 106, 1537–1547 (2014).
35. H. Shum, E. A. Gaffney, Hydrodynamic analysis of flagellated bacteria swimming near one and between two no-slip plane boundaries. Phys. Rev. E Stat. Nonlin. Soft Matter Phys. 91, 033012 (2015).
36. J. Hu, A. Wysocki, R. G. Winkler, G. Gompper, Physical sensing of surface properties by microswimmers–Directing bacterial motion via wall slip. Sci. Rep. 5, 9586 (2015).
37. Y. Park, Y. Kim, S. Lim, Flagellated bacteria swim in circles near a rigid wall. Phys. Rev. E 100, 063112 (2019).
38. E. Lauga, Bacterial hydrodynamics. Annu. Rev. Fluid Mech. 48, 105–130 (2016).
39. H. Shum, E. A. Gaffney, Hydrodynamic analysis of flagellated bacteria swimming in corners of rectangular channels. Phys. Rev. E Stat. Nonlin. Soft Matter Phys. 92, 063016 (2015).
40. E. K. Sackmann, A. L. Fulton, D. J. Beebe, The present and future role of microfluidics in biomedical research. Nature 507, 181–189 (2014).
41. J. Zhang et al., Fundamentals and applications of inertial microfluidics: A review. Lab Chip 16, 10–34 (2016).
42. D. Erickson, D. Q. Li, Integrated microfluidic devices. Anal. Chim. Acta 507, 11–26 (2004).
43. G.-X. Zheng et al., An integrated microfludic device for culturing and screening of Giardia lamblia. Exp. Parasitol. 137, 1–7 (2014).
44. C.-X. Xu, X.-F. Yin, Continuous cell introduction and rapid dynamic lysis for high throughput single-cell analysis on microfluidic chips with hydrodynamic focusing. J. Chromatogr. A 1218, 726–732 (2011).
45. D. Yuan et al., Sheathless separation of microalgae from bacteria using a simple straight channel based on viscoelastic microfluidics. Lab Chip 19, 2811–2821 (2019).

46. L. Y. Yeo, H. C. Chang, P. P. Chan, J. R. Friend, Microfluidic devices for bio applications. Small 7, 12–48 (2011).
47. T. Kalisky, S. R. Quake, Single-cell genomics. Nat. Methods 8, 311–314 (2011).
48. R. U. Sheth, S. S. Yim, F. L. Wu, H. H. Wang, Multiplex recording of cellular events over time on CRISPR biological tape. Science 358, 1457–1461 (2017).
49. B. J. Kim, M. Wu, Microfluidics for mammalian cell chemotaxis. Ann. Biomed. Eng. 40, 1316–1327 (2012).
50. K. L. Hanson et al., Fungi use efficient algorithms for the exploration of microfluidic networks. Small 2, 1212–1220 (2006).
51. M. Held, A. P. Lee, C. Edwards, D. V. Nicolau, Microfluidics structures for probing the dynamic behaviour of filamentous fungi. Microelectron. Eng. 87, 786–789 (2010).
52. J. Wang et al., Detection of size spectrum of microalgae cells in an integrated underwater microfluidic device. J. Exp. Mar. Biol. Ecol. 473, 129–137 (2015).
53. Z. Liu, K. D. Papadopoulos, Unidirectional motility of Escherichia coli in restrictive capillaries. Appl. Environ. Microbiol. 61, 3567–3572 (1995).
54. G. S. Kijanka, I. K. Dimov, R. Burger, J. Ducrée, Real-time monitoring of cell migration, phagocytosis and cell surface receptor dynamics using a novel, live-cell opto microfluidic technique. Anal. Chim. Acta 872, 95–99 (2015).
55. M. Nayak, A. S. Perumal, D. V. Nicolau, F. C. M. J. M. Van Delft, Bacterial motility behaviour in sub-ten micron wide geometries" in 2018 16th IEEE International New Circuits and Systems Conference, R. Izquierdo, A. Miled, Eds. NEWCAS 2018 (Montreal, QC, 2018), pp. 382–384.
56. A. S. Perumal, M. Nayak, V. Tokárová, O. Kašpar, D. V. Nicolau, "Space partitioning and maze solving by bacteria" in Proceedings of the lecture Notes of the Institute for Computer Sciences, Social-Informatics and Telecommunications Engineering, LNICST, A. Compagnoni, W. Casey, Y. Cai, B. Mishra, Eds. (Pittsburgh, PA, 2019), pp. 175–180.
57. A. P. Berke, L. Turner, H. C. Berg, E. Lauga, Hydrodynamic attraction of swimming microorganisms by surfaces. Phys. Rev. Lett. 101, 038102 (2008).
58. E. Lauga, W. R. DiLuzio, G. M. Whitesides, H. A. Stone, Swimming in circles: Motion of bacteria near solid boundaries. Biophys. J. 90, 400–412 (2006).
59. E. P. Ipina, S. Otte, R. Pontier-Bres, D. Czerucka, F. Peruani, Bacteria display optimal transport near surfaces. Nat. Phys. 15, 610–615 (2019).
60. A. S. Utada et al., Vibrio cholerae use pili and flagella synergistically to effect motility switching and conditional surface attachment. Nat. Commun. 5, 4913 (2014).

61. H. Shum, Microswimmer propulsion by two steadily rotating helical flagella. Micromachines (Basel) 10, 65 (2019).
62. K. Bente et al., High-speed motility originates from cooperatively pushing and pulling flagella bundles in bilophotrichous bacteria. eLife 9, e47551 (2020).
63. W. R. DiLuzio et al., Escherichia coli swim on the right-hand side. Nature 435, 1271–1274 (2005).
64. M. Theves, J. Taktikos, V. Zaburdaev, H. Stark, C. Beta, Random walk patterns of a soil bacterium in open and confined environments. EPL 109, 28007 (2015).
65. H. Shum, "Simulations and modelling of bacterial flagellar propulsion," PhD thesis, University of Oxford, Oxford, UK (2011).
66. S. Bianchi, F. Saglimbeni, R. Di Leonardo, Holographic imaging reveals the mechanism of wall entrapment in swimming bacteria. Phys. Rev. X 7, 011010 (2017).
67. P. D. Frymier, R. M. Ford, H. C. Berg, P. T. Cummings, Three-dimensional tracking of motile bacteria near a solid planar surface. Proc. Natl. Acad. Sci. U.S.A. 92, 6195–6199 (1995).
68. N. Figueroa-Morales et al., E. coli "super-contaminates" narrow ducts fostered by broad run-time distribution. Sci. Adv. 6, eaay0155 (2020).
69. J. Männik, R. Driessen, P. Galajda, J. E. Keymer, C. Dekker, Bacterial growth and motility in sub-micron constrictions. Proc. Natl. Acad. Sci. U.S.A. 106, 14861–14866 (2009).
70. P. C. Blainey, The future is now: Single-cell genomics of bacteria and archaea. FEMS Microbiol. Rev. 37, 407–427 (2013).
71. B. M. Paegel, G. F. Joyce, Microfluidic compartmentalized directed evolution. Chem. Biol. 17, 717–724 (2010).
72. P. Galajda, J. Keymer, P. Chaikin, R. Austin, A wall of funnels concentrates swimming bacteria. J. Bacteriol. 189, 8704–8707 (2007).
73. T. V. Phan et al. Bacterial route finding and collective escape in mazes and fractals. Phys. Rev. X 10, 031017 (2020).
74. F. K. Balagaddé, L. You, C. L. Hansen, F. H. Arnold, S. R. Quake, Long-term monitoring of bacteria undergoing programmed population control in a microchemostat. Science 309, 137–140 (2005).
75. H. Massalha, E. Korenblum, S. Malitsky, O. H. Shapiro, A. Aharoni, Live imaging of root-bacteria interactions in a microfluidics setup. Proc. Natl. Acad. Sci. U.S.A. 114, 4549–4554 (2017).

76. M. Held, O. Kašpar, C. Edwards, D. V. Nicolau, Intracellular mechanisms of fungal space searching in microenvironments. Proc. Natl. Acad. Sci. U.S.A. 116, 13543–13552 (2019).
77. L. Potvin-Trottier, S. Luro, J. Paulsson, Microfluidics and single-cell microscopy to study stochastic processes in bacteria. Curr. Opin. Microbiol. 43, 186–192 (2018).
78. S. Martel, Swimming microorganisms acting as nanorobots versus artificial nanorobotic agents: A perspective view from an historical retrospective on the future of medical nanorobotics in the largest known three-dimensional bio-microfluidic networks. Biomicrofluidics 10, 021301 (2016).
79. 79. S. Martel, C. C. Tremblay, S. Ngakeng, G. Langlois, Controlled manipulation and actuation of micro-objects with magnetotactic bacteria. Appl. Phys. Lett. 89, 233904(2006).
80. H. Terashima, S. Kojima, M. Homma, Flagellar motility in bacteria structure and function of flagellar motor. Int. Rev. Cell Mol. Biol. 270, 39–85 (2008).
81. D. Akin et al., Bacteria-mediated delivery of nanoparticles and cargo into cells. Nat. Nanotechnol. 2, 441–449 (2007).
82. S. Martel, Bacterial microsystems and microrobots. Biomed. Microdevices 14, 1033–1045 (2012).
83. B. P. Tracy, S. M. Gaida, E. T. Papoutsakis, Flow cytometry for bacteria: Enabling metabolic engineering, synthetic biology and the elucidation of complex phenotypes. Curr. Opin. Biotechnol. 21, 85–99 (2010).
84. D. Huh, W. Gu, Y. Kamotani, J. B. Grotberg, S. Takayama, Microfluidics for flow cytometric analysis of cells and particles. Physiol. Meas. 26, R73–R98 (2005).
85. J. Oakey et al., Particle focusing in staged inertial microfluidic devices for flow cytometry. Anal. Chem. 82, 3862–3867 (2010).
86. X. Wang, J. Atencia, R. M. Ford, Quantitative analysis of chemotaxis towards toluene by Pseudomonas putida in a convection-free microfluidic device. Biotechnol. Bioeng. 112, 896–904 (2015).
87. J. A. Crooks, M. D. Stilwell, P. M. Oliver, Z. Zhong, D. B. Weibel, Decoding the chemical language of motile bacteria by using high-throughput microfluidic assays. Chem- BioChem 16, 2151–2155 (2015).
88. H. H. Jeong et al., Microfluidic monitoring of Pseudomonas aeruginosa chemotaxis under the continuous chemical gradient. Biosens. Bioelectron. 26, 351–356 (2010).
89. H. Kim, J. Ali, K. Phuyal, S. Park, M. J. Kim, Investigation of bacterial chemotaxis using a simple three-point microfluidic system. Biochip J. 9, 50–58 (2015).

90. O. Sipos, K. Nagy, P. Galajda, Patterns of collective bacterial motion in microfluidic devices. Chem. Biochem. Eng. Q. 28, 233–240 (2014).
91. B. Kaehr, J. B. Shear, High-throughput design of microfluidics based on directed bacterial motility. Lab Chip 9, 2632–2637 (2009).
92. S. Park, D. Kim, R. J. Mitchell, T. Kim, A microfluidic concentrator array for quantitative predation assays of predatory microbes. Lab Chip 11, 2916–2923 (2011).
93. Z. Wu, B. Willing, J. Bjerketorp, J. K. Jansson, K. Hjort, Soft inertial microfluidics for high throughput separation of bacteria from human blood cells. Lab Chip 9, 1193–1199 (2009).
94. D. T. Chiu, E. Pezzoli, H. Wu, A. D. Stroock, G. M. Whitesides, Using three-dimensional microfluidic networks for solving computationally hard problems. Proc. Natl. Acad. Sci. U.S.A. 98, 2961–2966 (2001).
95. D. V. Nicolau Jr et al., Parallel computation with molecular-motor-propelled agents in nanofabricated networks. Proc. Natl. Acad. Sci. U.S.A. 113, 2591–2596 (2016).
96. D. V. Nicolau et al., Molecular motors-based micro- and nano-biocomputation devices. Microelectron. Eng. 83, 1582–1588 (2006).
97. F. C. M. J. M. van Delft et al., Something has to give: Scaling combinatorial computing by biological agents exploring physical networks encoding NP-complete problems. Interface Focus 8, 20180034 (2018).

Chapter 3

3. Navigation through uniform and non-uniform maze

Based on the previous fundamental understanding of the movement of different bacterial species through simple to complex confined geometrics, here our study introduces microfluidic maze networks (uniform /non-uniform) as a valuable tool for studying their efficient strategies for space searching and pathfinding by exploring the maze environment. Furthermore, different performance parameters such as average time required for finding the solutions to the maze, number of vertices explored during the navigation, the success rate for maze solving, and energy expenditure during their navigation were evaluated. These experimental characterizations can be beneficial in development of a practical, straight forward space searching, and partitioning algorithm relevant for real-world applications such as transportation system planning, development of urban transportation, and vehicle routing problem etc.

Navigation through uniform and non-uniform maze

Monalisha Nayak[1], Ayyappasamy Sudalaiyadum Perumal[1], Viola Tokárová[2], Ondej Kašpar[2], Dan V. Nicolau[1*]

[1]*McGill University, Faculty of Engineering, Department of Bioengineering, Montreal, Quebec, H3A 0C3, Canada.*

[2]*University of Chemistry and Technology, Prague, Department of Chemical Engineering, Prague, 166 28, Czech Republic.*

** Correspondence should be addressed: dan.nicolau@mcgill.ca*

Abstract

The microbial environment, where the bacteria inhabit is diverse and highly complex. Bacteria exhibit different patterns of motility for their specific needs to be adopted to such a broad spectrum of habitats. Also, bacterial space searching and partitioning in the highly complex environments such as soil or tissues is relevant in the context of infection and medical applications. Here, we evaluated the space searching efficiency of bacteria of different species and morphology (*Vibrio natriegens*, *Magnetococcus marinus, Pseudomonas putida*, *Vibrio fischeri*, and *Escherichia coli*) through microfluidic maze networks of different complexity. The velocity, average time, distance travelled, and energy expenditure was calculated to access the navigation efficiency of bacteria. First, we presented the ability of bacteria to explore the shortest path, and the ability to explore all possible paths through the maze in the shortest time. We observed that higher velocity is not correlated to the space searching efficiency of bacteria. Second, by varying the geometry of the maze, we also observed that the complex confinements strongly influence the motility near the boundaries, and as well as near the obstacles through the network. Specifically, the bacterial species, which preferred to move along the wall such as *V. natriegens* and *E. coli* presented adequate strategies to navigate through the maze efficiently with lower energy expenditure despite having lower velocity compared to other studied bacterial species. Conversely, *M. marinus* exhibited the highest velocity but was less efficient as they also get strongly affected by the obstacles during the navigation leading to chaotic movement. Precision evaluation of bacterial efficiency for navigating through a complex maze could ultimately be relevant to medical applications such as understanding the spreading of bacteria during the infection and most importantly to bacteria-mediated biocomputational approaches.

3.1. Introduction

Unicellular organisms like bacteria are ubiquitous on earth. Efficient navigation in the microbial habitats (a/biotic) is critical for microbial survival. The microbes need to interact with the physical and chemical environments to perform a myriad of microbial processes like searching for nutrients, space, and conductive spots for propagation [1, 2]. Consequently, bacteria have developed numerous motility strategies; the dynamics of their motility guide them to unfold their ability for decision-making, space partitioning and interactions with their surrounding environments. The decision-making ability allows the bacteria to collect the information from surrounding environments using strategies like chemotaxis and biofilm formation. Understanding bacterial motility on surfaces has been the focus of applied research in the food industry for preventing the fouling effects [3, 4] and in the paper industry to study the effective ness of enzymatic treatment [5]. Thus, substantial research has been devoted to study and model the motility pattern of different bacterial species [6-8]. Both physicists and biologists have also investigated the underlying mechanism behind the mechanics and hydrodynamic forces that drive the motility of bacteria [9-11]. The earlier mentioned study explains the consequence of fluid dynamics that are relevant to the motility of bacteria in viscous environments.

Additionally, the motility of bacteria is actively influenced by its surroundings, which generally restricts their growth in natural habitats. Various studies have explained the interaction of surfaces with a single microorganism [12] and a group of microorganisms (collective behavior) [9] that can be used in technological applications. The advances in the field of microfluidics have made it possible to study the growth and motility pattern of bacteria in narrow confinements [13]; the influence of micron-confined geometry on the flagellar motility which is the most common propulsion system [14, 15], and the effect of solid boundaries on the swimming pattern of bacteria [16]. Also, a quasi-two-dimensional porous medium has been presented to bacterial cells to investigate the changes in its motility pattern [17]. This extensive information about the motility makes the bacteria an attractive model candidate for studying and evaluating their decision-making behavior and path finding/space searching abilities in maze or labyrinths.

Mazes are a class of graphical puzzle that consists of a series of nodes, junctions, and connectors arranged to form a network of interconnected paths. The maze problem with increasing complexity, non-trivial exercise has been placed in the category of non-polynomial time complete (NP-complete) problems [18]. Maze solving is defined as finding a route from the start point to the end point in a geometrical constrained space. This includes finding the best route (shortest) and to trace all possible valid routes with several solutions. The simplest maze problems involve determining the shortest distance from the entrance to the exit and can be solved by digital computation in polynomial time

[19]. Solving the maze problem with increasing complexity that incorporates non-linear behavior can be very challenging if at all by computational algorithm. There are several different maze solving algorithms starting from random mouse algorithm to mathematical search algorithms, which operate sequentially to find the correct solution. The "wall follower" algorithm is the simplest and the best-known algorithm that follows the wall to find a solution to mazes, but it is not the most efficient for achieving multiple solutions in parallel. Other mathematical algorithms for maze solving and path planning are Dijkstra's algorithm, which is used to find the shortest routes by connecting the nodes. A* (A star) search algorithm [20], uses graph traversal and pathfinding processes for computer games and rapidly exploring random tree algorithm that was designed for complex environments to find optimal solutions [21]. However, these methods are limited because of the slow computation time with the complexity of the maze network as the solution time increases dramatically with the increasing complexity [22]. In those circumstances, the digital computation can be insufficient and inaccurate.

As a non-conventional approach, various chemical and biological systems have been explored by researchers to solve the maze problems like by the use of chemical waves [23], tube morphogenesis in an amoeboid organism [24] tracing the path of plasma [25] as well as different organisms like ants [26], bees [27], rats [28], octopi [29, 30], humans [31], robots [32, 33], rat cyborgs [32], crabs [34] and simple organisms like amoeba [35], slime mold and fungi [36-38]. Nonetheless, all these above-mentioned methods are partially inefficient. For example, propagations of chemical waves were very slow and were difficult to visualize. Also, these methods were not suitable for larger mazes with complex connectivity. Reconfiguration of slime mold occurred between two food sources within the maze network allowed them to explore only the shortest path. Tube morphogenesis is complex and has been experimented only for very simple mazes. Hanson et al, investigated the growth of filamentous fungi, which used long term directional memory and collision-induced branching for space searching in a micro confined maze network. This reported methodology showed potential for efficient and complex natural algorithms for space searching and space partitioning. However, those studies became inefficient for the exploration of simultaneous maze solving problems such as finding possible solutions to complex maze (NP-complete problems). Other successful approaches have also been presented based on classical chemotaxis, which makes the navigation/exploration biased [33, 36, 39]. This approach hinders the bacterial innate space searching capabilities. Here, we suggest and demonstrate different bacterial species for solving mazes based on massively parallel computation without any external cues but the geometry of the maze itself. Importantly, optimal pathfinding, which is one of the primary functions of the intelligent transportation systems has many applications in transportation problems, such as, efficient pathfinding over large-scale road networks

will slow down the traffic jam in the shortest path. Previous studies regarding maze solving have only targeted to determine the shortest route [38] or the most efficient route where there is a greater number of possible valid routes to the network. Therefore, the proposed approach of introducing the bacterial candidates in the maze network without any external cue is to explore all possible efficient paths along with the shortest path. So, the study is essentially different from earlier studies, which was entirely focused on finding the shortest path. The navigation of bacteria through complex geometrics is a synergistic effect of confined geometrics along with its motility pattern. Here our study introduces microfluidic maze networks (uniform /non-uniform) as a valuable tool for behavioral preferences and demonstrates the surprising ability of different bacterial species namely *E. coli*, *V. natriegens*, *M. marinus*, *P. putida*, *V. fischeri* (different motility characteristics, and different flagellar arrangements) for exploring the maze environment as individual navigators. Furthermore, different performance parameters such as average time required for finding the solutions to the maze, number of vertices explored during the navigation, the success rate for maze solving to compare the efficiency between the bacterial candidates and energy expenditure during their navigation has been evaluated. Those experimental characterizations can allow a practical, straight forward space searching, and partitioning algorithm towards the analysis of more complex geometrics relevant for real-world applications.

The paper is organized as follows; We start by describing the overall motility pattern of proposed bacterial species during their navigation through maze networks of different complexity. We then perform a detailed estimation of different performance parameters to classify the bacterial species based on the efficient navigation.

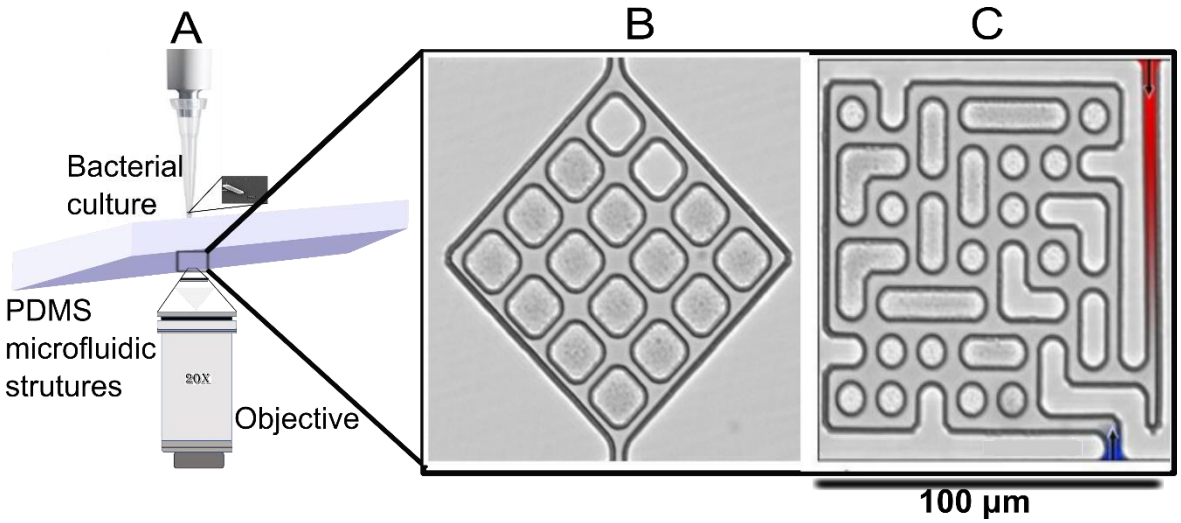

Figure 9. Experimental setup for bacterial navigation through microfluidic mazes B and C. PDMS microfluidic structures Uniform and Non-uniform strutures respectively.

3.2. Materials and Methods

Design and fabrication of the microfluidics networks. The overall design of the microfluidics chip (Figure 9B, C), used to probe various motility characteristics of bacteria, comprises parallel reservoirs with a width of 2 mm, connected through 1 mm-wide patterned areas (Figure 9B, C). All patterned areas are separated by the open spaces 'plazas' of 100 µm x 100 µm. The study of specific parameters of the bacterial motility required specific designs of the microfluidic structures, as follows: a 'diamond' structure: uniform maze (Figure 9B), presenting 45° and 90° angles, with a channel size with a width of 3 µm and a length of its edge of 12 µm designed to explore the bias for right-, or left-hand turns; and a complex maze structure: Non-uniform maze (Figure 9C) to observe the overall moving patterns in complex, randomly distributed geometrical obstacles with internal channels of 3 µm. The microfluidic chip devices were made by polydimethyl-siloxane (PDMS) through the replication process of a positive-relief silicon master, fabricated by standard photolithography [40, 41]. The mixture of PDMS and cross-linker in a weight ratio 10:1 was poured onto the silicon master, degassed inside the vacuum chamber to remove air bubbles, and cured at 65°C overnight to ensure full cross-linking. After cutting and peeling off, the PDMS replica was treated with air plasma for 30 seconds to render the surface hydrophilic before irreversibly bonding it onto the glass coverslip, also plasma-activated for 30 seconds.

Bacterial selection. Five bacterial species were selected for the study. *M. marinus*, *P. putida,* and *V. fischeri*, have similar lophotrichous morphology, i.e., they have multiple flagella at one end of the body. *E. coli* MG1665 (K12 wild type) is a rod-shaped bacterium with a peritrichous flagellar architecture. *V. natriegens* is a rod shaped, polar uniflagellated bacterium. *M. marinus* (MC-1) is a

marine bacterium with a spherical (‘coccus’) body of 1-2 μm in diameter and an average swimming speed of 110 μm·s-1 (maximum speed can exceed 200 μm. s^{-1}) [42]. As *M. marinus* is a microaerophilic bacterium, it prefers environments containing lower concentrations of O2, it is cultured in a chemo hetero lithotrophic medium at room temperature [43]. *E. coli* and *V. natriegens* were genetically transformed with a plasmid mCherry for visualization and tracking during the motility experiments. *E. coli* and *V. natriegens* were transformed to constitutively express the plasmid pMF440. The plasmids express mCherry, a red fluorescent protein in bacteria to visualize them in our experiments using fluorescence microscopy techniques. *P. putida* and *V. fischeri* were cultivated at room temperature in LB medium.

Motility experiments. While the PDMS surface was still hydrophilic, the microfluidics chip, comprising the PDMS stamp attached on the coverslip, was put in contact with the buffer/medium (LB medium in the case of *P. putida* and *V. fischeri*, *E. coli* and *V. natriegens*, and PBS buffer for *M. marinus*) for 1 hour to pre-wet all the channels in the structure; and then stored inside a wet chamber at 4°C before use. Prior to experiments, a bacterial suspension was introduced into the microfluidics chamber through the open ends of the PDMS stamps and let stay in contact for five minutes, to allow bacteria to enter the chip (Figure 9B, C). To ensure that the natural motility is the only mechanism at play, bacterial cells were let to randomly swim into the chips, without any guidance from external stimuli, or from a concentration gradient of the nutrients.

Image Acquisition and Analysis. For the image acquisition of *M. marinus* strain an inverted Zeiss AxioImager Z1m microscope with AxioVision Software Sonny HD-1000 camera (with VirtualDub 1.10.4 software), LD Epiplan 20x (NA 0.4) and N-Achroplan 10x (NA 0.25) objectives were used. The dark field imaging system was built to enhance the contrast between bacterial cell and surrounding structures, which is necessary for further image analysis of fast swimming bacteria such as *M. marinus*. On the other hand, the experiments with *P. putida* and *V. fischeri*, *E. coli* and *V. natriegens* were performed on an inverted - Spinning Disk Confocal Olympus IX83 microscope, with MetaMorph® (from Molecular Devices) Microscopy Automation & Image Analysis Software, and 10x (NA 0.4), 20x (NA 0.75) and 40x (NA 0.95) Differential Interference Contrast (DIC) objectives.

ImageJ 1.50a [44], a public domain software, has been used for image analysis, density map reconstructions, and time-resolved bacteria tracking. The density maps of bacterial movement inside confined structures were prepared from original RGB image stack as follows: (i) a median of 8-bit image stack (a background) was created using a ‘Z Project’ function; (ii) a new stack was created as a difference between the original stack and the background; (iii) the histogram of a new stack was adjusted and converted to a binary image; (iv) the binary operations ‘Close’ and ‘Dilate’ were applied

to remove the remaining noise; and (v) all binary images were added into one image, and a suitable 'Look Up Table' (LUT) was chosen. In some cases, the density map created by the above-mentioned procedure was accompanied by a high level of noise at the proximity of microfluidic channels, due to the non-uniform light conditions in the optically transparent PDMS chip. In such cases, the original stack of n-images was duplicated in the range of 1 to n-1 and 2 to n. However, the difference |Img2 - Img1| between stacks shifted by one frame highlighted the bacterial movement without background and light-related noise. The fact that this difference was used to calculate the absolute change between two images is important since bacteria have also free movement along the vertical z-axis, in and out of the focal plane, in the range limited by the depth of PDMS structures. The new image stack was processed by steps (iii)-(v) described above to create density map.

The trajectories of single bacterium cells were tracked by the automatic (TrackMate, ImageJ), and the manual (MTrackJ, ImageJ) plugins [45]. The TrackMate plugin, using LAP tracker algorithm, was used for *M. marinus*, which exhibits a quasi-linear motion behaviour, with a low deflection rate. The settings for this 2-parameter tracker were chosen to reach the maximum distance between the two consecutive points of one trajectory, at a given time, with a time gap set to 3 frames. To analyse the movement of these species the manual MTrackJ plugin, with a dark/white centroid snap feature, was employed with a point-and-click tracking. In all cases, the acquired x-y-time coordinates were used for calculating the velocity from single bacterial trajectories.

3.3. Results

3.3.1 Navigation through uniform maze

The navigation efficiency for all bacterial species was accessed by presenting them with a microfluidic uniform maze. The uniform maze is a simple, symmetric, diamond-shaped maze. The network has two types of routes from entry to exits, for instance, the outer boundary channel and the inner grid (the distance between two channels is 12μm and the channel width is 3μm) channels through a zigzagged path (Figure 9B). Because of the symmetrical nature, the shortest path (100 μm) is equivalent irrespective of the route the bacteria take (provided that bacterial species do not revisit the vertices of any route).

3.3.1.1 Overall motility pattern

The density map, which was created by the summation of individual bacterial trajectories through the network contributed towards the qualitative information. The boundaries of the network (Figure 10A) were explored densely by *M. marinus* for finding the valid routes towards the exit. Most of the

bacteria preferred to swim towards the right or left side of the network but the grids or inner channels. The density maps for the *V. natriegens*, and *E. coli* presented the highest propensity of bacterial trajectories along the walls of the network. (Figure 10A). The frequency of the bacterial trajectories in the inner channels of the network was not very evident, however *E. coli* exhibited a more even distribution of trajectories compared to *V. natriegens*. Another significant observation that was observed that the corners of the network were appeared to be denser with the trajectories of *V. natriegens*, and *E. coli* (Figure 10A). As suggested by the density maps, *P. putida* and *V. fischeri* showed high local densities in the boundary of the network and a smaller uniform density through the inner network channels like *V. natriegens*, and *E. coli*.

Individual trajectory analysis. To study the modulations in different performance parameters, the individual bacterial trajectories were evaluated thoroughly. Figure 10B presents a few of the successful representative bacterial trajectories in the network to substantiate the information conferred from the density maps. Around 30 individual trajectories were analyzed for 4 individual sets of experiments to calculate the average distance travelled to find a successful path from entry to exit. The average swimming velocity for *V. natriegens*, and *E. coli* was calculated to be 12±5 and 8±2 μm·s-1 respectively. To explore the successful route inside the network, the average distance travelled by *V. natriegens*, and *E. coli* were 130±30 μm and 144±45 μm (n=4) respectively. The average distance traveled by *M. marinus* was calculated to be 267±38 μm (n=4) with an average swimming velocity 69±19 μm·s-1. *P. putida* and *V. fischeri* swam slowly compared to *M. marinus* with a mean velocity around 30±12 and 15±6 μm·s-1, respectively. The average distance traveled by *P. putida* was 120±20 μm and 140±30 μm by *V. fischeri*. Furthermore, the distribution of the vertices (nodes) of the maze for a complete trajectory was calculated in each set of experiments. The distribution was presented statistically in Figure 10C. The complete trajectories for *V. natriegens* connected around 8 to 25 vertices. Most of the trajectories were found to be connected by 8 vertices which is the minimum number of vertices for a complete trajectory. We also observed few longest trajectories (vertices explored around 20) and the probability of longest trajectories was found to be around ~10 according to our analysis. The distribution of vertices in the case of *M. marinus* was between 8 to 30. Most of the trajectories traversed the minimum number (~8) of the vertices. *P. putida* and *V. fischeri* behaved like *E. coli* and explored the vertices distributed between 8 to 25 (n= 30 trajectories). *V. fischeri* could traverse a larger number of vertices (~25) as well.

3.3.1.2 Ability to find the shortest route

Success rate. Applications of maze solving through the shortest route include intelligent traffic control that benefits ambulances, firefighters, or rescuing robots to find accurately their shortest path to their destination [46]. Despite the simplicity, the bacterial species did explore the network differently. We first calculated the overall success rate, which was calculated as the number of trajectories that contributed to the shortest route, divided by the number of all successful trajectories in the network. The motility behavior of *V. natriegens* and *E. coli* in the network, which helped to find the shortest route resulted in high success rates which was calculated to be 95% (SD ±2%) and 90% (SD ±5%) respectively. The probability of finding the shortest paths in the case of *M. marinus* was evaluated to be 70% (SD ±7%). The success rate presented by *P. putida* and *V. fischeri* was calculated to be 80% (SD ±5%) and 75% (SD ±6%) respectively (Figure 10A).

Time and distance. Aside from analyzing the velocity and vertices with the success rate, we also calculated the time required to find the shortest route in the network. The average time spent in the network to find the shortest route for *E. coli* was estimated to be 16s (n=4) and 10s. (n=4) for *V. natriegens*. *M. marinus* spent around 5 s (n=4) to find the shortest route. *P. putida*, spent around 15 s and *V. fischeri* took around 8s to explore the shortest route in the network (Figure 10A)

Our further investigation was to determine the number of vertices traveled /unit time to comprehend the efficiency in finding the distinct routes for all studied bacterial species. The average number of vertices traveled during the successful pathfinding process was correlated with the swimming speed to calculate the number of vertices per unit time. *V. natriegens* and *E. coli* traveled a greater number of vertices/unit time (second) followed by. *V. fischeri* and *P. putida*. *M. marinus*, having the highest velocity traversed a lesser number of vertices per unit time compared to other bacterial species (Figure 12A).

Energy expenditure. We extended our analysis by calculating the energy expenditure by the bacterial cells during the navigation. These bacteria swim by means of flagella, which are rotated by a nanoscale motor embedded in the cell membrane. The rotation of the flagellar motor is energized by protons moving down the transmembrane gradient [47]. The energy expenditure was evaluated by multiplying the proton consumption rate, the power consumption for protons needed for rotation, and the number of flagella involved for the motility [47]. *V. natriegens* was found to spend less energy, hence presenting them as a more efficient candidate in exploring the shortest route (Figure 12A) followed by *E. coli*. The energy expenditure for *V. natriegens* was calculated to be 2 x 10^{-15} J and for *E. coli* was 1.4e x 10^{-14} J. Other bacterial species like *V. fischeri* and *P. putida* spent more energy compared to the earlier which was calculated to be 1 x 10^{-15} J and 1.2 x 10^{-14} J respectively. *M. marinus* spent more energy, which was calculated to be 2.8 x 10^{-14} J. (Figure 12A).

3.3.1.3 Ability to find all possible routes

Success rate. The success rate in finding the possible valid paths presented by *V. natriegens* and *E. coli* was evaluated to be 70% (SD ±5%) and 80% (SD ±5%) respectively. The success rate for *M. marinus* that presented the highest swimming velocity, was calculated to be 69% (SD ±8). *V. fischeri* and *P. putida* presented a lower success rate compared to other studied bacterial species and that was estimated to be 60 % (SD ±5%) and 50% (SD ±6%) respectively.

Time and Distance. The average time spent in the network to explore all possible valid routes was calculated for all bacterial species. The average time spent by *E. coli* and *V. natriegens* was calculated to be 16s and 10s respectively. *V. fischeri* and *P. putida* spent 15s and 8s respectively to explore the successful routes through the network. The average time spent by *M. marinus* was calculated to be 4s. (Figure 13A). The average number of vertices traversed during the navigation process was calculated along with the number of unique vertices explored (traveled only once). We observed that *V. natriegens* and *E. coli* traveled a greater number of vertices per unit time and explored a greater number of unique vertices, which means they were able to explore the unique junctions for any valid routes efficiently. The pathfinding mechanism has also been studied extensively for large-scale road networks [48], where connecting different locations to find an efficient path is important. *M. marinus*, spent less time in the network to explore the valid routes because of the highest swimming speed, however explored a smaller number of vertices per unit time. *V. fischeri* and *P. putida* also explored a smaller number of vertices/unit time, compared to *V. natriegens* and *E. coli*. However, *V. fischeri* was found to be efficient in finding the unique vertices like *V. natriegens* and *E. coli*. (Figure 13A). The average time and swimming speed were correlated with a number of vertices explored to investigate the efficiency in navigation. These counts of vertices suggest that these behavioral traits can afford advantages in exploring more routes per time during the pathfinding process.

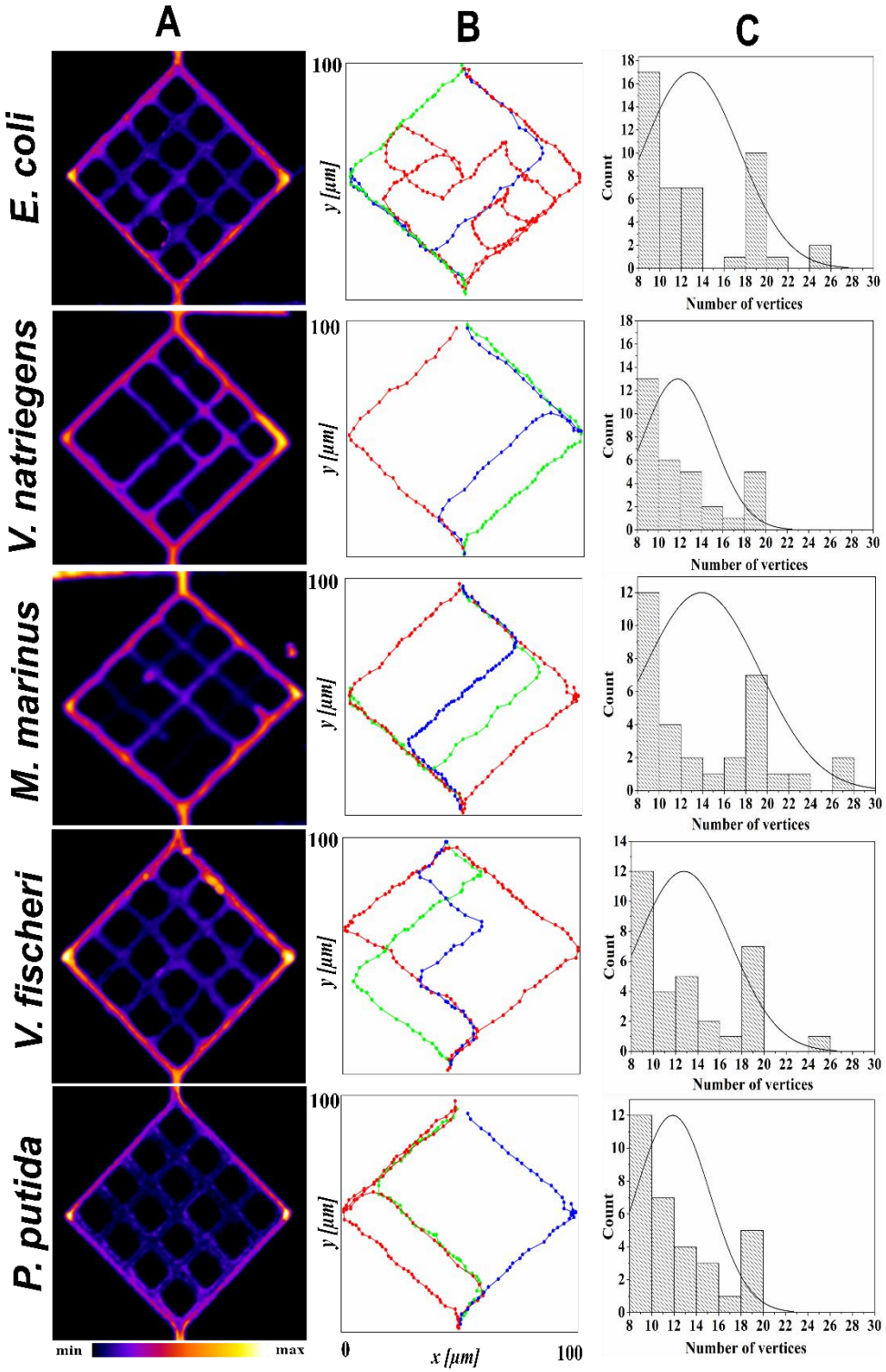

Figure 10. A. Density maps of movement for five bacterial strains through diamond like structure (uniform-MAZE), B. Few of the representative successful trajectories, that correspond to the bacteria movement through the structure, C. Probability of number of vertices traveled to complete a trajectory and their distribution in an individual experiment.

3.3.2 Navigation through non-uniform maze

Following the experiments with the uniform maze, we used a random non uniform maze to find out how the absence of regularity of the previously studied geometrics affects the motility pattern for studied bacterial species. This complex maze presented to bacterial candidates consists of geometries like circular pillars, corners and, barriers with multiple possible solutions along with one possible shortest route.

3.3.2.1 Overall motility pattern

Similarly, to the study in the uniform network, the density maps for the non-uniform maze network presented the information qualitatively at the first step. The density maps (Figure 11A) for *V. natriegens* and *E. coli* presented a stronger local density towards the corners and walls and the motility behavior correlates well with our previous observation for the uniform maze. *M. marinus* exhibited the strongest propensity to navigate through the centre of the network as the high-density clusters observed in the central and the upper-left corner of the maze. The qualitative observation for *P. putida* and *V. fischeri*, as suggested by the density maps (Figure 11A) offered information regarding the higher frequency of trajectories along the walls of the network. This observation was substantiated by a few representative individual successful trajectories (Figure 11B).

Individual trajectory analysis. The individual successful trajectories were evaluated to extract the information regarding the average swimming velocity along with the average time taken to find a successful route. *V. natriegens* and *E. coli* travelled around 268 ± 199 μm and 651± 450 μm respectively. The average swimming velocity presented by *V. natriegens* was 8 ±3 μm·s-1 and by *E. coli* 5±2 μm·s-1. The average distance traversed by the *M. marinus* is 1495 ± 1197 μm with an average swimming speed of 67±18 μm·s-1, which is 3.6x more than the distance made by *P. putida* (410 ± 243 μm) and 3.1x more when compared to the *V. fischeri* (477 ± 340 μm). While trying to find a way out of the maze, the distribution of each vertex of the maze in a single successful trajectory was estimated and compared between the bacterial species. The statistical analysis regarding the distribution of the average number of the vertices traveled to complete a successful trajectory shows apparent changes like skewed distribution in between studied bacterial species (Figure 11C). The distribution is skewed considerably towards a greater number of vertices count in the case of *M. marinus*. The distribution of the number of vertices in an individual experiment for *M. marinus* lies between 20 to 120.*V. natriegens* and *E. coli* presented the distribution towards a lesser number of average vertices compared to *M. marinus*. The majority of the successful trajectories included 20 to 60 vertices, and a few explored only 80 to 100. The distribution of the number of vertices for *P. putida* and *V. fischeri* was calculated between 20 to 100.

3.3.2.2 Ability to find the shortest route

To extend our understanding of the ability of the studied bacterial species to find the shortest path through the complex maze network, individual trajectories were thoroughly evaluated. We observed a significant difference in motility pattern with the increasing irregularity in the geometry. By analysing statistically, *E. coli*, and *V. natriegens* followed the shortest path to a lower extent but more efficiently than the other studied bacterial species. Success rate: *M. marinus* exhibited minimum possibilities of exploring the shortest route in the maze. *P. putida* and to a lesser extent *V. fischeri* appears to be less efficient in finding the shortest route as well. The probability of finding the shortest route in the presented network was found to be 15% (SD ±4%) and 13% (SD± 5%) for *V. natriegens* and *E. coli* respectively. The calculated success rate for *P. putida* and *V. fischeri* was found to be 2% (SD ±0.005%) and 7% (SD±0.1%).

Time. The average time calculated for finding the shortest route for *E. coli* was 18 s and *V. natriegens* was 16s. *V. fischeri* spent 10s to explore the shortest route and *P. putida* spent 8s for navigating through the shortest route in the network. Further the average time and swimming speed was correlated with number of vertices explored to investigate the efficiency in pathfinding process.

Vertices. We expanded the previous information regarding the traveled distance with the number of vertices traversed (in one complete trajectory) per unit time. These counts of vertices suggest that these behavioral traits can afford advantages in exploring more routes per time during the pathfinding process. *V. natriegens* traveled a greater number of vertices per second and it correlates well with the uniform maze. Strikingly these cells not only migrate through uniform maze remarkably to find the shortest path but also continued to be successful for finding the shortest route with increasing irregularity in the geometry. As can be seen (Figure 10 B), *E. coli* presented a significant number of vertices per second followed by *V. natriegens*. *V. fischeri* and *P. putida* presented a considerably lower number of vertices per unit time despite being the fastest candidates. (Figure 12 B).

Energy expenditure. Another performance parameter, that needed to be taken care of was the energy expenditure by the individual candidates. Here we observed that the energy expenditure achieved good agreement with the success rate. *V. natriegens* spent a lesser amount of energy that was calculated to be 3×10^{-14} J. The energy expenditure by *E. coli* was calculated to be 2.5×10^{-13} J. The average amount of energy spent by *V. fischeri*, and *P. putida* was calculated to be 1×10^{-13} J and 8.4×10^{-14} J. (Figure 10 B).

3.3.2.3 Ability to find all possible valid routes

All possible valid/unique routes to the maze network need to be analysed for important real-world applications. In our study, the studied bacterial species explored all possible valid solutions parallelly.

Success rate. The success rate for exploring the possible routes was calculated to be 50% (SD±8%) and 45% (SD±5%) for *E. coli*, and *V. natriegens* respectively. *M. marinus* presented a higher success rate among all the bacterial candidates that was calculated to be 55% (SD±7%). *P. putida* and *V. fischeri* were not able to succeed in exploring the path efficiently like the earlier candidates and presented as the success rate as 30% (SD±8%) and 40% (SD±7%) respectively (Figure 11B).

Time. We calculated the average time spent by each bacterial species and we observed that *E. coli*, and *V. natriegens* spent 96s and 58 s respectively to find the successful routes. The average time spent in the network by *M. marinus* was calculated to be 25s. The average calculated for *V. fischeri* was 41s and for *P. putida* was 21s.

Vertices. Also, the vertices traversed during the successful pathfinding process was calculated for all studied bacterial species. *E. coli*, and *V. natriegens* traversed though 6 and 11 vertices respectively per second. The frequency of exploring unique vertices were more for *E. coli*, and V. *natriegens. M. marinus* with the highest swimming speed travelled more distance but were able to explore only 1.5 vertices per second. It traveled more distance but were not able to explore the unique vertices for individual trajectories (Figure 13B), which was calculated to be 9%. They traveled the same vertices repetitively. *V. fischeri* was able to traverse through 2.5 vertices per second and the ability of exploring the unique vertices were also less compared to *E. coli*, and *V. natriegens*. The exploratory behavior for *P. putida* was very much like *V. fischeri* and they were able to traverse through 2 vertices per second.

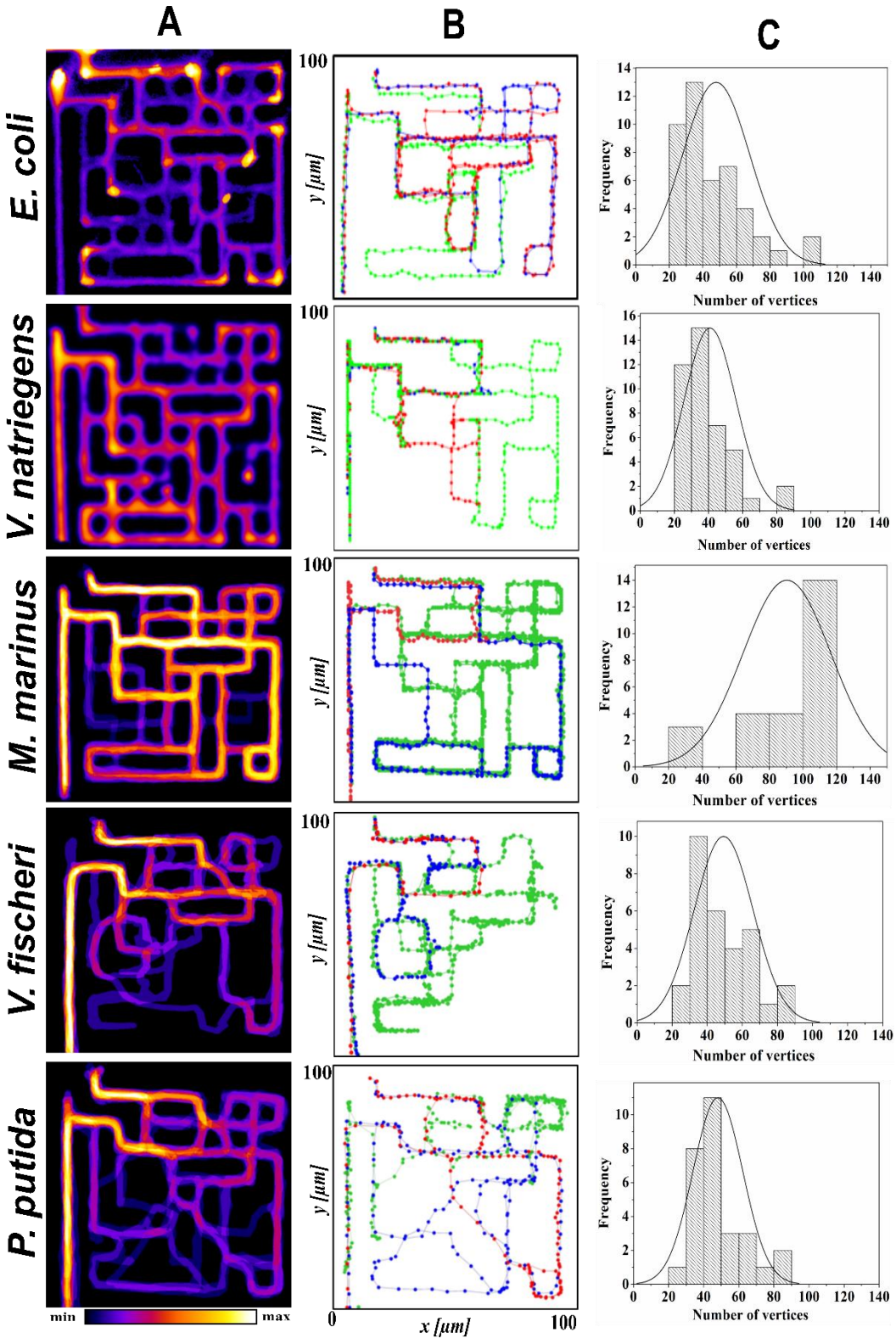

Figure 11. Bacterial Motility in non-uniform maze A. Density maps of movement for five bacterial strains through nonuniform-maze, B. Few of the representative successful trajectories, that correspond to the bacteria movement through the structure, C. Probability of number of vertices traveled to complete a trajectory and their distribution in an individual experiment.

Energy expenditure. Finding all possible valid solutions to a maze is an energy intensive process. Calculating the energy to investigate their efficiency during the energy efficient autonomous navigation inside the maze network is one of the crucial steps. *V. natriegens* spent a lesser amount of energy as observed earlier that was calculated to be 1.1 x 10^{-13} J. The amount of energy spent by *E. coli* was calculated to be 1.3 x 10^{-12} J. *M. marinus* spent more amount of energy that was determined to be 6.5 x 10^{-13} J. The energy expenditure for *V. fischeri* and *P. putida* was calculated to be 5.7 x 10^{-13} J and 1.4 x 10^{-13} J.

3.4 Discussion

Efficiency in exploring the shortest path. Finding the shortest path in a maze network is a classical problem, which is relevant to the fields such as the development of urban transportation [49], traffic engineering research, gaming optimization, and increasing the efficiency of board game creation [50]. Due to its wide applications for many practical problems, many researchers have developed hundreds of algorithms, silicon computing architectures and unconventional computation approaches to deal with this problem. Concerning more efficient computation, unconventional approaches have been demonstrated to compute the shortest path in a maze network. Previous studies presented neutrophil cells [51] and T cells [52], which navigated through the maze without any chemoattractant gradient, slime mold [38] *P. polycephalum*, which formed the biological network inside the maze by distributing its biomass, and nematodes, [53] which located the shortest route utilizing chemotaxis. However, there are still challenges in previously mentioned methods, such as the slime mold can build robust networks inside the maze but how the networks are formed are not clearly understood and do not seem to be suitable for complex mazes. The challenges arise with the complexity of the network and the unavailability of previous knowledge about the destination in the network. For instance, autonomous robots were unsuccessful in navigation after encountering any loop or obstacle in the network [54].

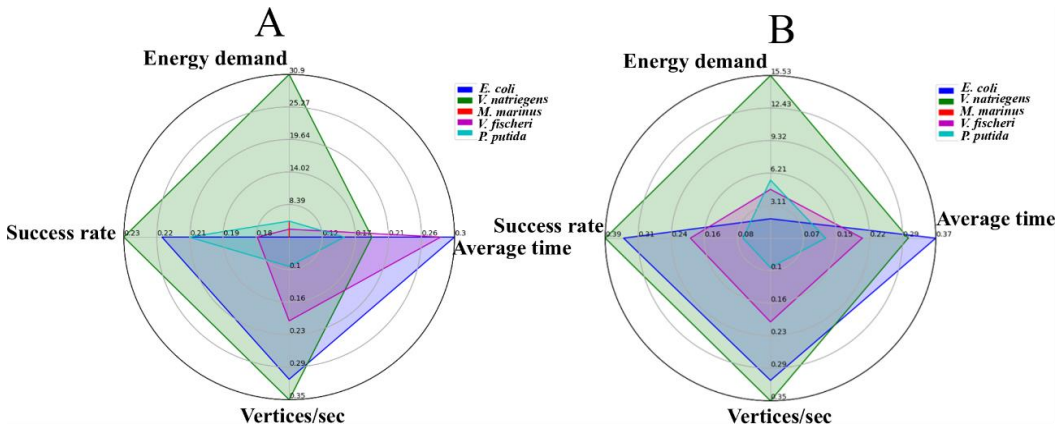

Figure 12. Comparison between multiple parameters (exploring the shortest path). Radar chart A. (Uniform maze), B. (Non-uniform maze) shows how the studied bacterial candidate behaves for different parameters like success rate, average time, energy demand, vertices travelled once and vertices travelled/sec. For each parameter larger area of the polygon represents a better candidate for solving the maze.

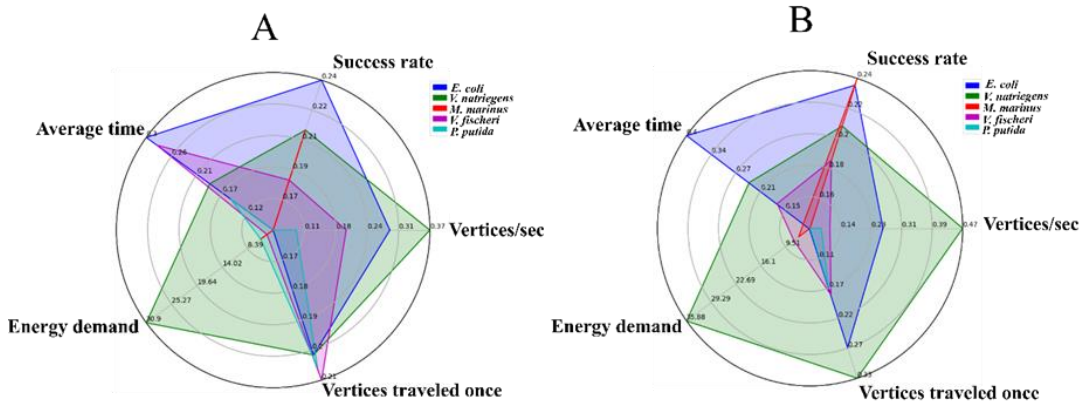

Figure 13. Comparison between multiple parameters (exploring all possible paths). Radar chart A. (Uniform maze), B. (Non-uniform maze) shows how the studied bacterial candidate behaves for different parameters like success rate, average time, energy demand, vertices travelled once and vertices travelled/sec. For each parameter larger area of the polygon represents a better candidate for solving the maze

Bacteria-based maze solving. The ability of bacteria to navigate through maze was demonstrated by many researchers. Nevertheless, previous experiments have typically been limited to the chemotaxis, where the intracellular biochemical noise significantly affects bacterial motility [55, 56]. Our result accessed the effect of the complex geometries on the random motility of bacteria without any external guidance. In the context of geometry of the network, Weber et al [57] studied the bacterial diffusion through a squared lattice maze and analyzed how the obstacles through the channels guided the swimming direction of bacteria. Here, we evaluated the motility pattern of different bacterial species through the maze network and the effect of micro confined geometries on the efficient navigation. We found that *V. natriegens* and *E. coli*, which moved parallel to the wall presented the highest success rate in exploring the shortest route in the mazes of different complexity. (Figure 12A & 12B). *M. marinus*, presented the highest velocity compared to other studied bacterial species in the networks but stands as an inefficient species for finding the shortest route. *P. putida* and *V. fischeri* explored the shortest route by some means, however, they presented a lower success rate compared to *V. natriegens* and *E. coli*. The complexity of the maze network holds a huge amount of effect on the bacterial ability for finding the shortest route. Even though *M. marinus* were able to find the shortest route through uniform mazes fairly, exhibit minimum possibilities with the non-uniform maze. One possible explanation for this observation is the chances of physical collision with the corners and walls with increasing complexity, which hindered the efficient navigation. These observations corelates well with our previous study [58], where we discussed about the species-specific motility pattern in micro-confinements such as hydrodynamic drag through the open spaces and steric interactions through the tight confinements. *P. putida* and *V. fischeri* also failed to efficiently explore the shortest route with increasing complexity. It must be noted that, the tight confinement with multiple junctions (angled junctions) limits the bacterial motility. The recurrence of U-turns for *P. putida* and *V. fischeri* through the linear channels were reported before, which also lower the efficient navigation. However, *V. natriegens* ranked first in the efficient exploration of the shortest route despite the lower swimming speed.

Exploring the shortest path in shortest time. To solve the shortest path problems in the shortest time, various methods have been reported earlier like the use of glow discharge [25, 59], thermal visualization of the path [60], and pathfinding using crystallization [61]. These above-mentioned methods trace the shortest path in a matter of milliseconds or seconds. Other methods that employ conductive particles [62], dyes [63] droplets [64, 65], and waves [66] find the optimal paths in minutes. Living organisms like slime mold [38], and epithelial cells [67] demand hours to days to trace the path. In the results presented here, all studied bacterial species explored the shortest route in a few seconds. *M. marinus* having the highest swimming speed explored the shortest route in the

uniform maze network in 5s followed by *V. fischeri*, which took around 8s to navigate through the shortest route. The average time spent to find the shortest route in the non-uniform maze for *V. fischeri* was found to be 10s. *V. natriegens* having the lowest swimming speed compared to earlier spent 10s in the uniform maze and 16s in the non-uniform maze network. *E. coli took* 16s to navigate through the shortest route in the uniform maze and 18s for the non-uniform maze. (Figure 12A & 12B)

Exploring unique vertices. One of the key features in the pathfinding process is the ability to get a target location while traversing through the environment without any redundant move. When traversing the maze to find the shortest route, *V. natriegens* and *E. coli* traveled a larger number of vertices per unit time with lower swimming velocity through the uniform maze network. The ability of *V. natriegens* and *E. coli* remain unaffected with increasing irregularities in the network. *V. fischeri* traversed a fair number of vertices per second during exploring the shortest path. The individual trajectories implied chaotic like movement for *M. marinus* and consequently, they visited the same vertices multiple times. So, they are less efficient at navigating through mazes with higher complexity. *M. marinus* and *P. putida* explored a lesser number of vertices per unit time despite having higher swimming speed. (Figure 12A & 12B) Energy efficient bacterium Calculating the energy to investigate the bacterial efficiency during the energy-efficient autonomous navigation inside the maze network is one of the crucial steps. When the *P. polycephalum* model was demonstrated to compute the shortest path problem, it needed a substantial number of iterations. Having demonstrated that, we aimed to present the most efficient bacterial species when dealing with the maze solving problem. We calculated the energy expenditure during the navigation through the shortest route and we observed that *V. natriegens* spent a lesser amount of energy followed by *E. coli*. The motility behavior of *M. marinus* was observed random and redundant along the same path and the energy expenditure was more making it less efficient compared with other studied bacterial species.

Efficiency in exploring all possible routes. While the scientific potential of the race to learn about the shortest path in a maze network is a goal, all possible valid/unique routes to the maze network needs to be analysed for important real-world applications. In the context of the computer game industry, [68] exploring unique paths is a crucial task. Navigating through a city to find new and simple paths is always a challenge. Generally, maze solving through graph theory, which is demonstrated for the pathfinding algorithms is more superior, accurate, and efficient. Meanwhile, most studies investigated the navigation through the maze network for finding the shortest path only. For the first time our study presents the bacteria-based computational approach to compute all the possible paths through the maze network along with the shortest path. The success rates for finding

the multiple routes were calculated and that described the ability of studied bacterial species to perform efficient navigation. *V. natriegens* and *E. coli* presented a higher success rate compared to all studied bacterial species through the uniform network. This can be explained as the preference of the bacterial species to move along the wall and preference to exit at 90° angles (at each junction). However, *M. marinus* was able to explore a greater number of possible paths with overall success rate 55% (SD±7%) with increasing complexity. Nevertheless, the success rate for all bacterial species in the non-uniform maze is comparable. (Figure 13A and 13B)

Exploring the unique vertices. In addition to the success rate, the average swimming velocity, travel time, and the traversed vertices were also compared between the bacterial species to classify them according to the efficient navigation. *M. marinus* spent the lowest amount of time because of the highest swimming velocity to explore multiple routes through maze networks of different complexity followed by *V. fischeri* and *P. putida*. *V. natriegens* and *E. coli* took higher amount of time compared to earlier and presented the lowest swimming velocity. However, the efficient navigation was realized to be independent of higher swimming velocity and the time required to trace any correct solution through the network. Traveling unique vertices in the maze and connecting them to find the path may provide advantages for route planning road networks [48]. *V. natriegens* and *E. coli* were found to be more efficient in traversing unique vertices through the uniform maze as well as the non-uniform maze (Figure 13A and 13B). *M. marinus* being in the wall escaper category showed redundant movement and was unsuccessful in finding the unique paths. The unique vertices traversed by *P. putida* was also not significant. Furthermore, *V. fischeri* was efficient in finding the unique vertices alike *V. natriegens* and *E. coli*. With respect to number of vertices explored per unit time (second), *V. natriegens* and *E. coli* presented a larger number of vertices irrespective of the network complexity (Figure 13A and 13B).

3.5 Conclusion

Our findings provide a description of how bacteria navigate the maze to explore the shortest path, and all possible valid paths. The performance parameters were evaluated with increasing variability to understand the strategy of bacteria to efficiently explore the maze network. Most notably, the modulations in the motility patterns of the bacteria with different flagellar arrangements may be critical for evaluating the efficiency for space partitioning. *V. natriegens* and *E. coli* presented efficient space partitioning strategies, hence can be used as independent computational agent for biocomputation and for development of space searching and partitioning algorithm.

3.6 Perspective of future work

The ability of different microorganisms and animals to perform a complex task for natural adaptation to the environment has become the basis for various optimization algorithms. Few examples of such algorithms are ant algorithm that has been inspired by the behavior of ants [69, 70], bee algorithms based on the foraging behavior of the honeybees [71], and many other methods. Present-day research projects concern the maze problems that are used as a prototype model in graph theory for practical problems like navigation-based problems, problems related to network routing agents, and exploring robots in a dangerous situation [72], etc. The “wall follower” algorithm is the simplest yet efficient algorithm that follows the right or left wall for navigating through the maze until the solution has arrived. One of the famous algorithms is Dijkstra algorithm that was proposed to solve the single source shortest path. Another well-known algorithm is the Bellman-ford algorithm [62] that has been demonstrated to compute the shortest path. However, these algorithms need an excessive amount of computation time with the very largescale network. The precision in developing and optimizing the algorithms, our bacteria-based maze solving can be beneficial in the fields of urban transportation [49], traffic engineering research, and gaming optimization and increasing the efficiency of board game creation [50].

Reference

[1] J. G. Mitchell and K. J. F. m. e. Kogure, "Bacterial motility: links to the environment and a driving force for microbial physics," vol. 55, no. 1, pp. 3-16, 2006.

[2] K. F. Jarrell and M. J. J. N. R. M. McBride, "The surprisingly diverse ways that prokaryotes move," vol. 6, no. 6, pp. 466-476, 2008.

[3] M. Simões, L. C. Simões, M. J. J. L.-F. S. Vieira, and Technology, "A review of current and emergent biofilm control strategies," vol. 43, no. 4, pp. 573-583, 2010.

[4] I. Banerjee, R. C. Pangule, and R. S. J. A. m. Kane, "Antifouling coatings: recent developments in the design of surfaces that prevent fouling by proteins, bacteria, and marine organisms," vol. 23, no. 6, pp. 690-718, 2011.

[5] C.-E. Marcato-Romain, Y. Pechaud, E. Paul, E. Girbal-Neuhauser, and V. J. B. Dossat-Letisse, "Removal of microbial multi-species biofilms from the paper industry by enzymatic treatments," vol. 28, no. 3, pp. 305-314, 2012.

[6] J. E. Johansen, J. Pinhassi, N. Blackburn, U. L. Zweifel, and Å. J. A. m. e. Hagström, "Variability in motility characteristics among marine bacteria," vol. 28, no. 3, pp. 229-237, 2002.

[7] S. L. Bardy, S. Y. Ng, and K. F. J. M. Jarrell, "Prokaryotic motility structures," vol. 149, no. 2, pp. 295-304, 2003.

[8] H. C. J. A. r. o. b. Berg, "The rotary motor of bacterial flagella," vol. 72, 2003.

[9] E. J. A. R. o. F. M. Lauga, "Bacterial hydrodynamics," vol. 48, pp. 105-130, 2016.
[10] Y. Sowa and R. M. J. Q. r. o. b. Berry, "Bacterial flagellar motor," vol. 41, no. 2, pp. 103-132, 2008.
[11] J. J. S. r. Lighthill, "Flagellar hydrodynamics," vol. 18, no. 2, pp. 161-230, 1976.
[12] K. Drescher, J. Dunkel, L. H. Cisneros, S. Ganguly, and R. E. J. P. o. t. N. A. o. S. Goldstein, "Fluid dynamics and noise in bacterial cell–cell and cell–surface scattering," vol. 108, no. 27, pp. 10940-10945, 2011.
[13] J. Männik, R. Driessen, P. Galajda, J. E. Keymer, and C. J. P. o. t. N. A. o. S. Dekker, "Bacterial growth and motility in sub-micron constrictions," vol. 106, no. 35, pp. 14861-14866, 2009.
[14] B. Libberton, M. Binz, H. Van Zalinge, and D. V. J. P. R. E. Nicolau, "Efficiency of the flagellar propulsion of Escherichia coli in confined microfluidic geometries," vol. 99, no. 1, p. 012408, 2019.
[15] H. Wioland, E. Lushi, and R. E. J. N. J. o. P. Goldstein, "Directed collective motion of bacteria under channel confinement," vol. 18, no. 7, p. 075002, 2016.
[16] M. Theves, J. Taktikos, V. Zaburdaev, H. Stark, and C. J. E. Beta, "Random walk patterns of a soil bacterium in open and confined environments," vol. 109, no. 2, p. 28007, 2015.
[17] J. E. Sosa-Hernández, M. Santillán, and J. J. P. R. E. Santana-Solano, "Motility of Escherichia coli in a quasi-two-dimensional porous medium," vol. 95, no. 3, p. 032404, 2017.
[18] M. Alviano, "The Maze Generation Problem is NP-complete," in ICTCS, 2009, pp. 12-18.
[19] R. L. Rivest and C. E. Leiserson, Introduction to algorithms. McGraw-Hill, Inc., 1990.
[20] N. H. Barnouti, S. S. M. Al-Dabbagh, M. A. S. J. J. o. C. Naser, and Communications, "Pathfinding in strategy games and maze solving using A* search algorithm," vol. 4, no. 11, p. 15, 2016.
[21] A. H. Qureshi, Y. J. R. Ayaz, and A. Systems, "Intelligent bidirectional rapidly-exploring random trees for optimal motion planning in complex cluttered environments," vol. 68, pp. 1-11, 2015.
[22] E. W. J. N. m. Dijkstra, "A note on two problems in connexion with graphs," vol. 1, no. 1, pp. 269-271, 1959.
[23] N. Rambidi and D. J. B. Yakovenchuck, "Finding paths in a labyrinth based on reaction–diffusion media," vol. 51, no. 2, pp. 67-72, 1999.
[24] T. Nakagaki, H. Yamada, and A. J. B. c. Toth, "Path finding by tube morphogenesis in an amoeboid organism," vol. 92, no. 1-2, pp. 47-52, 2001.

[25] D. R. Reyes, M. M. Ghanem, G. M. Whitesides, and A. J. L. o. a. C. Manz, "Glow discharge in microfluidic chips for visible analog computing," vol. 2, no. 2, pp. 113-116, 2002.
[26] M. Kohler, R. J. N. o. l. Wehner, and memory, "Idiosyncratic route-based memories in desert ants, Melophorus bagoti: how do they interact with path-integration vectors?," vol. 83, no. 1, pp. 1-12, 2005.
[27] N. Jin, T. Landgraf, S. Klein, and R. J. A. b. Menzel, "Walking bumblebees memorize panorama and local cues in a laboratory test of navigation," vol. 97, pp. 13-23, 2014.
[28] J. Cohen, P. Burkhart, N. Jones, and N. J. B. p. Innis, "The effects of an intramaze cue search rule on rat's spatial working memory," vol. 22, no. 1-2, pp. 73-88, 1990.
[29] P. G. J. J. o. e. m. b. Lee and ecology, "Chemotaxis by Octopus maya Voss et Solis in a Y-maze," vol. 156, no. 1, pp. 53-67, 1992.
[30] R. Schoenfeld, N. Moenich, F.-J. Mueller, W. Lehmann, and B. J. B. b. r. Leplow, "Search strategies in a human water maze analogue analyzed with automatic classification methods," vol. 208, no. 1, pp. 169-177, 2010.
[31] S. Slusný, R. Neruda, and P. J. N. n. t. o. j. o. t. I. N. N. S. Vidnerová, "Comparison of behavior-based and planning techniques on the small robot maze exploration problem," vol. 23, no. 4, pp. 560-567, 2010.
[32] Y. Yu et al., "Intelligence-augmented rat cyborgs in maze solving," vol. 11, no. 2, p. e0147754, 2016.
[33] E. Asenova, H.-Y. Lin, E. Fu, and D. V. J. I. t. o. n. Nicolau, "Optimal fungal space searching algorithms," vol. 15, no. 7, pp. 613-618, 2016.
[34] Y. P. Gunji, Y. Nishiyama, and A. Adamatzky, "Robust soldier crab ball gate," in AIP Conference Proceedings, 2011, vol. 1389, no. 1, pp. 995-998: AIP.
[35] T. Nakagaki, H. Yamada, and M. J. B. c. Hara, "Smart network solutions in an amoeboid organism," vol. 107, no. 1, pp. 1-5, 2004.
[36] K. L. Hanson, D. V. Nicolau Jr, L. Filipponi, L. Wang, A. P. Lee, and D. V. J. s. Nicolau, "Fungi use efficient algorithms for the exploration of microfluidic networks," vol. 2, no. 10, pp. 1212-1220, 2006.
[37] M. Held, A. P. Lee, C. Edwards, and D. V. J. M. E. Nicolau, "Microfluidics structures for probing the dynamic behaviour of filamentous fungi," vol. 87, no. 5-8, pp. 786-789, 2010.
[38] T. Nakagaki, "Smart behavior of true slime mold in a labyrinth," Res Microbiol, vol. 152, no. 9, pp. 767-70, Nov 2001.
[39] T. J. R. i. M. Nakagaki, "Smart behavior of true slime mold in a labyrinth," vol. 152, no. 9, pp. 767-770, 2001.

[40] C. Acikgoz, M. A. Hempenius, J. Huskens, and G. J. Vancso, "Polymers in conventional and alternative lithography for the fabrication of nanostructures," European Polymer Journal, vol. 47, no. 11, pp. 2033-2052, 11// 2011.
[41] M. Binz, A. P. Lee, C. Edwards, and D. V. Nicolau, "Motility of bacteria in microfluidic structures," (in English), Microelectronic Engineering, vol. 87, no. 5-8, pp. 810-813, May-Aug 2010.
[42] S. Taherkhani, M. Mohammadi, J. Daoud, S. Martel, and M. Tabrizian, "Covalent binding of nanoliposomes to the surface of magnetotactic bacteria for the synthesis of self-propelled therapeutic agents," ACS Nano, vol. 8, no. 5, pp. 5049-60, May 27 2014.
[43] D. A. Bazylinski et al., "Magnetococcus marinus gen. nov., sp. nov., a marine, magnetotactic bacterium that represents a novel lineage (Magnetococcaceae fam. nov., Magnetococcales ord. nov.) at the base of the Alphaproteobacteria," Int J Syst Evol Microbiol, vol. 63, no. Pt 3, pp. 801-8, Mar 2013.
[44] C. A. Schneider, W. S. Rasband, and K. W. Eliceiri, "NIH Image to ImageJ: 25 years of image analysis," Nat Methods, vol. 9, no. 7, pp. 671-5, Jul 2012.
[45] E. Meijering, O. Dzyubachyk, and I. Smal, "Methods for cell and particle tracking," Methods Enzymol, vol. 504, pp. 183-200, 2012.
[46] M. O. Aqel, A. Issa, M. Khdair, M. ElHabbash, M. AbuBaker, and M. Massoud, "Intelligent maze solving robot based on image processing and graph theory algorithms," in 2017 International Conference on Promising Electronic Technologies (ICPET), 2017, pp. 48-53: IEEE.
[47] M. Meister, G. Lowe, and H. C. J. C. Berg, "The proton flux through the bacterial flagellar motor," vol. 49, no. 5, pp. 643-650, 1987.
[48] S. Jun, L. Jian-Yuan, C. Han, W. J. J. o. A. Xi-Li, and C. Technology, "Study on near-optimal path finding strategies in a road network," vol. 2, no. 3, pp. 319-333, 2008.
[49] S. J. N. Pallottino, "Shortest-path methods: Complexity, interrelations and new propositions," vol. 14, no. 2, pp. 257-267, 1984.
[50] D. Połap, M. Wozniak, C. Napoli, E. J. I. J. o. E. Tramontana, and Telecommunications, "Is swarm intelligence able to create mazes?," vol. 61, no. 4, pp. 305-310, 2015.
[51] M. Skoge et al., "A worldwide competition to compare the speed and chemotactic accuracy of neutrophil-like cells," vol. 11, no. 6, 2016.
[52] N. G. Jain et al., "Microfluidic mazes to characterize T-cell exploration patterns following activation in vitro," vol. 7, no. 11, pp. 1423-1431, 2015.

[53] A. M. Reynolds, T. K. Dutta, R. H. Curtis, S. J. Powers, H. S. Gaur, and B. R. J. J. o. t. R. S. I. Kerry, "Chemotaxis can take plant-parasitic nematodes to the source of a chemo-attractant via the shortest possible routes," vol. 8, no. 57, pp. 568-577, 2011.
[54] A. B. S. Saman and I. Abdramane, "Solving a reconfigurable maze using hybrid wall follower algorithm," 2013.
[55] M. M. Salek, F. Carrara, V. Fernandez, J. S. Guasto, and R. J. N. c. Stocker, "Bacterial chemotaxis in a microfluidic T-maze reveals strong phenotypic heterogeneity in chemotactic sensitivity," vol. 10, no. 1, pp. 1-11, 2019.
[56] T. V. Phan et al., "Bacterial Route Finding and Collective Escape in Mazes and Fractals," vol. 10, no. 3, p. 031017, 2020.
[57] A. Weber, M. Bahrs, Z. Alirezaeizanjani, X. Zhang, C. Beta, and V. J. F. i. P. Zaburdaev, "Rectification of Bacterial Diffusion in Microfluidic Labyrinths," vol. 7, p. 148, 2019.
[58] V. Tokárová et al., "Patterns of bacterial motility in microfluidics-confining environments," vol. 118, no. 17, 2021.
[59] A. E. Dubinov, A. N. Maksimov, M. S. Mironenko, N. A. Pylayev, and V. D. J. P. o. P. Selemir, "Glow discharge based device for solving mazes," vol. 21, no. 9, p. 093503, 2014.
[60] S. J. P. E. Ayrinhac, "Electric current solves mazes," vol. 49, no. 4, p. 443, 2014.
[61] A. J. P. L. A. Adamatzky, "Hot ice computer," vol. 374, no. 2, pp. 264-271, 2009.
[62] A. Nair, K. Raghunandan, V. Yaswant, S. S. Pillai, and S. J. A. P. L. Sambandan, "Maze solving automatons for self-healing of open interconnects: Modular add-on for circuit boards," vol. 106, no. 12, p. 123103, 2015.
[63] M. J. Fuerstman et al., "Solving mazes using microfluidic networks," Langmuir, vol. 19, no. 11, pp. 4714-4722, 2003.
[64] I. Lagzi, S. Soh, P. J. Wesson, K. P. Browne, and B. A. J. J. o. t. A. C. S. Grzybowski, "Maze solving by chemotactic droplets," vol. 132, no. 4, pp. 1198-1199, 2010.
[65] J. Cejkova, M. Novak, F. Stepanek, and M. M. J. L. Hanczyc, "Dynamics of chemotactic droplets in salt concentration gradients," vol. 30, no. 40, pp. 11937-11944, 2014.
[66] K. Agladze, N. Magome, R. Aliev, T. Yamaguchi, and K. J. P. D. N. P. Yoshikawa, "Finding the optimal path with the aid of chemical wave," vol. 106, no. 3-4, pp. 247-254, 1997.
[67] C. Scherber et al., "Epithelial cell guidance by self-generated EGF gradients," vol. 4, no. 3, pp. 259-269, 2012.
[68] H. Kolivand and M. S. J. I. T. R. Sunar, "Survey of shadow volume algorithms in computer graphics," vol. 30, no. 1, pp. 38-46, 2013.

[69] L. Gambardella and M. J. I. T. E. C. Dorigo, "A cooperative learning approach to the traveling salesman problem," vol. 1, p. 5366, 1997.
[70] M. Dorigo, V. Maniezzo, A. J. I. T. o. S. Colorni, Man,, and P. B. Cybernetics, "Ant system: optimization by a colony of cooperating agents," vol. 26, no. 1, pp. 29-41, 1996.
[71] D. Karaboga and B. J. J. o. g. o. Basturk, "A powerful and efficient algorithm for numerical function optimization: artificial bee colony (ABC) algorithm," vol. 39, no. 3, pp. 459-471, 2007.
[72] R. Kumar et al., "Maze solving robot with automated obstacle avoidance," vol. 105, pp. 57-61, 2017.

Chapter 4

4. Agents-based network bio-computing solutions to high-density, compact NP-complete Subset Sum Problems

Ayyappasamy Sudalaiyadum Perumal[1#], Monalisha Nayak[1#], Falco C.M.J.M. van Delft[2] and Dan V. Nicolau[1]*

[1]McGill University, Faculty of Engineering, Department of Bioengineering, Montreal, Quebec, H3A 0C3, Canada

[2]Molecular Sense Ltd, Liverpool L36 8HT, UK
*Corresponding author: dan.nicolau@mcgill.ca
# Contributed equally

Abstract

Agent-based Network BioComputation (NBC) has been proposed as an advanced non-conventional computing method to solve combinatorial non-polynomial time complete (NP-complete) problems. Apart from the benchmark demonstration of NP-computation using molecular motor proteins and cytoskeletal filaments, actively replicating bacteria in microfluidic networks are proposed as alternative computing agents. Bacterial operated NBC, due to the inherent ability of bacteria to replicate in confined spaces, has the potential to exponentially scale-up the computing power at par with the problem size under optimal conditions. The Subset Sum Problem (SSP) is frequently used as model problem, specifically the Prime number series (SSP {2,3,5,7,11,13…}). The Prime numbers+1 SSP set translates into a relatively compact, but unary coded network, requiring large network areas and a large readout Field-of-View (FoV) when scaling up to cardinalities above N=7. To overcome this limitation and experimentally establish the solution exploration capability of bacterial NBC with sample sizes of cardinality higher than N=7, we chose a high density, ultra-compact SSP series – the unit (or Pascal's) series. This communication presents a preliminary experimental demonstration of scalability up to a cardinality of 10, i.e., for the SSP@10 {1,1,1,1,1,1,1,1,1,1} set. This work also shows the readouts obtained and demonstrates the time-point comparisons to achieve readouts for various cardinalities; this demonstration uses a small part of the larger network that was used. The available microscopy-based tools can monitor the network up to cardinalities of N=42, at which point, however, computer derived solutions will be intractable when using a brute force algorithm only.

4.1 INTRODUTION

In applied mathematics, combinatorial problems require exploring many candidate solutions by brute force. As the sample size increases, the number of solutions to explore raises exponentially [1]. Among the many different NP-complete problems such as, the graph colouring problem, the traveling salesman problem, the knapsack problem, etc. [2,3,4], the Subset Sum Problem (SSP) is a very commonly used model problem for demonstrating agent-based NBC [1,5]. In SSP, for a problem size of N numbers, referred to as cardinality, the total number of possible solutions is 2^N. When solving SSP problems, sequentially operating electronic computers must explore solutions by brute force and are shown to reach intractability for higher cardinalities, N≥40 (for a Pentium Core V processor with 1Gb RAM capacity) [1]. Also, no single best algorithm could scale up with the increasing problem size [2]. Non-conventional computing approaches use DNA [3-4], or molecular motor proteins [5] to solve NP-complete problems like SSP. However, a significant problem for all these bio-computational methods is scalability [1].

Recently, our group proposed bacteria as an alternative computation entity based upon computer-aided simulations; bacteria have manifold advantages compared to other entities [1]: they replicate and adapt in constrained channels and microfluidic spaces; they are resilient, genetically manipulatable, and autonomously motile [1]. However, the limiting factor to scaling up is the FoV needed to monitor the SSP networks that are of high density, but low compactness. For demonstrating SSP solving ability, we used the Prime numbers+1 set, i.e., {1,2,3,5,7,11,13} which translates into a relatively compact, but unary coded network, requiring large network areas and a large readout FoV when scaling up to cardinalities above N=7. The solution density corresponds to the number of combinations to reach the target solutions (complexity class I networks has one solution per exit, complexity class II network has more than one solution combination to reach the same exits) [1]. While solving SSP as an NP-complete problem, the computation approach has two questions to be answered. Q1: “Does a solution exist for a particular target sum?” and Q2: “If a solution exists, what is/are the subset(s) of the target sum?”. Q1 can usually be answered for the non-conventional NBC approach using a density or heat map or quantifying agents at the network exits. However, for answering Q2, full tracking of the bacterial trajectories in the network is necessary, unless otherwise tagging-based approaches as proposed in [1] can be employed.

The bacterial-driven NBC approach demonstrated a maximum Prime number +1 set has been solved up to a cardinality of N=7 (work in review). Although N=7 is the highest Cardinality set solved by bacteria, we could not further expand yet, due to limitations in the Field-of-View of our current set-up. However, to experimentally explore higher cardinality sets solvable by bacteria, we used an even more compact set, i.e., Pascal's series of 1s. Such a set with our present resolution and FoV could

expand up to a cardinality of N=42. The Pascal set SSP network consists of two types of junctions, namely split junctions and join junctions. Split junctions provide the bacteria exploring the networks an equal opportunity to go left or right. Join junctions are active on all routes that encode more than one solution to the same exit. Bacteria follow the junction rules detailed elsewhere [6], leading to exits that encode the solutions. The solutions are tracked either by density map profiles (solving Q1) [1,5] or by tracking individual agents, showing all individual routes taken (solving Q2 as well) [1,5]. The work here demonstrates a bacterial (*E. coli)* operated SSP network encoding the Pascal set of 1s for N=9, one of the highest Cardinality problems solved by bacteria. Our network here could experimentally run a problem of cardinality N=42, without any modification or new imaging technologies needed, while requiring advancements in NBC-specific tracking tools.

4.2 METHODS

The detailed protocols for network fabrication and operation by bacteria, image processing, and network tracking are provided in [6][8].

4.3 RESULTS AND DISCUSSION

The bacterial trajectory summation as heat patterns or density maps, shown in Figure 14, demonstrates the solutions explored by bacteria for a model Pascal set of 1s for the Cardinality N=5. A and B represent the density maps and individual trajectories for each exit, respectively. Except for the first and last exit, all the remaining exits have more than one route to reach the exit, meaning complexity class II exits with active join junctions. As a result, Fig 14A (bar graph) in black fonts represents the possible routes to reach the same exit (target sum). The same has been tracked and shown with individual bacterial trajectories in Figure 14B (the inset for exit 3 with ten possible solutions. Figure 13A shows a larger cardinality network, with N=9. In all the networks used for this demonstration, the bacterial counts have been quantified at the exit of the network (Figure 14B) with the computation time for Pascal series of 1s for the cardinality of up to N=9. It should be noted that, in the case of N=9, the exits, #4 and #5 have a total of 126 different paths to reach the same exit, while the bacteria that explored these networks were more than 6000, i.e., 6000 individual bacterial agents explored one of the subsets in the series (Figure 15A and 15B).

The model demonstration shown here is particularly useful to show the ability of bacteria to solve higher cardinality networks. While the Q1 for NP computation could be answered using density maps, as shown in Figure 14A (left), Figure 15A, for answering Q2, the effective solutions to these NBC of SSP require tracking the entire paths of the computing agents in real-time through the network, from the starting point until the exits, i.e., the entire network in a single FoV [1]. With the

increasing problem set size, the network's overall computing area explodes exponentially, too large to be recorded in one FoV. The image stitching of different frames benefits us to some extent, but there are chances of missing bacterial trajectories. Despite imaging advancements, e.g., lens-less microscopy, mobile phone-based microscopy [7], it appears that the scaling of networks for solving SSP is problematic, and the FoV for larger networks is not achievable easily without modification to the existing imaging techniques. The use of a Pascal set here is an alternative to test the efficiency of bacterial operated networks for high density, high compact networks. While we tested the network up till N=42, the results presented here are majorly of cardinality up to N=9, SSP {1,1,1,1,1,1,1,1,1}, answering both Q1 and Q2. For networks of cardinality N≥10 and up to N=42, Q1 could be readily achieved using existing imaging techniques using fluorescence microscopy, while Q2 would need extensive improvement in automatic tracking of bacteria. While we present here the solutions to the cardinality N=9 network (Fig. 15), one of the highest solved and first-ever compact series attempted, we aim to test the network to perform tracking and computation with N>10, high density, highly compact networks in the future.

4.4 FIGURES

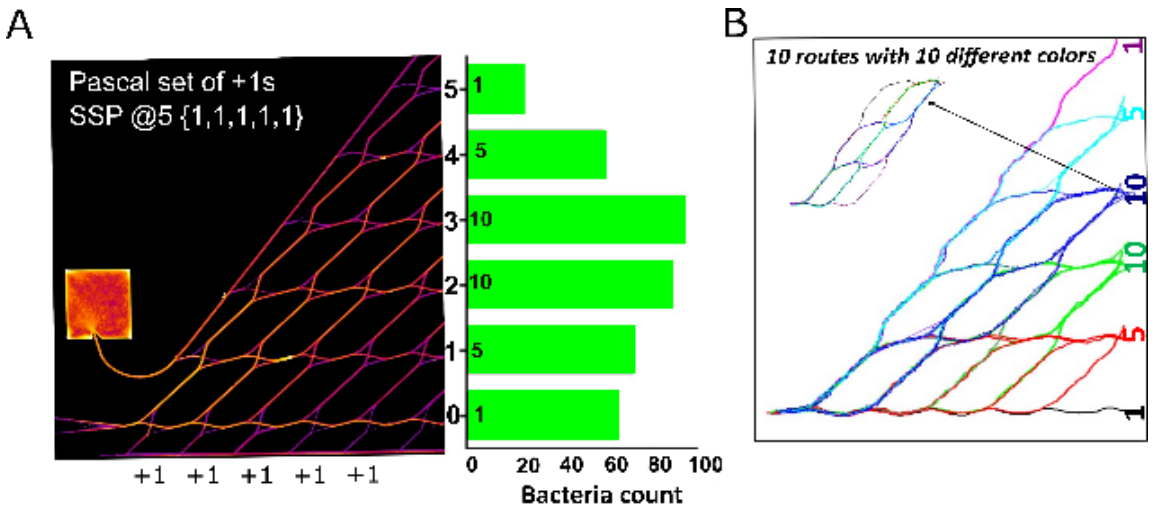

Figure 14. Demonstration of solutions for bacteria operated Pascal series of N+1 set (N=5, Pascal SSP@5 {1,1,1,1,1}). A and B represent the density maps, bar graphs (answering Q1), and individual trajectories (answering Q2) to each solution by NBC approach (different routes to one exit, i.e., target sum (highlighted with yellow) by *E. coli*.

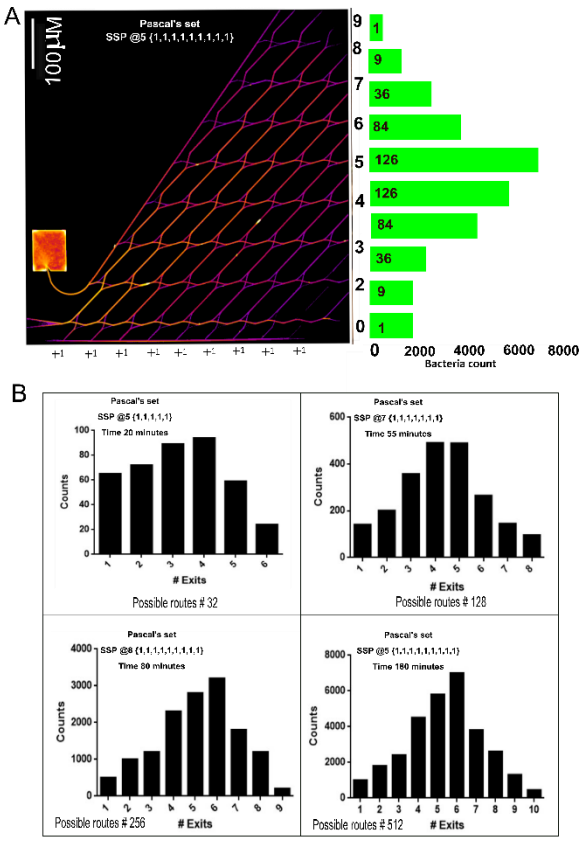

Figure 15. Demonstration of solutions for bacteria operated Pascal series of N+1 set (N=9, Pascal SSP@9 {1,1,1,1,11,1,1,1}). A represents the density map derived solutions to the SSP problem of N=9 explored by *E. coli*. B. Four bar graphs show the computation time for different cardinalities.

4.5 CONCLUSION

The important aim of this communication is to show experimental evidence for bacterial-operated NBC using the Pascal's series. Since the use of the Prime number series was limited by the FoV and readout achievable, a different series with compact network size and a complexity class II network have been experimented here. The presented proofs not only answer the Q1 for NP-complete problems but also Q2. While the current experimental setup with Pascal series could scale up immediately to N=42, with the ability to answer Q1, the approach needs detailed time-energy computation analysis, comparing different SSP sets and comparing the efficiency of a computer solving SSP of Pascal series by brute force. Also, any advancement in advanced imaging with large FoV in the future will further the non-conventional NBC approach using bacteria.

REFERENCES

1. F. C. van Delft et al., "Something has to give scaling combinatorial computing by biological agents exploring physical networks encoding NP-complete problems, *" Interface focus "* vol.8, no.6, p.0034, 2018.
2. M. R. J. C. Garey, "A Guide to the Theory of NP-Completeness, "*Computers and intractability*" 1979.
3. L. M. J. S. Adleman, "Molecular computation of solutions to combinatorial problems, *" Science* " vol. 266, no. 5187, pp. 1021-1024, 1994
4. C. V. Henkel, T. Bäck, J. N. Kok, G. Rozenberg, and H. P. J. B. Spaink, "DNA computing of solutions to knapsack problems, *" Biosystems "* vol. 88, no. 1-2, pp. 156-162, 2007.
5. D. V. Nicolau et al., "Parallel computation with molecular-motor-propelled agents in nanofabricated networks,*" Proceedings of the National Academy of Sciences",* vol. 113, no. 10, pp. 2591-2596, 2016.
6. M. Nayak, A. S. Perumal, D. V. Nicolau, and F. C. van Delft, "Bacterial motility behaviour in sub-ten micron wide geometries,*" 16th IEEE (NEWCAS),* pp. 382-384, 2018.
7. S. Kheireddine, A. Sudalaiyadum Perumal, Z. J. Smith, D. V. Nicolau, and S. Wachsmann-Hogiu, "Dual-phone illumination-imaging system for high resolution and large field of view multi-modal microscopy,*", Lab Chip",* vol. 19, no. 5, pp. 825-836, Feb 26 2019.
8. Tokárová, Viola, et al. "Patterns of bacterial motility in microfluidics-confining environments." *Proceedings of the National Academy of Sciences"* 118.17 (2021).

Chapter 5

5. Discussion

This thesis provides an in-depth experimental and simulation-based comprehension of bacterial motility in confinement, for five bacterial species with significantly diverse morphologies, dimensions, and flagellar complexities, through microfluidic networks of different levels of confinement. More crucially, these observations can be used as a foundation for the design of microfluidic devices for biocomputational and biosimulation approaches, bacteria entrapment for diagnostics, and single-cell genome screening. Maze solving and solution exploration by bacteria reveal species specific and genus specific space searching and path finding abilities of the studied bacterial species individually. Also, the study demonstrates a small instance of bacteria operated network-based computation as a proof of concept to address the limitation with scaling and Field-of view.

The chapter 1 described a theoretical introduction to the insights into microbial motility in the natural environments and methods to understand the underlying mechanisms of microbial motility. The methods include traditional microbiological assays, [31, 32], microscopic analysis of bacterial motility [35, 36], and microfluidics-based approaches [45, 46]. This chapter also briefly explained the relevant applications in the areas of biocomputation and biosimulation with the rules of the motility. Chapter 2 provided comprehensive research of motility of five individual bacterial species of diverse dimensions and morphologies, through microfluidic networks of different confinement and complexity. Chapter 3 evaluated the efficiency of individual bacterial species for space searching and pathfinding through the maze networks of different complexity such as uniform and non-uniform maze. This study also explained species specific strategies to find the shortest path along with maximum number of possible paths, which can be advantageous for developing bio-inspired algorithms. Agent-based Network BioComputation approach was demonstrated in Chapter 4 by using bacteria as an ideal computing agent. The work also presented experimental evidence for bacterial-operated NBC using the Pascal series.

Chapter 2 described the modulations in the motility patterns of five individual bacteria, i.e., *V. natriegens*, *M. marinus*, *P. putida*, *V. fischeri*, and *E. coli* through microfluidic structures of different confinement. The motility behavior was accessed through microfluidic structures with high (6 µm), or low (4 µm) ceilings (Figure 3B), large chambers with quasi-open spaces (‘plazas’), linear channels with various widths, channels presenting lateral exits at various angles, and meandered channels with various widths by 2D and 3D imaging. The 2D and 3D imaging/z-stack sectioning of bacterial trajectories through plaza presented the motility close to the walls and corners. *V. natriegens*, *V.*

fischeri, and *E. coli* presented trajectories in the proximity to, and parallel with the horizontal walls, where the motility behavior for *P. putida* and *M. marinus* was frequently fluctuated between z-planes (Figure S7, S8).

Correlation between experimental and theoretical classification. An in-depth hydrodynamic modeling of monotrichous bacteria revealed that the geometrical parameters of the cell and the helical flagellum determines the motility behavior near a stable flat surface [157]. The experimental results were correlated with the theoretical modeling and the bacterial species were classifies into various categories based on the geometry of the bacterium. The bacterial species that exhibit an active propensity for swimming adjacent to the wall were classified as "Wall accumulators". When the movement of the bacteria was away from the wall but maintain a near constant distance from the wall and presented circular motility patterns were classified as "stable swimmers parallel to the wall". The last classified group was "wall escapers as the hydrodynamic interactions result in bacterial movement away from surfaces. Experimentally, *M. marinus* as an monotrichous model bacteria exhibited a 'ping-pong'-like movement resulting in higher density localized near the walls due to frequent collisions and is predicted as wall escapers, but it is near the boundary between accumulators and escapers. Another theoretical model of the movement of a polar bi-flagellate bacterium based on *M. marinus* [158] demonstrated that, *V. natriegens, E. coli*, and *V. fischeri* presented two patterns of movement: movement along vertical and horizontal walls, and circular motion when detached.

Experimentally, *V. natriegens* and *V. fischeri* were grouped in the category of movement parallel to the wall alike theoretical predictions. *P. putida* and *E. coli* exhibited both escapers motility pattern, and movement parallel to the wall.

The theorical classification was determined by two geometrical parameters such as; cell body aspect ratio and the length of the flagellum. Even though, the theoretical models depict a single, polar flagellum [159], *E. coli,* with multiple flagella was reproduced accurately by these theoretical models. Thus, this classification is expected to serve as a useful conceptual framework for the characterization of motility behavior in relation to a solid surface, although most species in the current study are architecturally more complex than the monotrichous model.

Motility in linear channels. Our observations provide several insights to straight and U-turn movements, the effect of different channel widths on the motility, and the effect of local steric interactions between the walls and the flagella during the movement through extreme confinements. The motility of *V. natriegens* and *E. coli* through the wider channels (6 to 8 μm) correlates well with their behavior through plaza (Figure 4). These species presented the lowest overall proportion of U-turns, with an apparent decrease of U-turns with the channel width for the larger *E. coli*. Due to

extreme steric interactions with both the walls through the narrower channels and because of large cell body, *M. marinus* exhibited higher ratio of U-turns. This could also be the result of frequent collision with the walls.

V. fischeri and *P. putida* presented intermittent wall contact and presented highest ratio of U-turns. According to the previous studies, the velocity decreases significantly in narrower channels because of various mechanical constraints for *E. coli*, [160, 161] *B. subtilis*,[98] and *S. marcescens* [99] that is supported well by our observation for *V. natriegens* and *E. coli*. Another interesting pattern of motility was observed, which is sinusoidal pattern of motility. *P. putida, V. natriegens, V. fischeri*, and to a much less extent *E. coli* present sinusoidal movement pattern with increasing channel widths. One of the studies for monotrichous wall escaper bacterial species [156] demonstrated distorted helical motility pattern through the channels of large rectangular transversal section. These observations are useful for the design of biocomputation of networks and also the different patterns of motility such as; wall accumulators, or wall escapers, can translate into different geometrics for bacterial cell sorting; and also, for microfluidics-based flow cytometry.

Motility in channels with angled exits. Microfluidic structures presenting angled exits were used to reveal the additional mechanism responsible for determining the exit probabilities in angled channels in addition to the species-specific hydrodynamics driven spread of deflection angles in open spaces (plazas). The exiting probability decreased with increasing the exit angle due to species specific details, and it was observed for all the studied bacterial species. In the tight confinements, the species-specific pattern was the result of local hydrodynamics interactions. The movement of the larger bacterial species were guided by the steric interactions of flagella with the walls. These findings are interesting topic for selection of bacterial candidates, and the designs of computational microfluidic networks for cancelling of errors, such as U-turns in narrow channels, and the optimization of the angles of logic gates channels.

Motility in meandered channels. The meandered channel, which was comprised of three channels of different width made the movement of all bacterial species difficult, more specifically the tightly confined 5μm–wide meandered channels. *M. marinus* presented considerably lower overall success rate than the other species because of elastic-like collisions that resulted in frequent trappings through the channels. The movement of all bacterial species through the channels with large gaps between comb teeth was found to be mostly directed by hydrodynamics, with only occasional interference of the local steric interactions between the flagella and the walls. The bacterial species were also successful to pass through the tight confinements due to local steric interaction between flagella and the 90°-angled walls. And the movement in the channels in the meso-scale region, i.e., 10 μm distance between the comb teeth, all species had difficulties in passing through the channel

and the hydrodynamics-based mechanism governs the motility. Another intriguing phenomenon, which was observed that steric interactions–driven movement in tight confinement is also modulated by bacterial shape and not only by size. *P. putida*, a much shorter species had some success in passing, while *V. natriegens* and *E. coli* are both very effectively trapped in mesoscale-sized meandered channels. *V. fischeri* being the largest among all largest of the species appeared to have the best success rate. To conclude, in the mesoscale region, hydrodynamics and local steric interaction mechanism do not act synergistically, and as a result, the bacteria get trapped and their movement gets modulated by their characteristic shape ratios. These observations can be useful in the areas of cell sorting and single cell genomics [162, 163].

Maze solving by bacteria. We extended the study about the motility of different bacterial species by evaluating their space searching efficiency through the microfluidic maze networks. Maze solving with increasing complexity is a non-trivial exercise, which has been placed in the category of NP-complete problems [113]. We used microfluidic maze networks (uniform /non-uniform) as a complex network for studying the behavioral preferences of the bacterial species and evaluating the motility parameters by presenting them as individual navigators. These experimental characterizations can allow a practical, straight forward space searching, and partitioning algorithm towards the analysis of more complex geometrics relevant for real-world applications.

The efficiency was calculated by evaluating various performance parameters such as velocity, ability to explore unique paths/unique vertices, shortest time, and distance traveled through the network.

Shortest path. Solving the shortest path problem in a maze has various applications, most notably in the fields of urban transportation [164], traffic engineering research, and gaming optimization and increasing the efficiency of board game creation [132]. Hundreds of algorithms, silicon computing architectures, and unconventional computation approaches have been developed to address this problem. Neutrophil cells [165], T cells [166], and slime mold [167] navigated through the maze to connect the shortest path with/out chemotaxis. However, challenges arise with the complexity of the network, and obstructions on a possible route. For instance, autonomous robots were unsuccessful in navigation after encountering any loop or obstacle in the network [168]. Many implementations require external assistance of hardware/software for detecting the shortest path [169, 170]. Using bacteria to study the space searching mechanism, behavioral preference, and modulations in motility parameters [171] were studied by many researchers but were also related to biased motility such as chemotaxis. Our study demonstrates the fundamental behavioral characteristic of bacterial species to find the shortest path in mazes of different complexity without any external inference. Addressing the shortest path in the shortest time various methods have been reported previously by tracing the path through thermal visualization [172], through crystallization [173], employing conductive

particles [174], and also by living organisms like slime mould [167], and epithelial cells [175]. All these reported studies took hours to days for tracing the path. *V. natriegens* and *E. coli* exhibited a higher success rate in exploring the shortest route in few seconds. Other bacterial species exhibit chaotic motility in tightly confinements, which present a lower success rate for exploring the shortest route in less time.

All possible valid paths. During traffic simulation processes, navigating through a city to find new and unique paths are always a challenge. Other real-world applications such as optimizing computer games with unique solutions need better pathfinding/intelligence algorithms [134]. We evaluated the efficiency of bacterial species for exploring all possible valid/unique routes through the network. Previously reported hydrodynamics interaction and species steric interactions with the surrounding channel walls in tight confinements were observed as well with the increasing complexity of the network [176]. The angled junction through the networks influenced the motility of the bacterial species. *V. natriegens* and *E. coli* presented lower velocity but were successful in finding unique possible paths. In the end, the precision in the evaluation of the efficiency of bacteria can guide us to choose an ideal bacterial candidate as a computing agent for biocomputation approach, and bacteria-based space partitioning will help in developing and optimizing algorithms in urban transportation, board game creation/optimization, and traffic engineering research. We evaluated one of the important performance parameters, which is unique vertices traversed through the navigation. The ability was quantified with increasing complexity (while tracing all possible paths) as well and compared between all the bacterial species. *V. natriegens* and *E. coli* traversed a fair number of vertices per second when compared to other bacterial species. This observation is an important aspect in the pathfinding process to eliminate the redundant steps.

Bacteria operated network-based computation. The advantages of using bacteria as a model organism for network-based computation approaches are manifold compared to other computation agents [155] as they replicate and adopt in constrained channels, microfluidic spaces; they are resilient, genetically manipulatable, and autonomously motile. The proof of concept of network based biocomputation has been proposed by using self-propelled cytoskeletal filaments, i.e actin filaments, or microtubules [177]. However, this approach was challenged with computational errors and scalability issues [155]. Real-time tracking of the computing agents through the network is essential during the computation, hence the requirement to capture the complete network in one optical FoV is necessary. With the increasing problem set, the network's overall computing area explodes exponentially, too large to be recorded in one FoV. Image stitching of different frames, lens-less microscopy, mobile phone-based microscopy benefits us by some means [156], but it appears that the scaling of networks for solving SSP is problematic, and the field-of-view for larger

networks is not achievable easily without modification to the existing imaging techniques. Thus, our present study advanced the network-based computation for solving SSP with bacteria as a computing agent. Our work shows experimental evidence for bacterial-operated NBC using the Pascal's series (high density and ultra compact). we present here the solutions to the cardinality N=9 network (Fig. 15), one of the highest solved and first-ever compact series attempted, we aim to test the network to perform tracking and computation with N>10, high density, highly compact networks in the future.

Chapter 6

6. Conclusion

The objective of this thesis is to address the motility behavior of individual bacterial cells of five species of varying size and morphologies using microfluidic networks with various levels of confinement and complexity. This in-depth study of bacterial motility will facilitate further advances in biosensing, cell sorting, biocomputation, and biosimulation approaches.

This study provided a detailed description of the bacterial motility pattern through complex geometries. Here, we presented the impact of the hydrodynamic effect and local steric interaction of species-specific morphology with varying confinements. For lesser confinements, such as an open space with one limiting wall, the motility behavior can be comprehended with qualifications compared to that of monotrichous bacteria with identical size. With increasing confinements, such as straight channels with various widths, in networks with exits at various angles and meandering channels, *V. natriegens*, *E. coli*, and *V. fischeri* were classified as swimmers parallel to the walls, while *P. putida* and *M. marinus* were wall escapers. However, *E. coli* and *P. putida* also presented wall escaper behavior partially with increasing complexity. The variation in the behavior was a result of the impact of local steric interaction of species-specific morphology with tight confining geometries. The detailed description of bacterial motility, especially the motility of *M. marinus*, in microfluidic channels can be used to mimic the microvascular system surrounding the tumors of micrometer range sizes and for the optimization of microrobots outside for medical applications. Additionally, for designing microfluidic biocomputational networks, the selection of an ideal biological candidate is essential, which can be achieved by studying their motility pattern to avoid any errors, such as U-turns in narrow channels, and the optimization of the angles of logic gates channels.

The study also focused on the space searching ability of bacteria through micro-confined maze networks of different complexity along with additional motility parameters. The modulations in different performance parameters during the navigation were evaluated, which revealed the efficiency of five individual bacterial species for finding maximum number of possible paths along with the shortest path all possible in the maze networks. *V. natriegens* and *E. coli* possess an incredible ability to find the shortest path along with the most possible valid paths through the network with minimum redundant trajectories. Although *M. marinus* being the fastest swimmer among all the studied species traveled a larger distance with increasing complexity and the paths traversed were repetitious. Maze networks are commonly studied for chemotactic cell sorting, whereas our research has the potential to choose the efficient bacteria to solve mazes without any

external clue. The bacterial random motility parameters can allow a practical, straightforward space searching, and partitioning algorithm towards the analysis of more complex geometrics relevant for real-world applications, such as transportation system planning, development of urban transportation, and vehicle routing problem, etc.

A proof of concept of the bacteria-operated biocomputational network was attempted with a comprehensive understanding of the bacterial motility behavior. A high compact SSP series – Pascal's series was computed using *E. coli*. The study stands as a promising approach towards the limitations of scalability and smaller FoV with microscopy.

References

1. Storz, G. and R. Hengge, *Bacterial stress responses*. 2010: American Society for Microbiology Press.
2. Durham, W.M., J.O. Kessler, and R.J.s. Stocker, *Disruption of vertical motility by shear triggers formation of thin phytoplankton layers.* 2009. **323**(5917): p. 1067-1070.
3. Bortolaia, C. and L. Sbordone, *[Biofilms of the oral cavity. Formation, development and involvement in the onset of diseases related to bacterial plaque increase].* Minerva Stomatol, 2002. **51**(5): p. 187-92.
4. de Weert, S., et al., *Flagella-driven chemotaxis towards exudate components is an important trait for tomato root colonization by Pseudomonas fluorescens.* 2002. **15**(11): p. 1173-1180.
5. Auger, J., et al., *[Sperm motility and fertilization].* Contracept Fertil Sex, 1994. **22**(5): p. 314-8.
6. Kearns, D.B., *A field guide to bacterial swarming motility.* Nature Reviews Microbiology, 2010. **8**(9): p. 634-644.
7. Henrichsen, J.J.B.r., *Bacterial surface translocation: a survey and a classification.* 1972. **36**(4): p. 478.
8. Harshey, R.M.J.M.m., *Bees aren't the only ones: swarming in Gram-negative bacteria.* 1994. **13**(3): p. 389-394.
9. Macnab, R.J.E.c. and Salmonella, *Flagella and motility.* 1996.
10. Mattick, J.S.J.A.R.i.M., *Type IV pili and twitching motility.* 2002. **56**(1): p. 289-314.
11. McBride, M.J.J.A.R.i.M., *Bacterial gliding motility: multiple mechanisms for cell movement over surfaces.* 2001. **55**(1): p. 49-75.
12. Lauga, E. and T.R.J.R.o.P.i.P. Powers, *The hydrodynamics of swimming microorganisms.* 2009. **72**(9): p. 096601.
13. Turner, L., W.S. Ryu, and H.C.J.J.o.b. Berg, *Real-time imaging of fluorescent flagellar filaments.* 2000. **182**(10): p. 2793-2801.
14. Berg, H. and D. Brown, *Chemotaxis in Escherichia coli analyzed by three-dimensional tracking*, in *Chemotaxis: Its Biology and Biochemistry*. 1974, Karger Publishers. p. 55-78.
15. Webre, D.J., P.M. Wolanin, and J.B. Stock, *Bacterial chemotaxis.* Current Biology, 2003. **13**(2): p. R47-R49.
16. Berg, H.C. and D.A.J.N. Brown, *Chemotaxis in Escherichia coli analysed by three-dimensional tracking.* 1972. **239**(5374): p. 500-504.
17. Macnab, R.M. and D.E.J.P.o.t.N.A.o.S. Koshland, *The gradient-sensing mechanism in bacterial chemotaxis.* 1972. **69**(9): p. 2509-2512.
18. Darnton, N.C., et al., *On torque and tumbling in swimming Escherichia coli.* 2007. **189**(5): p. 1756-1764.
19. Leifson, E., et al., *MOTILE MARINE BACTERIA I.: Techniques, Ecology, and General Characteristics.* 1964. **87**(3): p. 652-666.
20. Stocker, R.J.P.o.t.N.A.o.S., *Reverse and flick: Hybrid locomotion in bacteria.* 2011. **108**(7): p. 2635-2636.
21. Xie, L., et al., *Bacterial flagellum as a propeller and as a rudder for efficient chemotaxis.* 2011. **108**(6): p. 2246-2251.
22. Son, K., J.S. Guasto, and R.J.N.p. Stocker, *Bacteria can exploit a flagellar buckling instability to change direction.* 2013. **9**(8): p. 494-498.
23. Xie, L. and X.-L.J.B.j. Wu, *Bacterial motility patterns reveal importance of exploitation over exploration in marine microhabitats. Part I: Theory.* 2014. **107**(7): p. 1712-1720.
24. Taktikos, J., H. Stark, and V.J.P.o. Zaburdaev, *How the motility pattern of bacteria affects their dispersal and chemotaxis.* 2013. **8**(12).

25. Engelmann, T.W.J.A.f.d.g.P.d.M.u.d.T., *Bacterium photometricum.* 1883. **30**(1): p. 95-124.
26. Berg, H.C.J.B.j., *Torque generation by the flagellar rotary motor.* 1995. **68**(4 Suppl): p. 163S.
27. Aizawa, S.I.J.M.m., *Flagellar assembly in Salmonella typhimurium.* 1996. **19**(1): p. 1-5.
28. Berg, H.C. and L.J.N. Turner, *Movement of microorganisms in viscous environments.* 1979. **278**(5702): p. 349-351.
29. Shapiro, L., *The bacterial flagellum: from genetic network to complex architecture.* Cell, 1995. **80**(4): p. 525-527.
30. Morimoto, Y.V. and T. Minamino, *Structure and function of the bi-directional bacterial flagellar motor.* Biomolecules, 2014. **4**(1): p. 217-234.
31. Ha, D.-G., S.L. Kuchma, and G.A. O'Toole, *Plate-based assay for swimming motility in Pseudomonas aeruginosa*, in *Pseudomonas Methods and Protocols*. 2014, Springer. p. 59-65.
32. Adler, J.J.S., *Chemotaxis in bacteria.* 1966. **153**(3737): p. 708-716.
33. Tso, W.-W. and J.J.J.o.b. Adler, *Negative chemotaxis in Escherichia coli.* 1974. **118**(2): p. 560-576.
34. Li, J., et al., *The chemical-in-plug bacterial chemotaxis assay is prone to false positive responses.* 2010. **3**(1): p. 77.
35. Vigeant, M.A.-S., et al., *Reversible and irreversible adhesion of motile Escherichia coli cells analyzed by total internal reflection aqueous fluorescence microscopy.* 2002. **68**(6): p. 2794-2801.
36. Chemla, Y.R., et al., *A new study of bacterial motion: superconducting quantum interference device microscopy of magnetotactic bacteria.* 1999. **76**(6): p. 3323-3330.
37. Calldine, C.J.J.o.m.b., *Change of waveform in bacterial flagella: the role of mechanics at the molecular level.* 1978. **118**(4): p. 457-479.
38. Scharf, B., *Real-time imaging of fluorescent flagellar filaments of Rhizobium lupini H13-3: flagellar rotation and pH-induced polymorphic transitions.* Journal of Bacteriology, 2002. **184**(21): p. 5979-5986.
39. Barbara, G.M. and J.G.J.F.m.e. Mitchell, *Bacterial tracking of motile algae.* 2003. **44**(1): p. 79-87.
40. Weibel, D.B., W.R. DiLuzio, and G.M.J.N.R.M. Whitesides, *Microfabrication meets microbiology.* 2007. **5**(3): p. 209-218.
41. Tabeling, P., *Introduction to microfluidics*. 2005: OUP Oxford.
42. Wang, X., Z. Liu, and Y.J.R.a. Pang, *Concentration gradient generation methods based on microfluidic systems.* 2017. **7**(48): p. 29966-29984.
43. Kaminski, T.S., O. Scheler, and P.J.L.o.a.C. Garstecki, *Droplet microfluidics for microbiology: techniques, applications and challenges.* 2016. **16**(12): p. 2168-2187.
44. Rusconi, R., J.S. Guasto, and R.J.N.p. Stocker, *Bacterial transport suppressed by fluid shear*. 2014. **10**(3): p. 212-217.
45. Ahmed, T., T.S. Shimizu, and R.J.I.B. Stocker, *Microfluidics for bacterial chemotaxis.* 2010. **2**(11-12): p. 604-629.
46. Kim, S., H.J. Kim, and N.L.J.I.B. Jeon, *Biological applications of microfluidic gradient devices.* 2010. **2**(11-12): p. 584-603.
47. Adler, M., et al., *Studies of bacterial aerotaxis in a microfluidic device.* 2012. **12**(22): p. 4835-4847.
48. Kalinin, Y., et al., *Responses of Escherichia coli bacteria to two opposing chemoattractant gradients depend on the chemoreceptor ratio.* 2010. **192**(7): p. 1796-1800.
49. Yawata, Y., et al., *Competition–dispersal tradeoff ecologically differentiates recently speciated marine bacterioplankton populations.* 2014. **111**(15): p. 5622-5627.
50. Wong, I., C.-M.J.M. Ho, and nanofluidics, *Surface molecular property modifications for poly (dimethylsiloxane)(PDMS) based microfluidic devices.* 2009. **7**(3): p. 291.

51. Cheng, S.-Y., et al., *A hydrogel-based microfluidic device for the studies of directed cell migration.* 2007. **7**(6): p. 763-769.
52. Weibel, D.B., et al., *Bacterial printing press that regenerates its ink: contact-printing bacteria using hydrogel stamps.* 2005. **21**(14): p. 6436-6442.
53. Bren, A. and M.J.J.o.b. Eisenbach, *How signals are heard during bacterial chemotaxis: protein-protein interactions in sensory signal propagation.* 2000. **182**(24): p. 6865-6873.
54. Paster, E. and W.S.J.P.o.t.N.A.o.S. Ryu, *The thermal impulse response of Escherichia coli.* 2008. **105**(14): p. 5373-5377.
55. Frankel, R.B., et al., *Magneto-aerotaxis in marine coccoid bacteria.* 1997. **73**(2): p. 994-1000.
56. Stocker, R. and J.R.J.M.M.B.R. Seymour, *Ecology and physics of bacterial chemotaxis in the ocean.* 2012. **76**(4): p. 792-812.
57. Stocker, R.J.s., *Marine microbes see a sea of gradients.* 2012. **338**(6107): p. 628-633.
58. Dong, L., et al., *Automated chemotactic sorting and single-cell cultivation of microbes using droplet microfluidics.* Scientific reports, 2016. **6**(1): p. 1-8.
59. Nagy, K., et al., *Microfluidic study of the chemotactic response of Escherichia coli to amino acids, signaling molecules and secondary metabolites.* 2015. **9**(4): p. 044105.
60. Lambert, B.S., et al., *A microfluidics-based in situ chemotaxis assay to study the behaviour of aquatic microbial communities.* 2017. **2**(10): p. 1344-1349.
61. Waite, A.J., et al., *Non-genetic diversity modulates population performance.* 2016. **12**(12).
62. Kalinin, Y.V., et al., *Logarithmic sensing in Escherichia coli bacterial chemotaxis.* 2009. **96**(6): p. 2439-2448.
63. Rieke, F. and M.E.J.N. Rudd, *The challenges natural images pose for visual adaptation.* 2009. **64**(5): p. 605-616.
64. Hol, F.J. and C.J.S. Dekker, *Zooming in to see the bigger picture: Microfluidic and nanofabrication tools to study bacteria.* 2014. **346**(6208): p. 1251821.
65. Berg, H.C., *E. coli in Motion*. 2008: Springer Science & Business Media.
66. Montgomery, J.C., C.F. Baker, and A.G.J.N. Carton, *The lateral line can mediate rheotaxis in fish.* 1997. **389**(6654): p. 960-963.
67. Miki, K. and D.E.J.C.B. Clapham, *Rheotaxis guides mammalian sperm.* 2013. **23**(6): p. 443-452.
68. Kaya, T. and H.J.B.j. Koser, *Direct upstream motility in Escherichia coli.* 2012. **102**(7): p. 1514-1523.
69. Stocker, R., H.C. Fu, and T.R. Powers, *Bacterial rheotaxis.* 2012.
70. Ishikawa, T., et al., *Separation of motile bacteria using drift velocity in a microchannel.* 2014. **14**(5): p. 1023-1032.
71. Menolascina, F., et al., *Logarithmic sensing in Bacillus subtilis aerotaxis.* 2017. **3**(1): p. 1-8.
72. Kim, B.J., et al., *Oxygen tension and riboflavin gradients cooperatively regulate the migration of Shewanella oneidensis MR-1 revealed by a hydrogel-based microfluidic device.* 2016. **7**: p. 1438.
73. Salman, H., et al., *Solitary modes of bacterial culture in a temperature gradient.* 2006. **97**(11): p. 118101.
74. Murugesan, N., et al., *Interplay of chemical and thermal gradient on bacterial migration in a diffusive microfluidic device.* 2017. **11**(2): p. 024108.
75. Zhuang, J., R.W. Carlsen, and M.J.S.r. Sitti, *pH-taxis of biohybrid microsystems.* 2015. **5**: p. 11403.
76. Wang, W., et al., *A Diffusion-Based pH Regulator in Laminar Flows with Smartphone-Based Colorimetric Analysis.* 2018. **9**(12): p. 616.

77. Felfoul, O. and S.J.B.m. Martel, *Assessment of navigation control strategy for magnetotactic bacteria in microchannel: toward targeting solid tumors.* 2013. **15**(6): p. 1015-1024.
78. Myklatun, A., et al., *Microfluidic sorting of intrinsically magnetic cells under visual control.* 2017. **7**(1): p. 1-8.
79. Perlova, T., M. Gruebele, and Y.R.J.J.o.b. Chemla, *Blue light is a universal signal for Escherichia coli chemoreceptors.* 2019. **201**(11): p. e00762-18.
80. Rosko, J., et al., *Osmotaxis in Escherichia coli through changes in motor speed.* 2017. **114**(38): p. E7969-E7976.
81. Berke, A.P., et al., *Hydrodynamic attraction of swimming microorganisms by surfaces.* 2008. **101**(3): p. 038102.
82. O'Toole, G., H.B. Kaplan, and R.J.A.R.i.M. Kolter, *Biofilm formation as microbial development.* 2000. **54**(1): p. 49-79.
83. Karimi, A., et al., *Interplay of physical mechanisms and biofilm processes: review of microfluidic methods.* 2015. **15**(1): p. 23-42.
84. Magariyama, Y., et al., *Difference in bacterial motion between forward and backward swimming caused by the wall effect.* 2005. **88**(5): p. 3648-3658.
85. Lauga, E., et al., *Swimming in circles: motion of bacteria near solid boundaries.* Biophys J, 2006. **90**(2): p. 400-12.
86. DiLuzio, W.R., et al., *Escherichia coli swim on the right-hand side.* 2005. **435**(7046): p. 1271-1274.
87. Utada, A.S., et al., *Vibrio cholerae use pili and flagella synergistically to effect motility switching and conditional surface attachment.* 2014. **5**(1): p. 1-8.
88. Gibiansky, M.L., et al., *Bacteria use type IV pili to walk upright and detach from surfaces.* 2010. **330**(6001): p. 197-197.
89. Marcos, et al., *Separation of microscale chiral objects by shear flow.* Phys Rev Lett, 2009. **102**(15): p. 158103.
90. Marcos, et al., *Bacterial rheotaxis.* Proc Natl Acad Sci U S A, 2012. **109**(13): p. 4780-5.
91. Hill, J., et al., *Hydrodynamic surface interactions enable Escherichia coli to seek efficient routes to swim upstream.* 2007. **98**(6): p. 068101.
92. Wu, X.-L. and A.J.P.r.l. Libchaber, *Particle diffusion in a quasi-two-dimensional bacterial bath.* 2000. **84**(13): p. 3017.
93. Zhang, H.-P., et al., *Collective motion and density fluctuations in bacterial colonies.* 2010. **107**(31): p. 13626-13630.
94. Butler, M.T., Q. Wang, and R.M.J.P.o.t.N.A.o.S. Harshey, *Cell density and mobility protect swarming bacteria against antibiotics.* 2010. **107**(8): p. 3776-3781.
95. Ramia, M., D. Tullock, and N.J.B.j. Phan-Thien, *The role of hydrodynamic interaction in the locomotion of microorganisms.* 1993. **65**(2): p. 755-778.
96. Frymier, P.D. and R.M.J.A.j. Ford, *Analysis of bacterial swimming speed approaching a solid–liquid interface.* 1997. **43**(5): p. 1341-1347.
97. Biondi, S.A., J.A. Quinn, and H.J.A.j. Goldfine, *Random motility of swimming bacteria in restricted geometries.* 1998. **44**(8): p. 1923-1929.
98. Männik, J., et al., *Bacterial growth and motility in sub-micron constrictions.* 2009. **106**(35): p. 14861-14866.
99. Binz, M., et al., *Motility of bacteria in microfluidic structures.* Microelectronic Engineering, 2010. **87**(5-8): p. 810-813.
100. Ping, L., V. Wasnik, and E.J.F.m.e. Emberly, *Bacterial motion in narrow capillaries.* 2015. **91**(2): p. 1.
101. Kaehr, B. and J.B. Shear, *High-throughput design of microfluidics based on directed bacterial motility.* Lab on a Chip - Miniaturisation for Chemistry and Biology, 2009. **9**(18): p. 2632-2637.

102. Hulme, S.E., et al., *Using ratchets and sorters to fractionate motile cells of Escherichia coli by length.* 2008. **8**(11): p. 1888-1895.
103. Chen, J. and Y.J.J.o.c.h. Jin, *Motility of Pseudomonas aeruginosa in saturated granular media as affected by chemoattractant.* 2011. **126**(1-2): p. 113-120.
104. Galajda, P., et al., *A wall of funnels concentrates swimming bacteria.* 2007. **189**(23): p. 8704-8707.
105. Lagzi, I., et al., *Maze solving by chemotactic droplets.* 2010. **132**(4): p. 1198-1199.
106. Rao, N.S., et al., *Robot navigation in unknown terrains: Introductory survey of non-heuristic algorithms*. 1993, Oak Ridge National Lab., TN (United States).
107. Crowe, D.A., et al., *Mental maze solving.* 2000. **12**(5): p. 813-827.
108. Modesti, P. and A.J.E.J.o.O.R. Sciomachen, *A utility measure for finding multiobjective shortest paths in urban multimodal transportation networks.* 1998. **111**(3): p. 495-508.
109. Rivest, R.L. and C.E. Leiserson, *Introduction to algorithms*. 1990: McGraw-Hill, Inc.
110. Gupta, B. and S. Sehgal. *Survey on techniques used in autonomous maze solving robot*. in *2014 5th International Conference-Confluence The Next Generation Information Technology Summit (Confluence)*. 2014. IEEE.
111. Barnouti, N.H., et al., *Pathfinding in strategy games and maze solving using A* search algorithm.* 2016. **4**(11): p. 15.
112. Qureshi, A.H., Y.J.R. Ayaz, and A. Systems, *Intelligent bidirectional rapidly-exploring random trees for optimal motion planning in complex cluttered environments.* 2015. **68**: p. 1-11.
113. Alviano, M. *The Maze Generation Problem is NP-complete*. in *ICTCS*. 2009.
114. Funke, S., A. Nusser, and S. Storandt. *The simultaneous maze solving problem*. in *Proceedings of the AAAI Conference on Artificial Intelligence*. 2017.
115. Steinbock, O., Á. Tóth, and K.J.S. Showalter, *Navigating complex labyrinths: optimal paths from chemical waves.* 1995. **267**(5199): p. 868-871.
116. Scriven, L. and C.J.N. Sternling, *The marangoni effects.* 1960. **187**(4733): p. 186-188.
117. Cejkova, J., et al., *Dynamics of chemotactic droplets in salt concentration gradients.* 2014. **30**(40): p. 11937-11944.
118. Lovass, P., et al., *Maze solving using temperature-induced Marangoni flow.* 2015. **5**(60): p. 48563-48568.
119. Wang, Y., et al., *Directional and path-finding motion of polymer hydrogels driven by liquid mixing.* 2012. **28**(31): p. 11276-11280.
120. Adamatzky, A., A. Chiolerio, and K.J.a.p.a. Szaciłowski, *Liquid metal solves maze.* 2019.
121. Seelig, G.J.N.m., *Navigating through a maze.* 2019. **18**(3): p. 198-199.
122. Nakagaki, T., H. Yamada, and Á.J.N. Tóth, *Maze-solving by an amoeboid organism.* 2000. **407**(6803): p. 470-470.
123. Hanson, K.L., et al., *Fungi use efficient algorithms for the exploration of microfluidic networks.* 2006. **2**(10): p. 1212-1220.
124. Asenova, E., et al., *Optimal Fungal Space Searching Algorithms.* IEEE Trans Nanobioscience, 2016. **15**(7): p. 613-618.
125. Held, M., et al., *Intracellular mechanisms of fungal space searching in microenvironments.* Proceedings of the National Academy of Sciences, 2019. **116**(27): p. 13543-13552.
126. Law, J.W., *Do Caenorhabditis elegans exhibit spatial learning? Using a t-maze to explore association of a spatial environment with an attractant.* 2009.
127. Qin, J. and A.R.J.L.o.a.C. Wheeler, *Maze exploration and learning in C. elegans.* 2007. **7**(2): p. 186-192.
128. Salek, M.M., et al., *Bacterial chemotaxis in a microfluidic T-maze reveals strong phenotypic heterogeneity in chemotactic sensitivity.* 2019. **10**(1): p. 1-11.
129. Weber, A., et al., *Rectification of Bacterial Diffusion in Microfluidic Labyrinths.* Frontiers in Physics, 2019. **7**(148).

130. Park, S., et al., *Influence of topology on bacterial social interaction.* Proc Natl Acad Sci U S A, 2003. **100**(24): p. 13910-5.
131. Aqel, M.O., et al. *Intelligent maze solving robot based on image processing and graph theory algorithms*. in *2017 International Conference on Promising Electronic Technologies (ICPET)*. 2017. IEEE.
132. Połap, D., et al., *Is swarm intelligence able to create mazes?* 2015. **61**(4): p. 305-310.
133. Shi, N., et al., *An adaptive routing strategy for freight transportation networks.* 2011. **62**(4): p. 799-805.
134. Kolivand, H. and M.S.J.I.T.R. Sunar, *Survey of shadow volume algorithms in computer graphics.* 2013. **30**(1): p. 38-46.
135. Fuerstman, M.J., et al., *Solving Mazes Using Microfluidic Networks.* Langmuir, 2003. **19**(11): p. 4714-4722.
136. Pershin, Y.V. and M.J.P.R.E. Di Ventra, *Solving mazes with memristors: A massively parallel approach.* 2011. **84**(4): p. 046703.
137. Kennedy, J. and R. Eberhart. *Particle swarm optimization*. in *Proceedings of ICNN'95-International Conference on Neural Networks*. 1995. IEEE.
138. Beaver, D., *Computing with DNA.* J Comput Biol, 1995. **2**(1): p. 1-7.
139. Nicolau, D.V., et al., *Parallel computation with molecular-motor-propelled agents in nanofabricated networks.* 2016. **113**(10): p. 2591-2596.
140. Jaderberg, M., et al., *Population based training of neural networks.* arXiv preprint arXiv:1711.09846, 2017.
141. Castro, L.N., L.N. De Castro, and J. Timmis, *Artificial immune systems: a new computational intelligence approach*. 2002: Springer Science & Business Media.
142. Dorigo, M., et al., *Ant system: optimization by a colony of cooperating agents.* 1996. **26**(1): p. 29-41.
143. Adleman, L.M., *Molecular computation of solutions to combinatorial problems.* Science, 1994. **266**(5187): p. 1021-1024.
144. Winfree, E., et al., *Design and self-assembly of two-dimensional DNA crystals.* Nature, 1998. **394**(6693): p. 539-44.
145. Reif, J.H., *Biochemistry. Scaling up DNA computation.* Science, 2011. **332**(6034): p. 1156-7.
146. Freyre-Gonzalez, J. and L. Trevino-Quintanilla, *Analyzing Regulatory Networks in.* 2010.
147. Pitkänen, E., et al. *A computational method for reconstructing gapless metabolic networks*. in *International Conference on Bioinformatics Research and Development*. 2008. Springer.
148. Dasika, M.S., A. Burgard, and C.D. Maranas, *A computational framework for the topological analysis and targeted disruption of signal transduction networks.* Biophysical journal, 2006. **91**(1): p. 382-398.
149. Dunne, J.A., R.J. Williams, and N.D. Martinez, *Food-web structure and network theory: the role of connectance and size.* Proceedings of the National Academy of Sciences, 2002. **99**(20): p. 12917-12922.
150. Fraenkel, A.S., *Complexity of protein folding.* Bull. Math. Biol., 1993. **55**(6): p. 1199-1210.
151. Pierce, N.A. and E. Winfree, *Protein design is NP-hard.* Protein Engineering, 2003. **15**(10): p. 779-782.
152. Hopfield, J.J. and D.W. Tank, *"Neural" computation of decisions in optimization problems.* Biological Cybernetics, 1985. **52**(3): p. 141-152.
153. Valiant, L.G. and V.V. Vazirani, *NP is as easy as detecting unique solutions.* Theoretical Computer Science, 1986. **47**(C): p. 85-93.
154. Nicolau, D.V., Jr., et al., *Parallel computation with molecular-motor-propelled agents in nanofabricated networks.* Proc Natl Acad Sci U S A, 2016. **113**(10): p. 2591-6.

155. Van Delft, F.C., et al., *Something has to give: scaling combinatorial computing by biological agents exploring physical networks encoding NP-complete problems.* 2018. **8**(6): p. 20180034.
156. Kheireddine, S., et al., *Dual-phone illumination-imaging system for high resolution and large field of view multi-modal microscopy.* Lab on a Chip, 2019. **19**(5): p. 825-836.
157. Shum, H., E.A. Gaffney, and D.J. Smith, *Modelling bacterial behaviour close to a no-slip plane boundary: The influence of bacterial geometry.* Proceedings of the Royal Society A: Mathematical, Physical and Engineering Sciences, 2010. **466**(2118): p. 1725-1748.
158. Shum, H., *Microswimmer propulsion by two steadily rotating helical flagella.* Micromachines, 2019. **10**(1).
159. Giacché, D., T. Ishikawa, and T. Yamaguchi, *Hydrodynamic entrapment of bacteria swimming near a solid surface.* Physical Review E, 2010. **82**(5): p. 056309.
160. Libberton, B., et al., *Efficiency of the flagellar propulsion of Escherichia coli in confined microfluidic geometries.* Physical Review E, 2019. **99**(1).
161. Figueroa-Morales, N., et al., *E. coli "super-contaminates" narrow ducts fostered by broad run-time distribution.* 2020. **6**(11): p. eaay0155.
162. Blainey, P.C., *The future is now: Single-cell genomics of bacteria and archaea.* FEMS Microbiology Reviews, 2013. **37**(3): p. 407-427.
163. Wang, X., et al., *Enhanced cell sorting and manipulation with combined optical tweezer and microfluidic chip technologies.* Lab on a Chip, 2011. **11**(21): p. 3656-3662.
164. Pallottino, S.J.N., *Shortest-path methods: Complexity, interrelations and new propositions.* 1984. **14**(2): p. 257-267.
165. Skoge, M., et al., *A worldwide competition to compare the speed and chemotactic accuracy of neutrophil-like cells.* 2016. **11**(6).
166. Jain, N.G., et al., *Microfluidic mazes to characterize T-cell exploration patterns following activation in vitro.* 2015. **7**(11): p. 1423-1431.
167. Nakagaki, T., *Smart behavior of true slime mold in a labyrinth.* Res Microbiol, 2001. **152**(9): p. 767-70.
168. Saman, A.B.S. and I. Abdramane, *Solving a reconfigurable maze using hybrid wall follower algorithm.* 2013.
169. Agladze, K., et al., *Finding the optimal path with the aid of chemical wave.* Physica D: Nonlinear Phenomena, 1997. **106**(3-4): p. 247-254.
170. Adamatzky, A., et al., *Experimental reaction–diffusion chemical processors for robot path planning.* Journal of Intelligent and Robotic Systems, 2003. **37**(3): p. 233-249.
171. Weber, A., et al., *Rectification of Bacterial Diffusion in Microfluidic Labyrinths.* 2019. **7**: p. 148.
172. Ayrinhac, S.J.P.E., *Electric current solves mazes.* 2014. **49**(4): p. 443.
173. Adamatzky, A.J.P.L.A., *Hot ice computer.* 2009. **374**(2): p. 264-271.
174. Nair, A., et al., *Maze solving automatons for self-healing of open interconnects: Modular add-on for circuit boards.* 2015. **106**(12): p. 123103.
175. Scherber, C., et al., *Epithelial cell guidance by self-generated EGF gradients.* 2012. **4**(3): p. 259-269.
176. Tokárová, V., et al., *Patterns of bacterial motility in microfluidics-confining environments.* 2021. **118**(17).
177. Nicolau Jr., D.V., et al., *Parallel computation with molecular-motor-propelled agents in nanofabricated networks.* Proceedings of the National Academy of Sciences, 2016. **113**(10): p. 2591-2596.

Appendix A

SUPPORTING INFORMATION

Patterns of bacterial motility in microfluidics-confining environments

Viola Tokárová, Ayyappasamy Sudalaiyadum Perumal, Monalisha Nayak, Henry Shum, Ondřej Kašpar, Kavya Rajendran, Mahmood Mohammadi, Charles Tremblay, Eamonn Andrew Gaffney, Sylvain Martel, Dan V. Nicolau Jr., Dan V. Nicolau*

1. Detailed Experimental Section

1.1. Experimental protocols

1.1.1. *Bacterial species*

Five bacterial species living in micro-environments were studied, presented here in an increased order of architectural complexity. *Vibrio natriegens* is a rod-shaped, polar uni-flagellated bacterium. (1, 2) *Magnetococcus marinus* (MC-1) is a spherical bacterium with two clusters of seven flagella at one polar end (3, 4), *Pseudomonas putida* (ATCC® 12633™) (5, 6) and *Vibrio fischeri* (Ward's Science 15-5722) have rod-shaped bodies, (7, 8) and are polar-multi-flagellated bacteria. *Escherichia coli*MG1665 (K12-wild type) is a rod-shaped bacterium with a peritrichous flagellar machinery. (9-12) **Figure 3** (main text) and **Table S1** present the characteristics of the five bacterial strains used in this study, and **Figure S1** presents detailed SEM images of individual bacterial cells. All the cultures, except *M. marinus*, were maintained in agar plates and cultured in Luria-Bertani (LB) medium prior to the experiments. *P. putida* and *V. fischeri* were cultivated at room temperature (RT), as reported else where (5) while *E. coli* and *V. natriegens* were cultivated at 30ºC. *E. coli* and *V. natriegens* were genetically transformed with a plasmid to express mCherry for visualization and tracking in microfluidic devices. *E. coli* and *V. natriegens* were transformed to constitutively express the plasmid pMF440-mChe (a gift from Dr. Michael Franklin's lab, Addgene Plasmid #62550). The plasmids express mCherry, a red fluorescent protein in bacteria to visualize them in our experiments using fluorescence microscopy techniques. *M. marinus* was cultivated and maintained at École Polytechnique de Montréal, Canada, in a microaerophilic, chemo-hetero lithotrophic chemically-defined medium, rich with ferrous ions, grown in dark, at room temperature, as described earlier (3), while a 24hrs to 48hrs culture was used for microfluidic experiments.

1.1.2. Design and fabrication of the microfluidics networks

The microfluidic chip for probing bacterial motility (**Figure 3C**, first left) comprises parallel reservoirs with widths of 2mm, connected through 1 mm-wide 'bus' channel (**Figure 3C**, second left). Every area consists of 1 mm x 1 mm structures of 5 x 5 identical geometries separated by open spaces ('plazas') of 100µm x 100µm (**Figure 3C**, third left).

The quantification of specific motility parameters required specific designs of the microfluidic structures **(Figure 3C**,third left, clockwise direction), as follows: (i) a set of linear, 100 µm-long channels (**Figure S2A**) with various widths, i.e., 2, 3, 4, 5, 6, 7 and 8µm, probed the linear movement and possible U-turns (~ 180°); (ii) zig-zag channels, 'combs', with 5, 10, and 15µm-long teeth length (**Figure S2C**), presenting 90° angles for each tooth, probed the corner preference and wall guiding behavior; (iii) 3.5µm-wide channels (**Figure S2B**) presenting different sideways angles, i.e., 0°, 30°, 45°, 60°, 90°, 120°, 135°, and 150°, probed the deflection of movement and turn angle preferences; and (iv) 100 x 100 µm chambers, 'plazas', with two entrances opposite to each other on opposite walls (Figure S2). The microfluidic chip was made of polydimethylsiloxane (PDMS) through the replication of a positive-relief silicon master, fabricated by standard photolithography. (9, 13) The mixture of PDMS and cross-linker (weight ratio 10:1) was poured onto the silicon master, degassed inside vacuum chamber to remove air bubbles, and cured at 65°C overnight to ensure full cross-linking. After cutting and peeling off, the PDMS replica was treated in air plasma for 30 seconds to render the surface hydrophilic, before irreversibly bonding it onto the glass coverslip (also plasma-activated for 30 seconds).

1.1.3. *Impact of the distance between horizontal planes*

In chambers with lateral dimensions considerably larger than the size of bacterial cells, and if the horizontal surfaces are placed at a distance that allows the decoupling of their impact, bacterial motility is limited only by one of the horizontal planes (and by the vertical walls and corners placed at large distances from each other). However, to avoid the sagging, or outright collapse of the top horizontal plane in PDMS microfluidic chambers, the optimal height/width ratio is around 0.05, (14) i.e., approximately 5 µm for a 100x100 µm chamber. Because bacteria approach walls diagonally, a conservative design of the microfluidics structures required that the distance between the horizontal walls be larger than the vertical projection of the bacterium length (cell body and flagella) at a 45° diagonal. For the dimensions of the bacteria studied, this condition was fulfilled, for all species, by a height of 6 µm (**Figure 3A, Table S1**). Conversely, this condition was not fulfilled for any of the species studied at a height of 4 µm, with *E. coli, V. fischeri, M. marinus, P. putida,* and *V. natriegens*, exceeding the 4 µm clearance, in this order (**Figure 3B**).

Indeed, the motility behavior in large chambers with low ceilings presented evidence of the coupling of the impact on both horizontal planes on bacterial motility, i.e., a considerable alteration of the distribution of deflection angles of the 2D projections of bacterial trajectories (**Figures S3**), which appeared to be more pronounced for species with characteristic length larger than the 4 μm clearance. A finer analysis of the bacterial 3D trajectories revealed a much narrower distribution of the curvatures of these trajectories, for all species, for 4 μm tall plazas compared with those in 6 μm tall plazas (**Figure S4**). These streamlined trajectories appear be the result of the increased confinement by both horizontal walls of the chambers with 4 μm heights.

A similar analysis for plazas with 4μm heights (**Figure S5**) and the characteristic trajectories (presented in **Movie S1**) also showed important differences in the motility behavior of all bacteria. Consequently, more detailed motility experiments were performed extensively in 6μm-tall microfluidic structures.

1.1.4. *Motility experiments*

Immediately after sealing the PDMS structure on the coverslip, the microfluidics chip was flooded with the working buffer, i.e., LB medium for *V. natriegens. putida, V. fischeri, E. coli*, and Phosphate-Buffered Saline (PBS) buffer for *M. marinus*, for 1 hour to pre-wet the microfluidic structure, then stored inside a wet chamber at 4°C before use. Separately, a log-phase bacterial suspension was introduced into the microfluidics chamber through the open ends of the PDMS stamps and left in contact for few minutes to allow of bacteria to enter the channels and plazas (Figure 1 C, first on the left). To ensure that the bacterial chemotaxis free motility is the only, or the over riding mechanism at play, t he working fluids have an excess of nutrients, and the experimental time is short enough (few minutes inside the confined environment) to ensure that the level of nutrients remains practically constant. Furthermore, the bacterial population in microenvironments never reached the population density of log phase or stationary phase (15, 16), during which other factors, e.g., quorum sensing, or chemotaxis could play a role in space searching and foraging for nutrients.

1.1.5. Image acquisition and analysis

Bacterial flagella were stained using Hardy Diagnostics Flagella Stain following the product protocol and visualized by optical microscopy (Olympus IX83, U PLAN S APO 100X oil objective). The scanning electron microscopy images of b bacterial cells and PDMS structures were obtained using a Quanta FEI450 SEM and Hitachi S 3400N SEM system. The image acquisition of M. marinus used a specially designed inverted Zeiss AxioImager Z1m microscope with AxioVision

Software Sonny HD 1000 camera (with VirtualDub 1.10.4 software), LD Epiplan 20x (NA 0.4) and N Achroplan 10x (NA 0.25) objectives. The dark field imaging system enhances the contrast between bacterial cell and surrounding structures, which is necessary for further image analysis of fast swimming bacteria such as *M. marinus*. The experiments with *V. natriegens*, *P. putida*, *V. fischeri*, and *E. coli* were performed on a system mounted on an inverted, Spinning Disk Confocal Olympus IX83 microscope, with MetaMorph® Microscopy Automation & Image Analysis Software (Molecular Devices), and 10x (NA 0.4), 20x (NA 0.75) and 40x (NA 0.95) Differential Interfer ence Contrast (DIC) objectives. The duration of image acquisition was based on type of imaging like bright field microscopy (for *M. marinus* MC 1 and *P. putida*) or with fluorescence microscopy (*E. coli*, *V. natriegens*, and *V. fischeri*). Depending on the type of acquisition, a different exposure was used, and the frames used for plotting density maps, or another trajectory analysis were normalized accordingly. Density maps also used the average number of bacteria per frame.

ImageJ 1.50a (17), a public domain software, has been used for image analysis, density map reconstructions, and time resolved bacterial tracking. The density maps of bacterial movement inside confined structures were prepared from original RGB image stack as follows: (i) a median of 8 bit image stack (a background) was created using a 'Z Project' function; (ii) a new stack was created as a difference between the original stack and the background; (iii) the histogram of a new stack was adjusted and converted to a binary image; (iv) the binary operations 'Close' and 'Dilate' were applied to remove the remaining noise; and (v) all binary images w ere superimposed into one image. In some cases, the density map created by the procedure described above was accompanied by a high level of noise near the walls of the channels, due to the non uniform light

conditions in the optically transparent PDMS chip. In such cases, the original stack of n images was duplicated in the range of 1 to n 1 and 2 to n. Thus, the difference |Img2 Img1| between stacks shifted by one frame highlighted the bacterial movement without the background and light related noise. Th is difference, used to calculate the absolute change between two images, is important, since bacteria have also free movement along the vertical z axis, in and out of the focal plane, in the range limited by the height of the PDMS structures. The new image stack was processed by steps (iii) iii) --(v) described above to create the respective density maps. The trajectories of the single bacterium were tracked by the automatic (TrackMate, ImageJ), and the manual (MTrackJ, ImageJ) plugins (18). The TrackMate plugin, using LAP tracker algorithm, was used for *M. marinus*, which exhibits a quasi-linear motion, with low deflection angles thus making the analysis amenable to automation. The settings for this 2-parameter tracker were chosen to reach the maximum distance between the two consecutive points of one trajectory, at a given time, with a time gap set to three frames. However, because *P. putida* and *V. fischeri* tend to swim along the walls, thus leading to the possibility of

interrupted trajectories, the automatic tracking required more statistical data. The image analysis of these species used the manual MTrackJ plugin, with a dark/white centroid snap feature, with a point-and-click tracking. To facilitate automatic tracking, we used fluorescently labelled *E. coli* and *V. natriegens*. In all cases, the acquired x-y-time coordinates were used for calculating the velocity and the deflection angle from trajectories of individual bacteria. All experiments and image analysis were performed in biological replicates, with at least 3 sets of experiment for each bacterial species in each motility structure. For analysis and probability/fraction % representation, at least 200-300 independent bacterial count were used in multiple sets, to obtain a high confidence data and a statistical significance of $P<0.005$. For the density map, a fixed number of frames with average bacterial count ($n=18\pm7$) on each frame in any particular motility structure for any bacterial species was kept standard, so that the density map intensity was comparable to minimum and maximum values for each motility structure under discussion.

For imaging bacterial trajectories in 3D, we used the piezo-stage controller of Olympus IX83, confocal microscope for rapid acquisition of z-stacking of the bacterial trajectory. The devices of 6µm tall plaza were z-stacked at a step size of 2µm for 12µm. In total 7 images were captured at an exposure of 10ms (a total of ~90ms to 100ms per time point). For plotting trajectory analysis, the tracking was done manually, followed by the intensity-based segregation of trajectory points for each z-planes with highest fluorescence or bright field intensity. (19) This highest intensity bacterial corresponds to 'in focus' bacterial trajectories and marks the z-plane maximum for each time point. We used 'Origin' software for plotting the 3D tracks as described in the Results and discussion section.

1.1.6. Imaging for mapping 3D motility patterns of bacteria in 6µm plaza

For imaging bacterial trajectories in 3D, we used the piezo-stage controller of Olympus IX83, confocal microscope for rapid acquisition of z-stacking of the bacterial trajectory. The devices of 6µm tall plaza were z-stacked at a step size of 2µm for 12µm. In total 7 images were captured at an exposure of 10ms (a total of ~90ms to 100ms per time point). For plotting trajectory analysis, the tracking was done manually, followed by the intensity-based segregation of trajectory points for each z-planes with highest fluorescence or bright field intensity. (19) This highest intensity bacterial corresponds to 'in focus' bacterial trajectories and marks the z-plane maximum for each time point. We used 'Origin' software for plotting the 3D tracks as described in the Results and discussion section.

1.2. Bacterial species

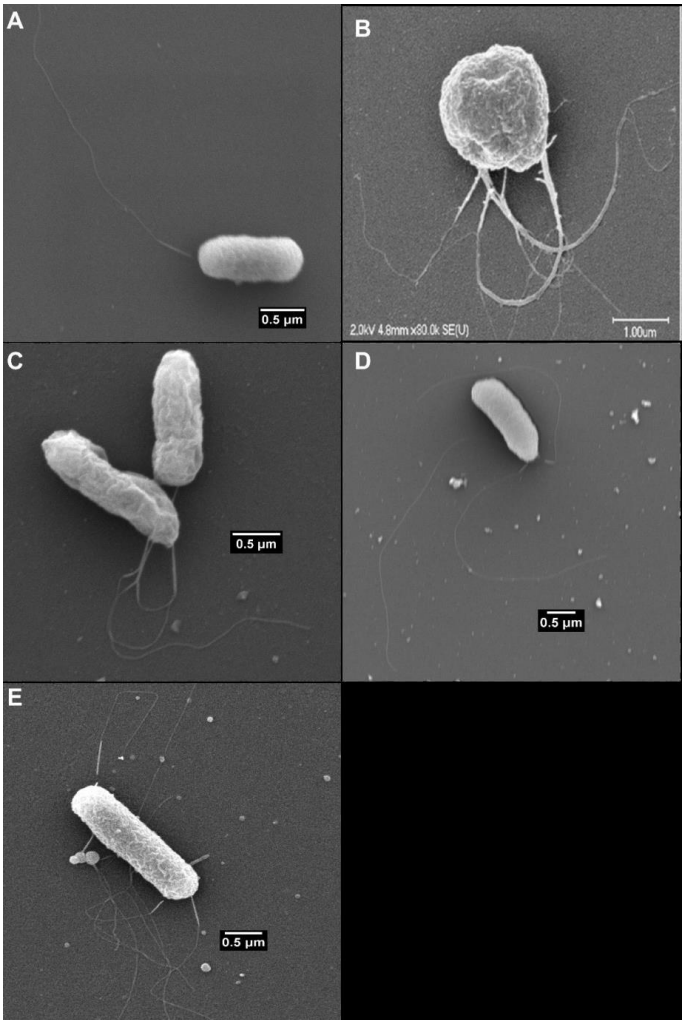

Figure S1. Scanning electron images of the bacteria used in this study, having different flagellar architectures. (**A**) *V. natriegens* with single polar flagella; (**B**) *M. marinus*, bi-flagellated (**C**) *P. putida* with multiple polar flagella; (**D**) *V. fischeri* with multiple polar flagella; (**E**) *E. coli* K12 with multiple lateral flagella (peritrichous arrangement).

Bacteria	***V. natriegens***	***M. marinus***	***P. putida***	***V. fischeri***	***E. coli***
Cell: Length [µm] Width [µm]	1.5 ± 0.5 0.9 ± 0.1	1.9 ± 0.2 1.9 ± 0.2	1.6 ± 0.3 0.6 ± 0.2	1.8 ± 0.1 0.6 ± 0.1	1.9 ± 0.6 1.0 ± 0.2
Flagellum/-a Architecture Length [µm]	One 4.7 ± 0.9	Two bundles 4.0 ± 0.8	Polar multiple 3.9 ± 0.8	Polar multiple 5.1 ± 1.1	Peritrichous 4.7 ± 1.4
Velocity[µm. s-1]	15-20	Up to200	27 -44	60-100	< 20
Habitat	Marine, or fresh water	Marine	Soil	Marine (free; or fish, squid)	Ubiquitous, intestine/gut
Aerobic	Aerobic	Micro-aerophilic	Aerobic	Aerobic	Facultative anaerobic
Media	LB, LB-V2 salt medium	Chemo-hetero-lithotrophic	LB broth/agar	LB broth/agar	LB broth/agar

Table S1. Characteristics of the motile bacteria used in this study

1.3. Microfluidics structures and their characteristic dimensions

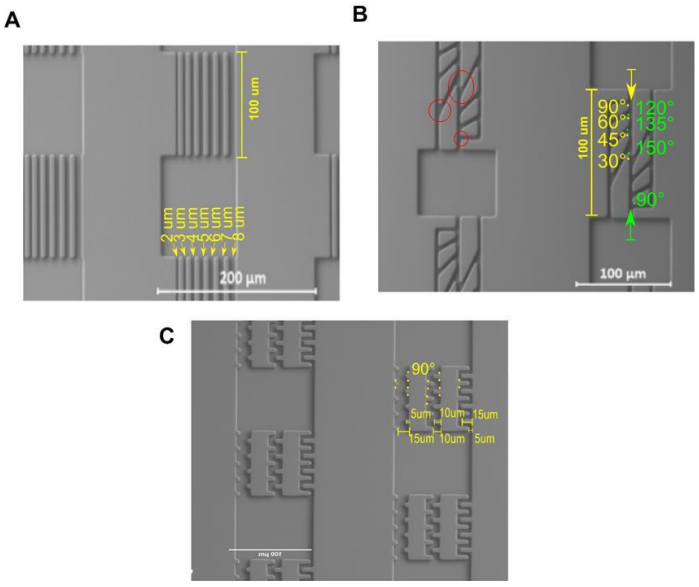

Figure S2. Scanning electron microscopy (SEM) images of PDMS microfluidic structures for the probing of the bacterial motility, separated by quasi-open spaces. **A**. Linear channels with different widths, from 2 µm to 8 µm. **B.** Turn-angle chip presenting eight different angles (0°, or straight path, and 30°, 45°, 60°, 90°, 120°, 135°, and 150° angles). Note the various volumes available for motility at the intersection of the axial and lateral angle, for 90°, 30°/150°, and 150° angles (red circles, top left). **C.** Meandered channels with three different tooth lengths (5 µm, 10 µm, and 15 µm).

2. Results and Discussion

2.1. Motility in large chambers

2.1.1. Impact of the distance between horizontal planes

2.1.1.1. Turn angle preference from 2D trajectories

To assess the possible coupling of the interaction of the horizontal plane in plazas, for 4 and 6 μm heights, respectively, the *turn angle preference* of motility was calculated, in the first instance, using 2D projections of the 3D trajectories (**Figure S3**).

It was found that the turn angle preference was considerably different for plazas with 4 μm, and 6 μm heights, respectively. Importantly, this difference appears to be larger for bacteria whose characteristic lengths are larger than the clearance of 4 μm heights (**Figure 3B**), with the notable exception of *E. coli*.

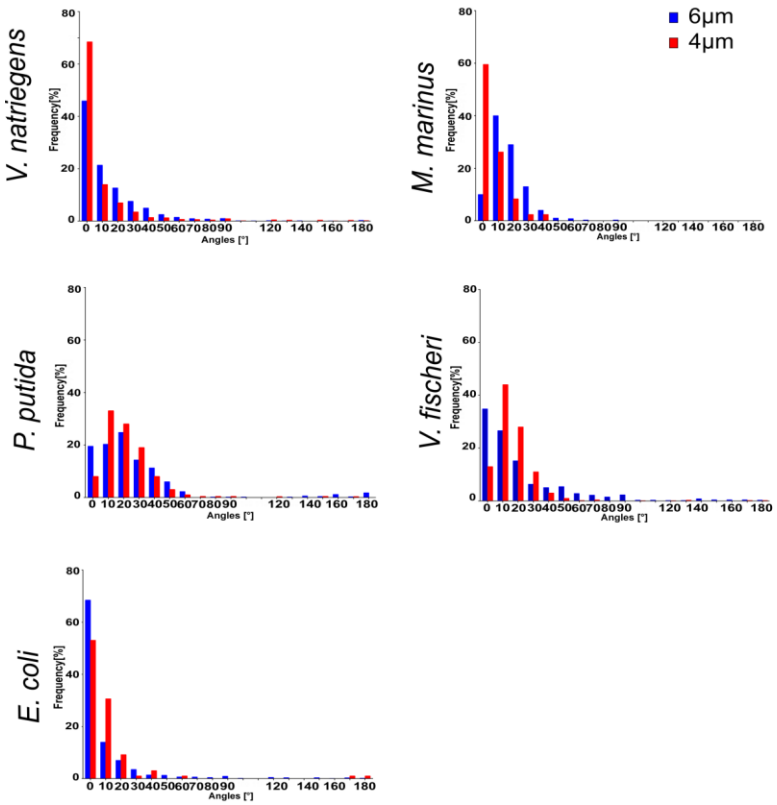

Figure S3. Frequency of the deflection patterns for five different bacterial species, i.e., *V. natriegens, M. marinus, P. putida, V. fischeri,* and *E. coli,* each labelled at the side of the graph, analyzed from the 2D projections of trajectories data collected in the 4 and 6 μm-high plazas.

2.1.1.2. Curvature analysis from 3D trajectories

A finer analysis of the possible coupling of the interaction of the top and bottom horizontal walls of the plazas is possible through the analysis of the representative 3D trajectories. To this end, twenty individual trajectories, each for each plaza with both 6µm, and 4µm heights, and for each bacterial species, respectively, were used for *curvature analysis*, with positive values corresponding to clockwise, and negative values corresponding to counter clockwise rotations. The median curvature value was calculated for each trajectory and twenty trajectories of each species and both heights were compared (**Figure S4**), as follows: for parametrized trajectories [x(t), y(t)], the curvature k is k (x0, y0) = [x-1·y-1–x1·y1]/ [(x-12+ y-12)3/2], where -1, 0, 1, represent the temporal sequence. Even a cursory inspection of the distribution of the average curvature for all bacteria showed much streamlined trajectories, that is, the considerably narrower distribution of curvatures, which could be understood only by the constrained applied by both horizontal walls.

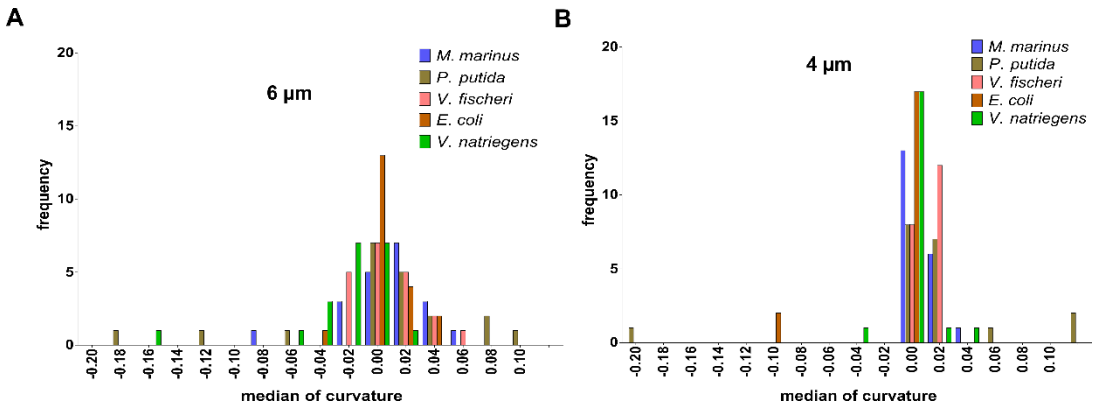

Figure S4. Curvature analysis of trajectories in plazas with 6 µm (A) and 4 µm (B) heights.

2.1.1.3. Preliminary analysis of bacterial motility in 4 µm tall plazas

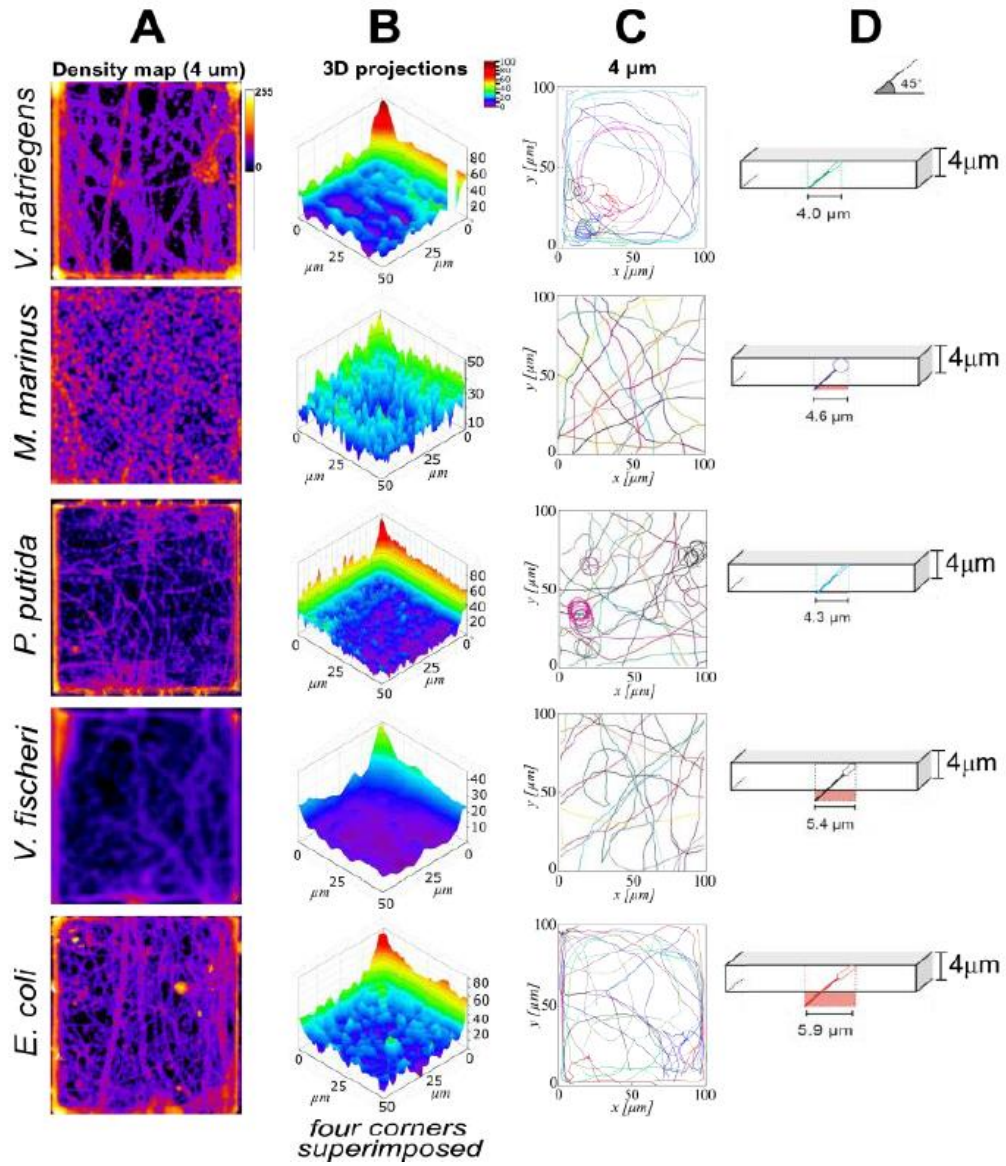

Figure S5. Motility in plazas with 4µm heights. **A**. Density maps of bacterial locations. **B**. Probabilities of bacterial positions. Note the differences in spatial distribution of probabilities compared with those for plazas with 6µm heights**. C.** Characteristic longest trajectories of bacterial motility. Note the differences in trajectory features compared with those for plazas with 6µm heights. **D**. Projection of bacterial length fit across the height of the chamber at 45º.

Detailed explanations for Figure S5. **A.** Density maps of bacterial locations in plazas. Left column; "0 (min)" and "255 (max)" represent the color-coded heat map of no/highest bacterial population, respectively. **B.** Estimation of probabilities of positions, estimated from the 2D projections of the bacterial positions on a horizontal plane, followed by superimposition of the four corners of the density maps of the plaza (similar procedures as in **Figure 4B**, but presented here in 3D). Left

column; “0 (blue, min)” and “100 (red, max)” represent the color code for bacterial density along the corners and the walls. **C.** Characteristic longest trajectories of bacterial motility, as 2D projections. **D**. Graphical projection of bacterial length fit across the height of the at 45º. By rows, from top to bottom: *V. natriegens* (average count of bacteria in each frame, n = 14/frame); *M. marinus* (n = 12/frame); *P. putida* (n = 15/frame); *V. fischeri* (n = 15/frame); and *E. coli* (n = 13/frame). Movie S1 presents bacterial overall movement in plazas, and representative trajectories **(similar to C).** Note the rather considerable difference between the long trajectories **(column C)** compared with equivalent representation for trajectories in **Figure 4C**.

2.1.2. Overall spatial density.

2.1.2.1. Quantification of bacterial positions at a distance from the horizontal walls in the plazas

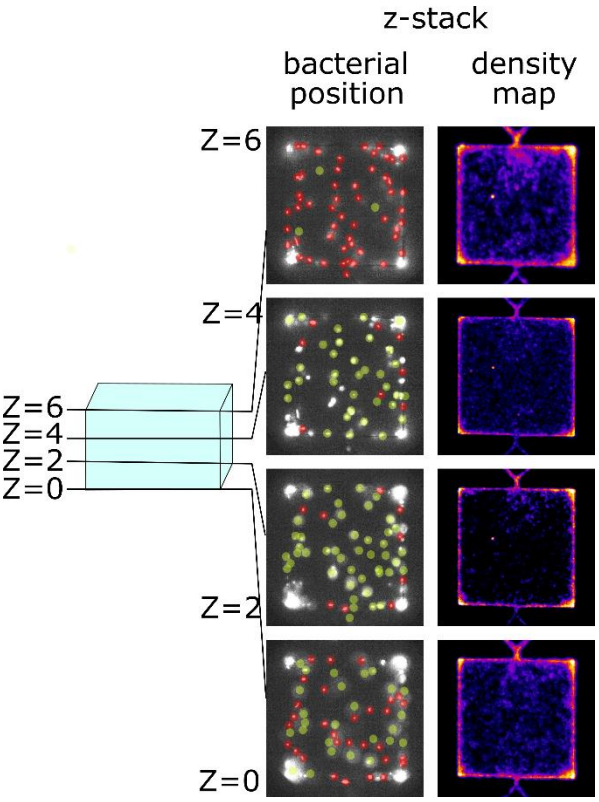

Figure S6. Quantification of bacterial positions using z-stack imaging of the plazas volume (representative analysis for *E. coli*). **A.** Schematic representation of the chamber, with four z-stacked planes, distanced by 2 μm step size. **B**. Assigning of the position of bacteria. The yellow circles over fluorescent signal represent the bacterial species that are out of focal plane, while the red circled overlapped over the fluorescing bacteria represent the bacterial outside the focal planes. **C.** Density maps for the representative z-resolved *E. coli* imaging at different levels. The density maps show that most of bacteria were placed close to the top and bottom horizontal planes.

2.1.2.2. 3D trajectory analysis and z-positioning of five bacterial species in tall plazas.

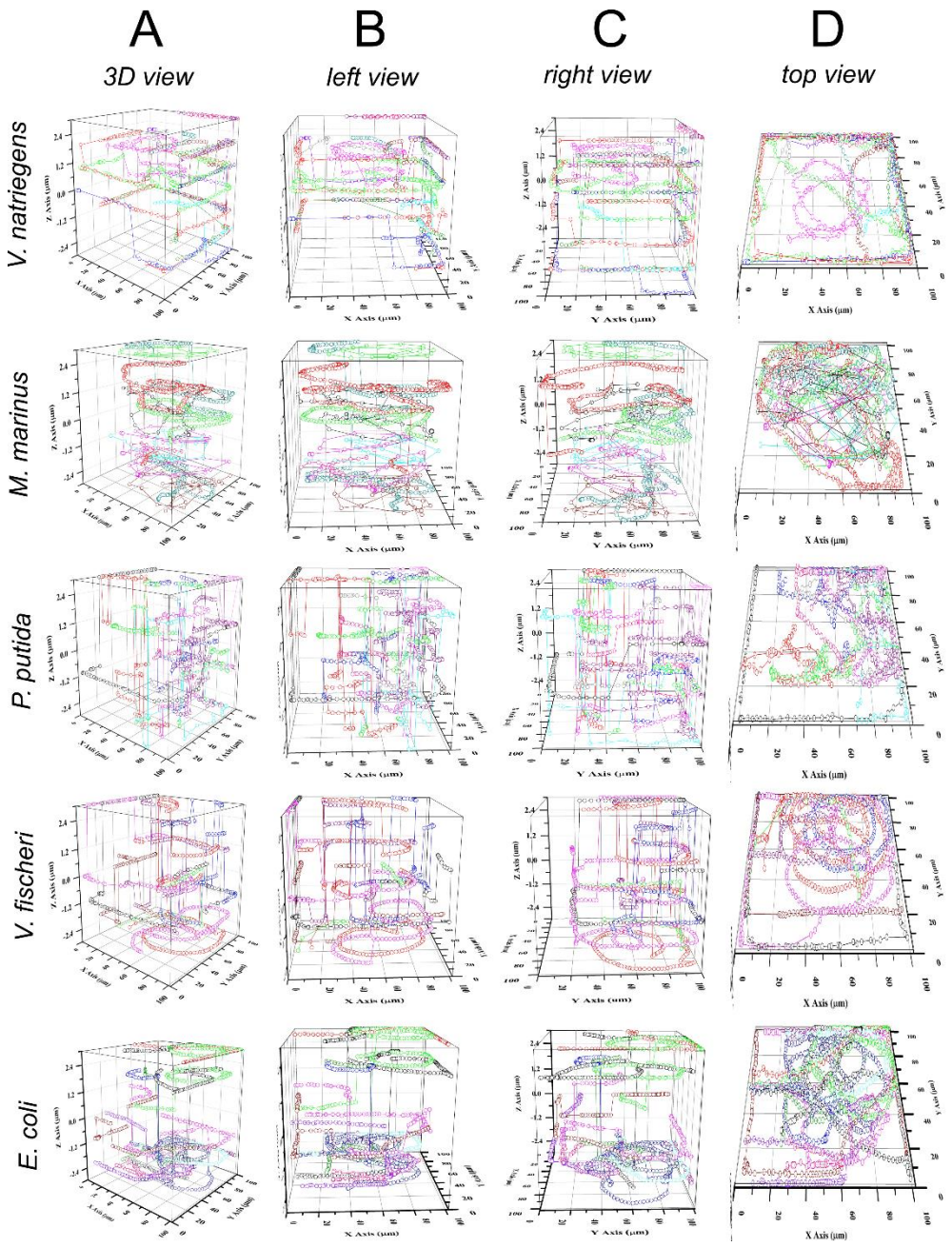

Figure. S7. Representation of bacterial trajectories in 3D using z-stack imaging in plazas. Most of trajectory lengths (density of bacterial positions) were close, and often parallel to the adjacent wall. The transitions between one plane to the opposing one occurred quickly (few points, in few ms). For *M. Marinus* (presenting helical motility patterns) and *P. Putida*, most trajectories were placed away for the horizonal planes, especially in the center for the plaza. Images represent different view angles of the 3D trajectories (complementing **Figure 2D**).

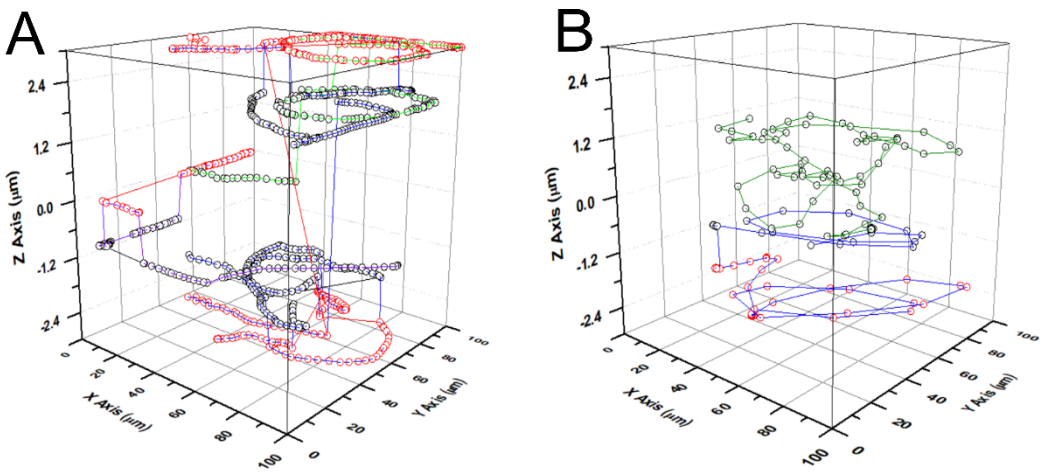

Figure S8. Comparison of two bacterial species with opposite motility behavior. **A**. *E. coli* moves in planes parallel to the walls, at different distances. **B**. *M. marinus* does not move in a parallel plane, thus flipping from a wall accumulator to a wall escaper behavior.

2.1.2.3. Estimation of the distance of swimming parallel to the walls

The first estimation of the distance bacteria swim away from the wall was provided by the "probability map" **(Figure 4B).** This estimation was statistically precise, but it suffered from the edge effects, as the walls the bacteria are swimming near are only 6 µm in width. A fundamentally better (but statistically weaker) option is to collect the z coordinates of the 3D trajectories in the central region of the plazas, i.e., away from edge effects, and then to construct histograms of the bacterial presence away from the horizontal walls **(Figure S9).**

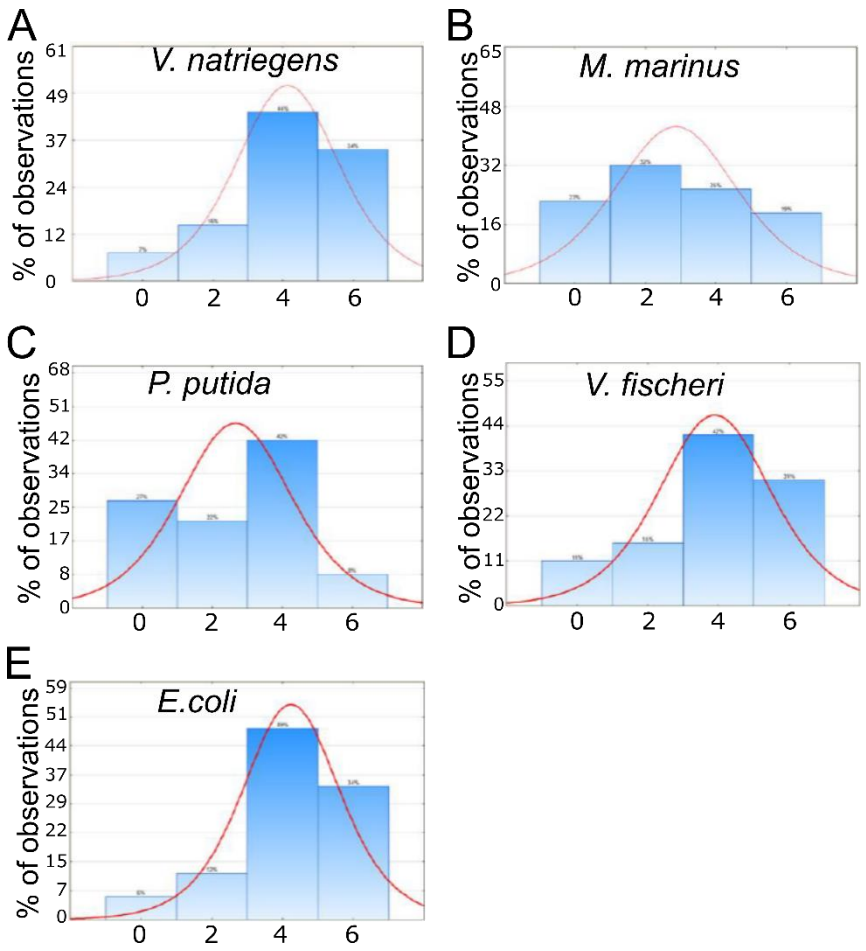

Figure S9. Histograms of the positions of bacteria away from horizontal walls (either ceiling, or floor) of the plazas. From top to bottom: **A.** *V. natriegens;* **B**. *M. marinus;* **C**. *P. putida*; **D.** *V. fischeri*, and **E.** *E. coli*. The logistic fit was used to determine the average bacterial position along vertical axis, and it does not reflect an actual distribution for *M. marinus* and *P. putida*.

2.1.2.4. Simulation of motility of monotrichous bacteria near wall

Numerical results for boundary interactions shown in **Figure 5** are upgraded from previous work. (20) The data were generated as follows. A model bacterium is considered consisting of a spheroidal cell body propelled by a single rigidly rotating flagellum. Body and flagellum shapes based on experimental measurements are depicted in **Figure 5**. The variable $\bar{a}$ is defined as the characteristic length scale of the body. The choice of semi-major axis a_1 and semi-minor axis a_2 of the body result in various aspect ratios a_1/a_2 while maintaining a fixed cell volume

$V = (4/3)\pi a_1 a_2^2 = (4/3)\pi \bar{a}^3$

The values of $\bar{a}$ based on cell lengths andwidths for the studied bacteria are given in **Table S2**. In addition to the body aspect ratio, the length of the model flagellum is varied, keeping its helical pitch and amplitude fixed.

For each set of geometry parameters, a Boundary Element Method was used to numerically calculate the velocity of the bacterium placed in a given configuration specified by the distance h and orientation angle θ relative to a solid wall. The instantaneous translational and rotational velocities of the bacterium are determined by satisfying the equations of Stokes flow subject to no-slip boundary conditions on the surface of the cell body, flagellum, and wall. The propulsive thrust generated by rotating the flagellum is generally not exactlyaligned with the axis of the body, leading to a slight wobbling motion. To determine the average velocity over timescales longer than a motor revolution, the instantaneous velocities was calculated at uniform increments of the angular phase of the flagellum relative to the body and take the mean value. This process allows us to define an average vertical speed $\frac{dh}{dt}$ and rate of turning $\frac{d\theta}{dt}$ that depend on h the current and θ

For some bacterial shapes, it was found that there is a certain combination of distance and orientation, denoted (h^*, θ^*) at which $\frac{dh}{dt} = 0$ and $\frac{d\theta}{dt} = 0$. This is an equilibriumconfiguration because the swimmer remains at this height and orientation indefinitely. Moreover, this is a stable equilibrium because bacteria starting at other configurations, provided they are not pointing too sharply away from the surface, would approach the equilibrium point. Bacteria with such an equilibrium point are referred in this study as‘swimmers parallel to wall’ because they tend to remain in this plane (which is close to boundaries). This regime is placed at the top right quadrant in **Figure 5**. The stable configuration was computed for various combinations of the cell body aspect ratio andflagellum length and the stable height was graphically presented by a color scale in $h^*$the upper right of **Figure 5**.

As the body aspect ratio decreases (approaching a spherical shape) for a fixed flagellum length, it was found that the stable height decreased until the bacterium became too close to the wall for numerical methods to be reliable. Since these model bacteria also have a strong attraction to walls, in fact descending into walls, they are classified in this study as ‘boundary accumulators. This regime is placed, approximately, at the top left quadrant in **Figure 5**.

Starting from boundary accumulators with a computed stable configuration, decreasing the flagellum length increases the stable height. There is a region of rapid transition from $h^*/\bar{a} \approx 1$ (where the cell body is very close to the wall) to $h^*/\bar{a} > 5$. Beyond this point, the stable height

is far enough from the wall that hydrodynamic interactions are negligible. In this regime, located in the lower portion of Figure 5, the bacteria turn and swim away fromthe wall even if they are initially approaching the wall, thus referred ‘boundary escapers.

The hydrodynamic explanation for why changes in the geometry of the bacterium affect its motion near walls is that the shape determines the distribution of stresses acting on the cell membrane and flagellum. The flow field generated by a swimming bacterium can be approximated by combinations of a force dipole, source dipole, and higher order terms that each produce different interactions with a wall. (21) The relative strengths of these terms, and hence the net behavior near walls, depend on the shape of the organism.

Table S2. Characteristic geometrical parameters of the bacteria studied used for the simulation of motility behavior (monotrichous architecture model), as in Figure 3.

Parameter→ Bacteria↓	**a_1/a_2**	**$L/\bar{a}$**	**$h^*/\bar{a}$**	**$L+a_1$ (μm)**
V. natriegens	1.75 ±0.75	9.51 ±3.48	3.05	5.45 ± 2.30
M. marinus	10.2 ±0.21	4.35 ±1.30	1.35	4.95 ± 1.80
P. putida	3.19 ±1.56	10.84 ±5.03	2.47	4.70 ± 1.90
V. fischeri	3.11 ±0.69	12.34 ±4.15	3.73	6.00 ± 3.40
E. coli	2.10 ±1.02	8.64 ±4.33	2.74	5.65 ± 2.30

Legend (32):

a_1 = polar radius of cell body (half the cell length); a_2 = equatorial radius of cell body (half of the diameter diameter); [a_1/a_2] = aspect ratio of the cell body; L = curvilinear length of the flagellum (approximated by the axial length of the flagellum); $\bar{a}$ = radius of sphere with volume of cell body; $L/\bar{a}$ = aspect ratio of the bacterium; h^* = optimal distance from the wall(for swimmers parallel to the walls), determined in this study from the z-stack analysis (**Figure S9**); and $h^*/\bar{a}$ = non-dimensional distance from the wall.

2.2. Motility in tightly confining geometries

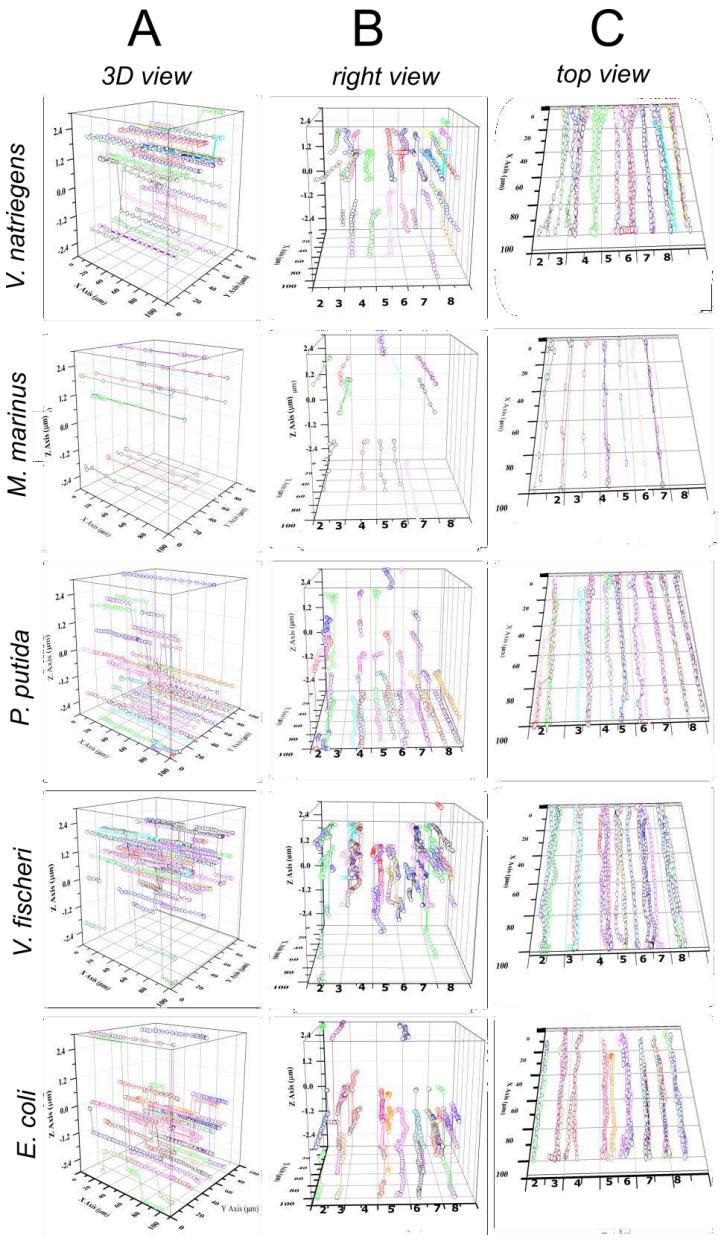

Figure. S10. Cumulative representation of trajectories of five different bacterial speciesprojected in 3D space using z-stack imaging in linear channels.

2.2.1.2. Analysis of the possible sinusoidal motion of bacteria in straight channels

2.2.1.2.1. Detecting potential helical motion from 2-dimensional camera data with multiple waveforms

We consider the general problem of determining, from 2D tracking data, whether a bacteriumis executing 3D helical motion or 2D, planar "sinusoidal" motion. To do this, we aim to convert 2D data to three dimensions, under the assumption the helical motion is taking place. This then allows us to essentially test the hypothesis of helical motion.

We begin by considering the directional components of the bacterial velocity, derived from positional data. Given a 2D track, we can compute $v_x(t)$ and $v_y(t)$, i.e., the x and y components, as a function of time, while $v_z(t)$, the z-component, is hidden from us due to the use of a point of view placed orthogonally to this axis. Given $v_x(t)$ and $v_y(t)$, our specific goal is to estimate the unobserved velocity component v_z.

Observe that the (unknown) magnitude of the total velocity is given by

$$V(t) = \sqrt{v_x(t)^2 + v_y(t)^2 + v_z(t)^2}$$

At any point where the bacterium is moving orthogonal to the axis of the camera, we have $v_z = 0$, such that the total velocity follows

$$V_\perp = \sqrt{v_x(t)^2 + v_y(t)^2}$$

We now assume (but see below) that the movement of the bacterium has no net drift in the z-direction. This implies the bacterium is moving orthogonal to the camera axis twice in each spiral of its 3D helix.

The total magnitude of velocity can be estimated as a smooth curve fit over the peaks of the $V_\perp$ curve, for instance using spline interpolation. At each peak, $v_z = 0$ and its sign alternates as the helically moving bacterium completes each corkscrew. This allows the estimation of v_z at all other points.

This approach has limitations, because of the loss of information from 3D information being projected into 2D. If the bacterium is moving toward or away from the camera for significant portions of its trajectory, our method is unable to estimate its total v_z component, absent further assumptions about the specific pattern of swimming. In addition, this estimation procedure is inaccurate if the trajectory is not close to a symmetrical, repeatable helix, e.g., if the helical motion

is highly stochastic. The technique is inaccurate in the absence of a sufficiently high number of data points, allowing a smooth spline to fit to be applied to the

$V_{\perp} = \sqrt{v_x(t)^2 + v_y(t)^2}$ curve. Lastly, it is not possible, by this approach, to determine the "handedness" of the helix. However, we note that for many bacterial species, the handedness is known or can be determined experimentally, because it is genetically controlled.

Perhaps most crucially, however, this method requires the available tracking data from the camera to contain multiple peaks and troughs of the trajectory, otherwise the spline fitting to the peaks of the $V_{\perp}$ curve is not possible. For situations where only one or less peak-to-troughsections are available, a different approach is needed.

2.2.1.2.2. Detecting potential helical bacterial motion from 2D camera data where only fragments of sinusoidal tracks are present

In this situation, it is possible to estimate the wavelength of the sinusoidal motion from fragments containing one or two peak-to-trough sections by employing a Fast Fourier Transform (FFT) analysis. Specifically, the FFT spectrum of the *x-y* curve (in 2D) will exhibit one dominant frequency if sinusoidal (potentially resulting from helical motion projected two-dimensionally) is present; otherwise, the spectrum will be highly noisy and/or flat.

We ran all tracks in different channel widths for all five bacterial species through an FFT analysis, leading to the ability to directly fit sine curves to the *x-y* trajectories and estimate thewavelength of the motion in the channel. This approach is illustrated (using a randomly chosen bacterial track from the data set) in Figure X.1 below, in which the right-hand side panel shows the results of the fitting procedure, and the left-hand panel shows the FFT spectrum, exhibiting a dominant frequency. From this, the motion wavelength can be estimated as the inverse of the dominant frequency (code available on request).

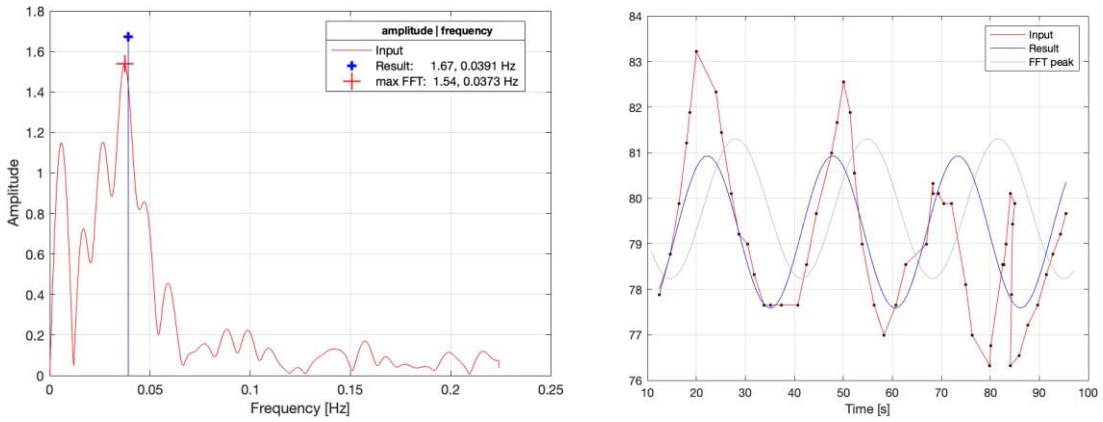

Figure S11. Left: FFT analysis of a bacterial track in a channel, allowing the identification of the frequency of the sinusoidal motion (and thereby the wavelength) as the peak of the FFT spectrum (blue line and red cross). Right: in red, the bacterial track projected as an x-y trajectory; in blue and gray, the resulting sine curve fits corresponding to the FFT peak frequency (gray) and average weighted frequency (blue).

2.2.1.2.3. Estimation of sinusoidal characteristics of bacterial motility in straight channels

We used this method to study the variation in sinusoidal movement (resulting from 3D helical movement) of different bacterial species in different channel widths from 2µm to 8µm. The results are shown in **Figure S12C**.

The sinusoidal character of the motion of *P. putida* and *V. natriegens* varies strongly with the widths of the linear channels, possibly due their shortest body lengths of all species studied. The increase of the wavelength of motion with the increase of the channel widths is probably due to the larger volume available for 3D helical movement. It is notable that a sinusoidal movement has been predicted (22) for monotrichous bacteria (such as *V. natriegens*) and for wall escapers (as partially exhibited by *P. putida*, **Figure 5**).

At the other end of the spectrum, *M. marinus*, with its frequent collisions with and bouncing from the walls, appeared to be insensitive to channel widths with regard to a sinusoidal character of movement.

Finally, in a medium class, *V. fischeri* and especially *E. coli* appear to have only a modest evolution of the sinusoidal character of movement with the increase of the channel widths, possibly due to their longest body lengths in all species studied.

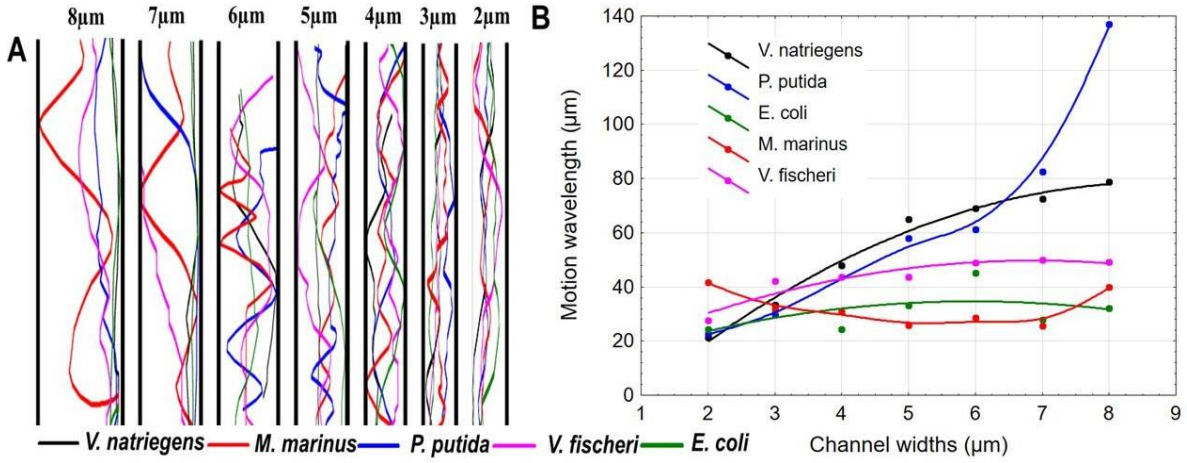

Figure S12. Representative trajectories in the linear channels (A, left); and the variation of the estimated motion wavelengths versus channel widths (B, right).

2.2.1.3. *Velocity in straight channels*

To assess the impact of confinement on bacterial velocity, the average velocity of bacteria was measured, in straight channels, and in plazas, the latter seen as straight channels with 100 µm widths (**Figure S13**).

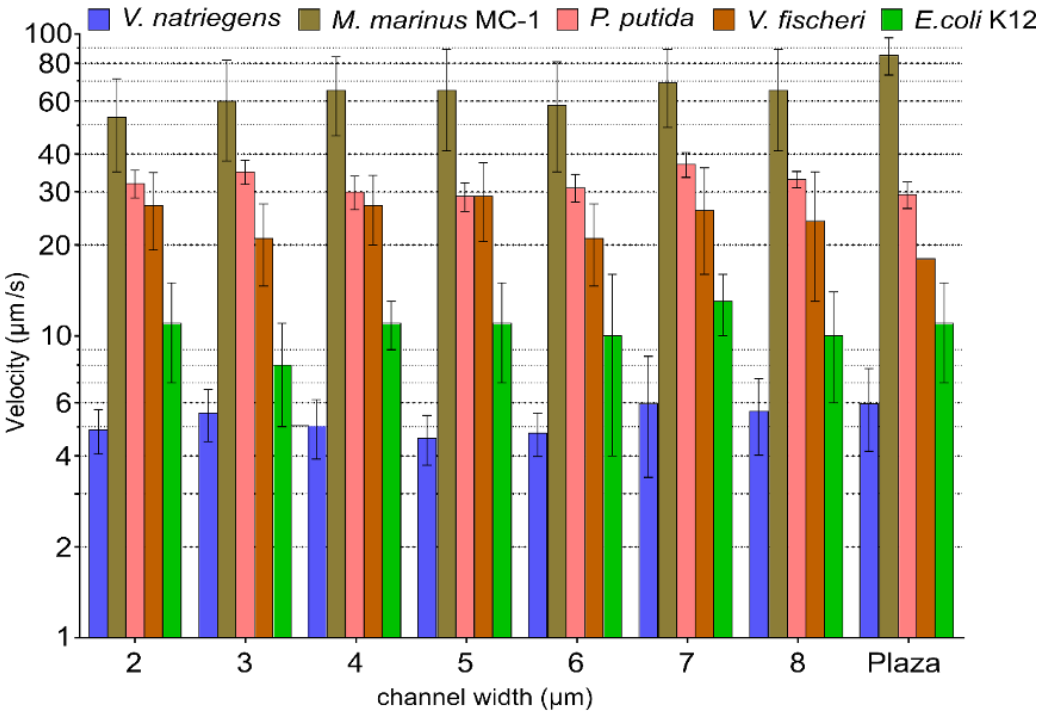

Figure S13. Bacterial velocities (logarithmic scale) in straight channels and plazas.

A moderate decrease was observed for the velocity of *M. marinus*, assumed to be a result of the amplification of the collisions with the walls, but for all other species the velocity does not vary importantly with the channel width.

This observation is further substantiated by the more precise and more detailed measurementsof velocities offered by double histograms of velocities in channels (**Figure S14**). Also, with the exception of *M. marinus*, for which extreme narrow channel 'force' motility at the walls, and *V. natriegens* and *E coli*, presenting a bimodal distribution of velocities, towards the channel center, and again a secondary bimodal distribution at the walls (as presented above), all other species behave as swimming parallel to the walls, that is, near the center of the channels, as predicted by **Figure 5**.

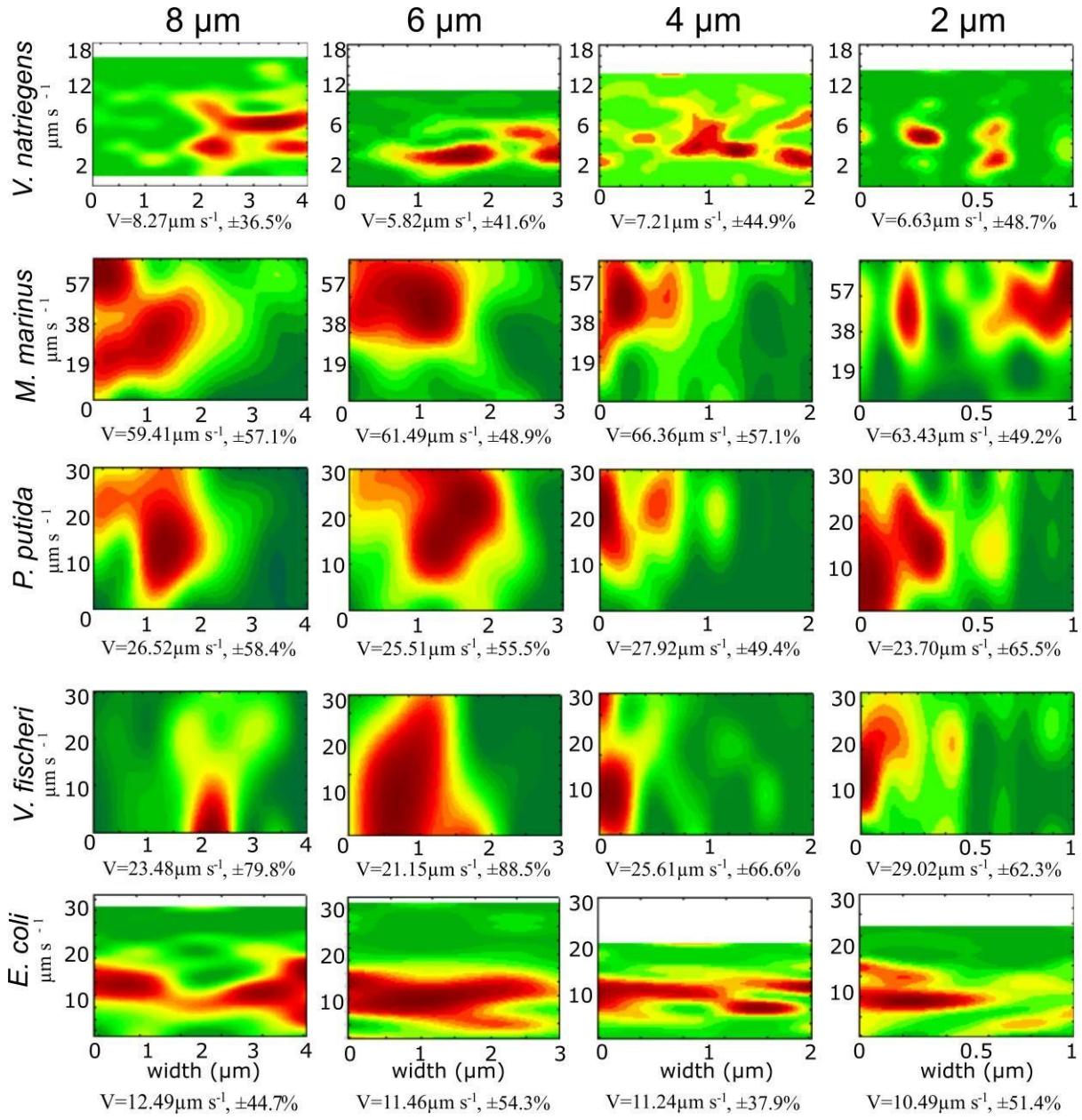

Figure S14. Double histograms of bacterial velocities in linear channels with 2 µm, 4 µm,6 µm, and 8 µm widths. All velocities values are normalized, i.e., top y-axis value is the maximum. The channel widths are also normalized, i.e., left value on the x-axis representsthe channel center, and the right value represents the wall. Note the resilient bimodal distribution, at the walls, for both *V. natriegens* and *E. coli*.

2.3. Motility in channels with angled exits

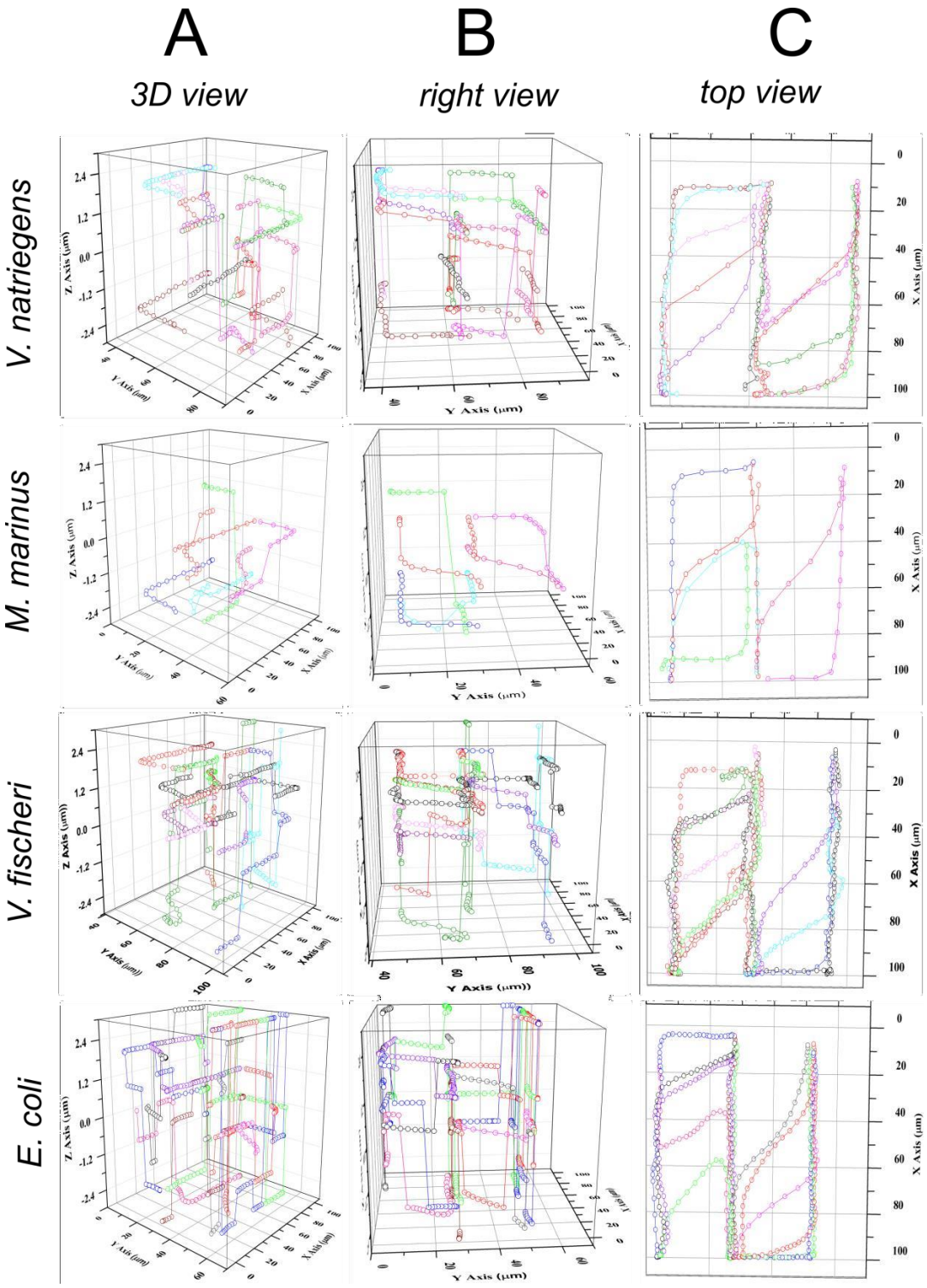

Figure. S15. 3D trajectories of five different bacterial species projected in 3D space using z-stack imaging in angled channels.

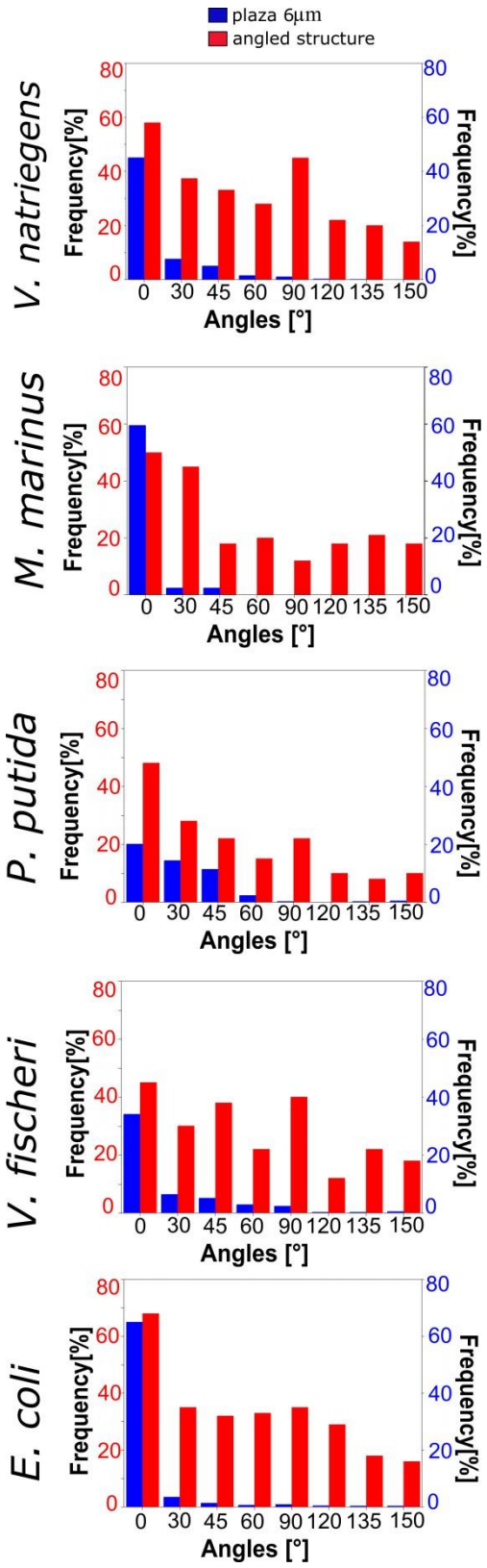

Figure. S16. 3D trajectories of five different bacterial species projected in 3D space using z-stack imaging in angled channels.

2.4 Motility in meandered channels

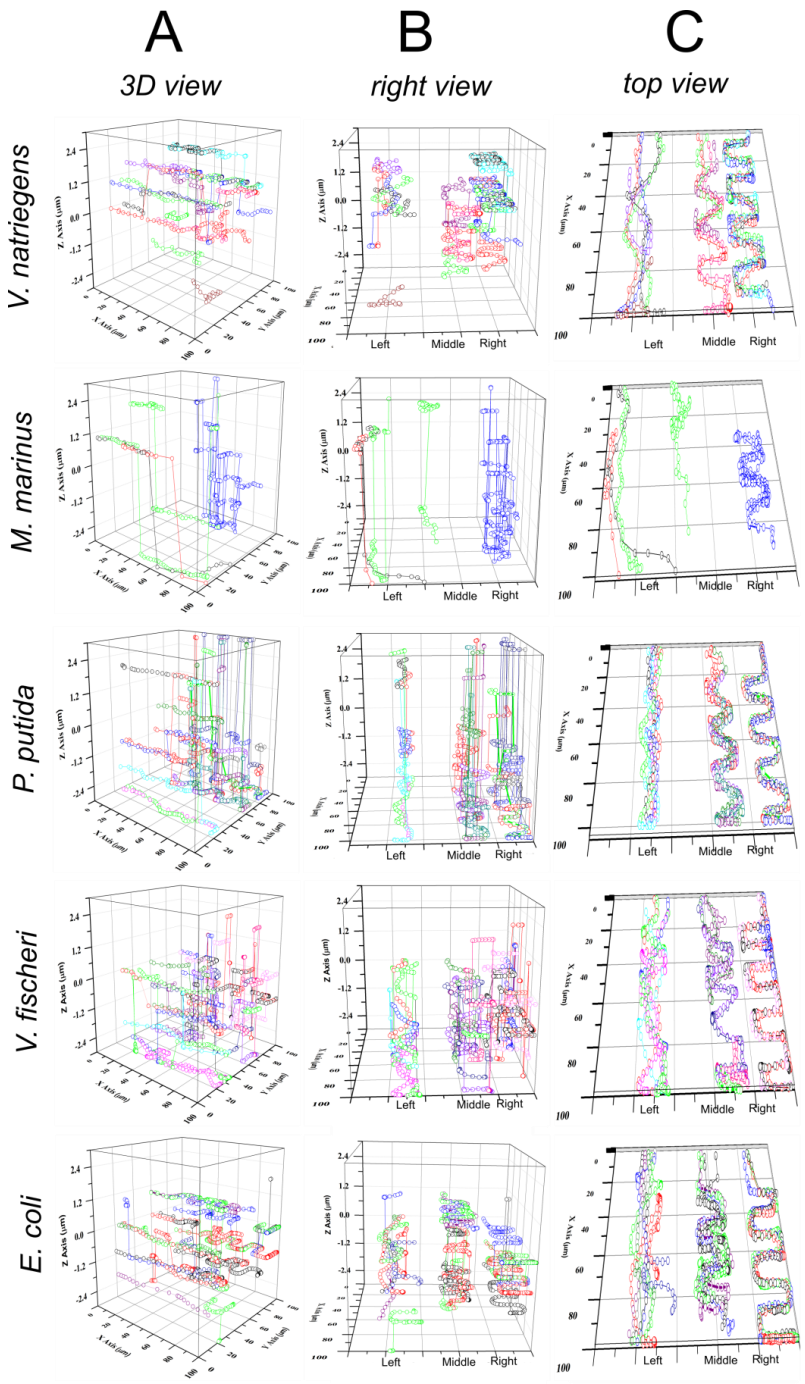

Figure. S17. 3D trajectories of five different bacterial species in meandered channels.

Table S3. Comparison of the average time-spent (seconds) by bacteria in meandered channels with different tooth widths (left-middle-right channels as in **Figure S2C**).

Meandered channels: **Bacteria↓ Tooth length→**	**Left** 5 µm	**Middle** 10 µm	**Right** 15 µm
V. natriegens	4.5 ±1.8	24.0 ±10.2	27.5 ±7.3
M. marinus	3.2 ±2.0	5.5 ±3.3	7.3 ±3.2
P. putida	7.9 ±5.1	11.2 ±4.4	15.4 ±5.6
V. fischeri	9.9 ±5.8	49.1 ±8.9	38.8 ±16.3
E. coli	24.3 ±19.3	43.1 ±14.9	65.9 ±22.3

Table S4. Comparison of the average time-spent (seconds) by bacteria that succeeded in traversing the meandered channels with different tooth widths (left-middle-right channels as in **Figure S2C**).

Meandered channels **Bacteria↓ Tooth length→**	**Average time spent in succeeding the trapping (seconds)**		
	Left 5 µm	**Middle** 10 µm	**Right** 15 µm
V. natriegens	5 ±1.8	NA	28 ±7.4
M. marinus	3 ±2.0	5 ±3.3	7.5 ±3
P. putida	7.5 ±5	11.8±4.4	15.4 ±5.6
V. fischeri	10 ±5.6	38.1 ±8	38.8 ±16.3
E. coli	20.5±18	NA	30 ±22.3

Note that bacterial species like *V. natriegens* and *E. coli* has a zero or negligible success rate in traversing the middle-sized meandered channel during experimental observation.

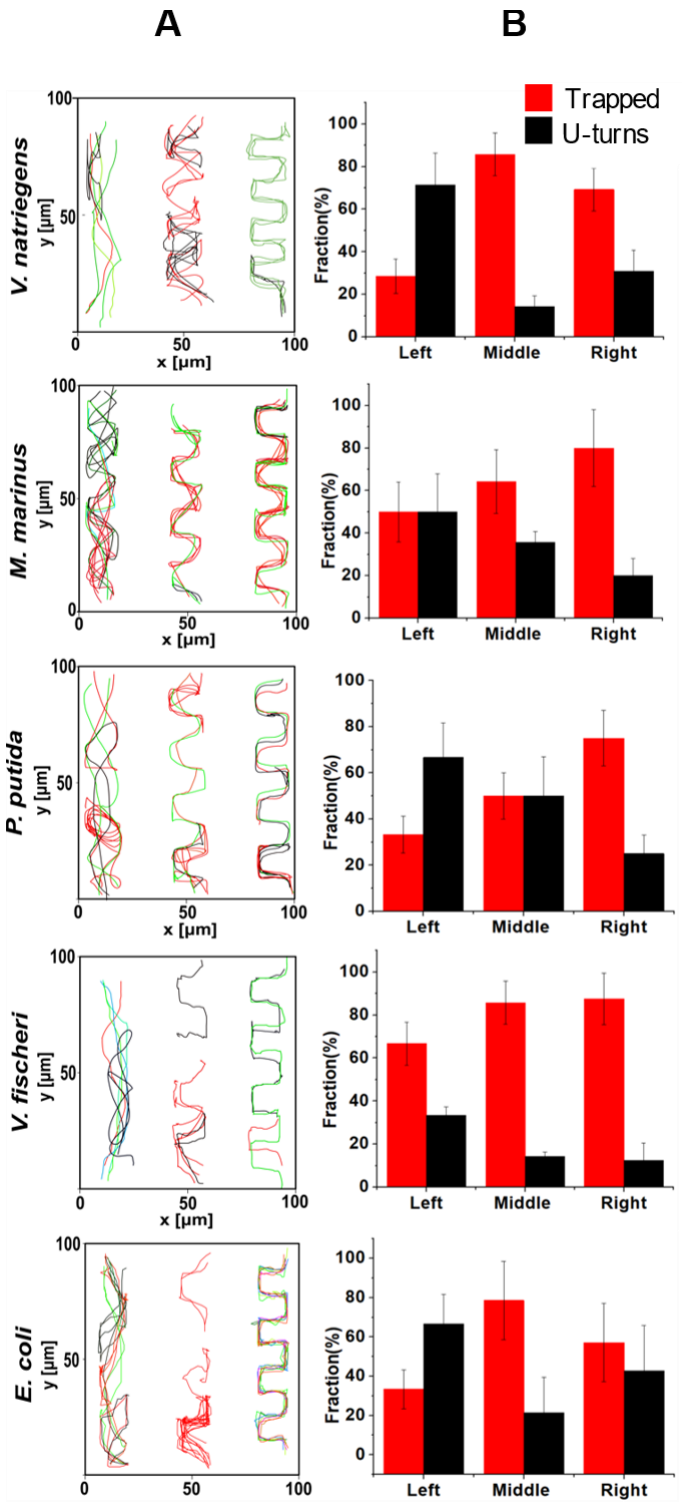

Figure S18. Bacterial motility in meandered, comb-like channels. A. Representative tracks of the bacterial motility: red trajectories - bacteria took U-turns; black trajectories - bacteria got trapped; any other color - bacteria successfully traversed. B. Distribution of unsuccessful bacteria that made either a U-turn or are trapped. By rows, from top to bottom: *V. natriegens* (average count of bacteria each frame, n = 18/frame); *M. marinus* (n = 12/frame); *P. putida* (n = 22/frame); *V. fischeri* (n = 25/frame); and *E. coli* (n = 19/frame).

2.4. Velocity distribution for bacterial species in different motility structures

The velocity observed in various microfluidics structures were expected to be related to the respective levels of confinement, with the highest confinement levels present in the meandered channels ("combs" in **Figure S17**); and the lowest in plazas. However, while the variation of velocity due to confinement were obvious for *M. marinus*, it is far less obvious for other species. However, among the different structures studied here, the motility in the meandered channels present the most noticeable decrease of apparent velocity (with the notable exception of *V. natriegens*). For instance, *E. coli* and *V. fischeri* decreased their velocities by more than 75% compared to its velocity in plazas, and P. putida with almost 50%, This behavior is easily understood if connected with the frequent trapping in the cornersof the meandered channels, reducing its overall average velocity. Such steep changes werenot observed in the other species, suggesting there was not a strong corner preference for rest of the members of bacteria tested. The velocity differences observed with *E. coli* and *M. marinus* are classical examples of steric interactions-based confinement where *M. marinus* was restricted with space leading to reduction in velocity while for *E. coli* it was the geometrical preferences. Finally, it should be noticed that *V. natriegens* is the species withthe smallest aspect ratio of the dimension of cell body, and one the species with the lowest ratio of length/cell diameter (**Figure 5**) which suggest an easier negotiation of convoluted geometries.

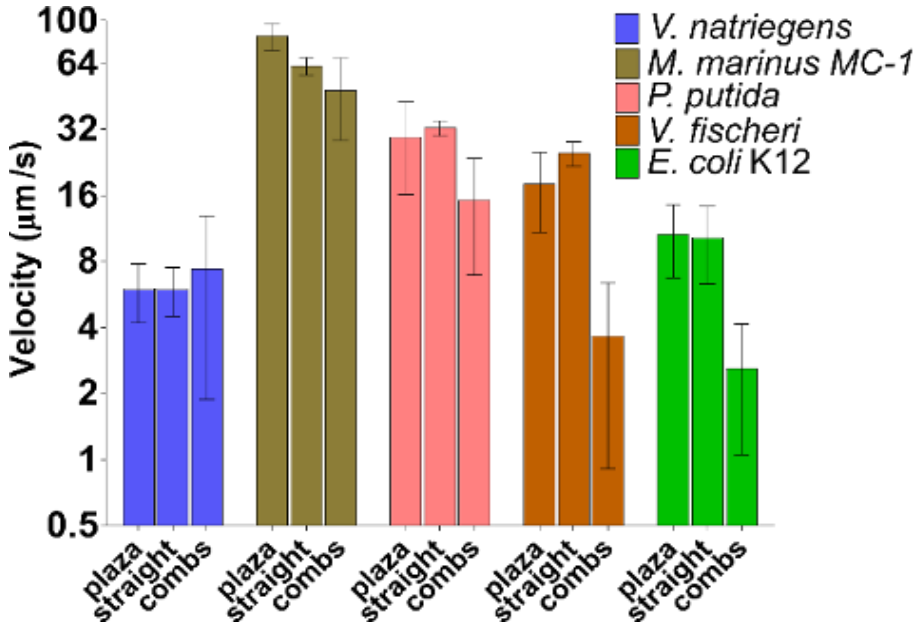

Figure S19. Comparison of bacterial velocities (logarithmic scale) in plazas, straight channels ("straight" label) and meandered channels ("combs" label)

2.5 Tight geometrical like confinements from nature

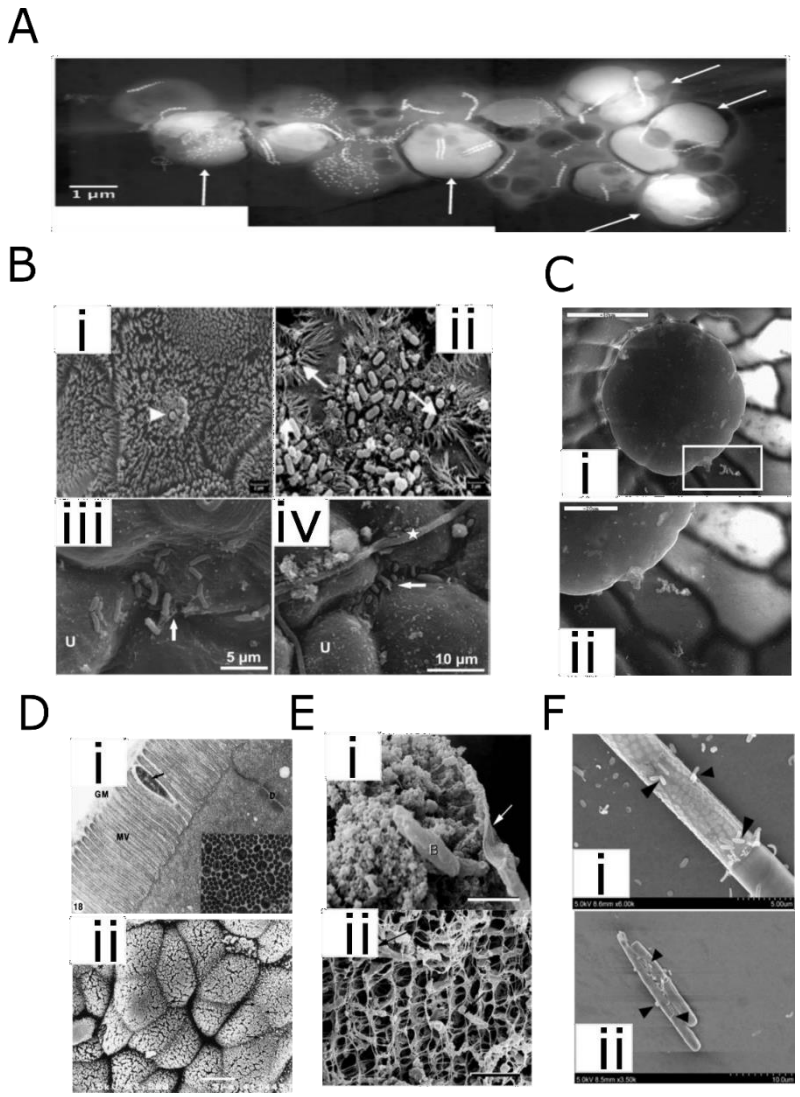

Figure S20. Closer look into the microbial habitats and tight confinements in nature. The above images are adopted from several reported communications, which shows high-definition microenvironment that are bacterial habitats and the tight confinements that are common observations among these figures. **A.** *Magnetotactic species* in the soil sediments of lake (23, 24), spherical bacteria in the constrained environments. **B**. *Escherichia species* inthe gut (B I & ii) and on plant surfaces (25) (B iii & iv). The image shows constricted patterns with tight channel like features and different turn angles (iii & iv). **C**. Rod shaped bacterial species (26). The image shows several straight and different turn angles, like the feature that we used in the devices for studying angled preferences. **D**. *Vibrio species* in the gut of fishes (27). The image D(i) shows straight channel like feature present in the microvilli(MV) and image D (ii) shows different angled and zig-zag patterns, like the structures with higher complexity that we explored

in our studies. ***E***. *Pseudomonas species* in soil sediments (i &ii) shows features with different pore sizes and highly complex structures (28). **F**. rod shaped bacterium on surface of phytoplankton (29). The figure shows straight lines withmany turn angles and most notably 90° turn angles.

Supporting Movies

The movies present typical motility patterns of all bacterial species studied. *E. coli* and *V. natriegens* were labelled with fluorescent expressing plasmids (either GFP or mCherry) andthe movies were recorded with a fluorescence microscope. Other species were observed in bright field (all species) or in dark field (*M. marinus* only). All the movies are played at original speed to show different behaviors like the velocity differences among the different species, U-turn types, wall-accumulating and wall repelling motions, circular, chaotic trajectories etc.

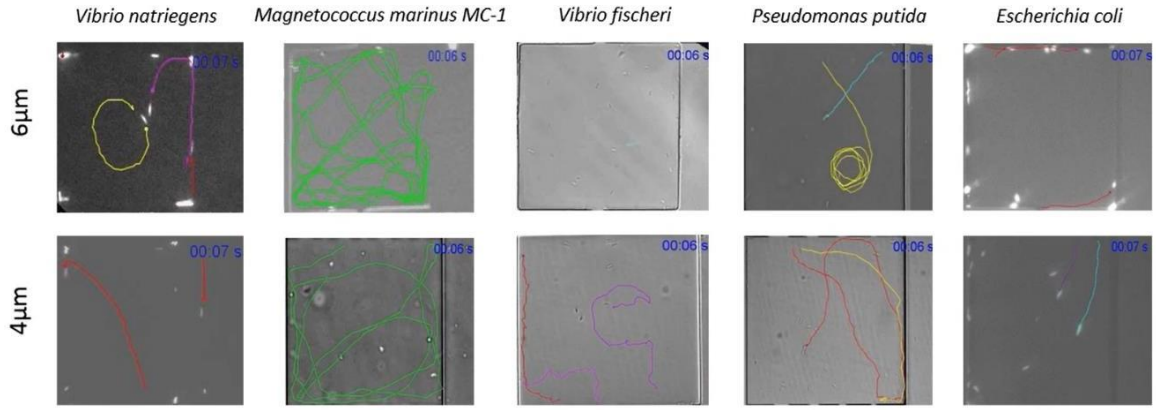

Supporting Movie 1 – Bacterial motility in quasi open spaces (plazas) of two different heights

Trajectories along the walls: Red, Ping-Pong like trajectories: Green, Circular trajectories (longest): Purple, Circular trajectories (Smallest): Yellow, Random trajectories: Cyan

Movie S1. Motility in quasi-open spaces (plazas). Bacterial specific motility observed from the movies and discussed in the main text – Screen shots of the videos is presented here, while the actual movies can be downloaded.

V. natriegens: Preference towards the corners and wall-directed motility. *M. marinus:* Wall-bouncing, ping-pong ball like motility pattern. Restricted motility and few straight trajectories in 4 µm tall plazas, as an effect of confinement. *V. fischeri:* Wiggling, chaotic motion with frequent pauses and change of directions. Observable frequently in 4 µm low plazas. *P. putida:* Typical circular motions with high deflection angles. The diameter of the circular motion decreases due to vertical confinement in 4 µm low plazas. *E. coli:* Wall- dependent motility with corner preferences. Also, small circular motions observed in both high and low plazas.

Linear channels

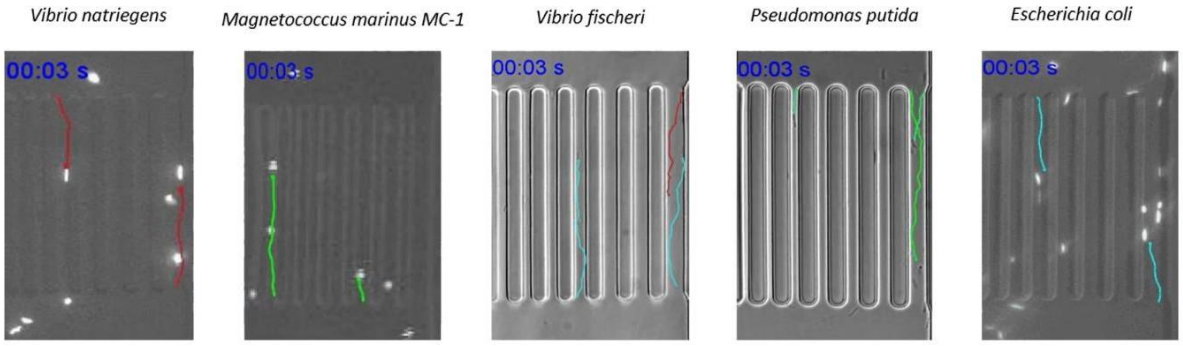

Supporting Movie 2 – Bacterial motility in linear channels

Trajectories along the walls: Red, Sinusoidal like trajectories: Green, Random trajectories: Cyan

Movie S2. Bacterial motility in linear channels. *V. natriegens:* Lowest U-turn frequency with high accumulating. *M. marinus:* High U-turn frequency in narrow channels due to repeated sinusoidal (bouncing) motility and deflection from the walls. *V. fischeri:* Chaotic motility pattern with considerable U-turn frequency, irrespective of the channel dimensions. *P. putida:* Sinusoidal (bouncing) motility and deflection from the walls. *E. coli:* Second highest propensity for wall-accumulating and a low U-turn frequency.

Angled channels

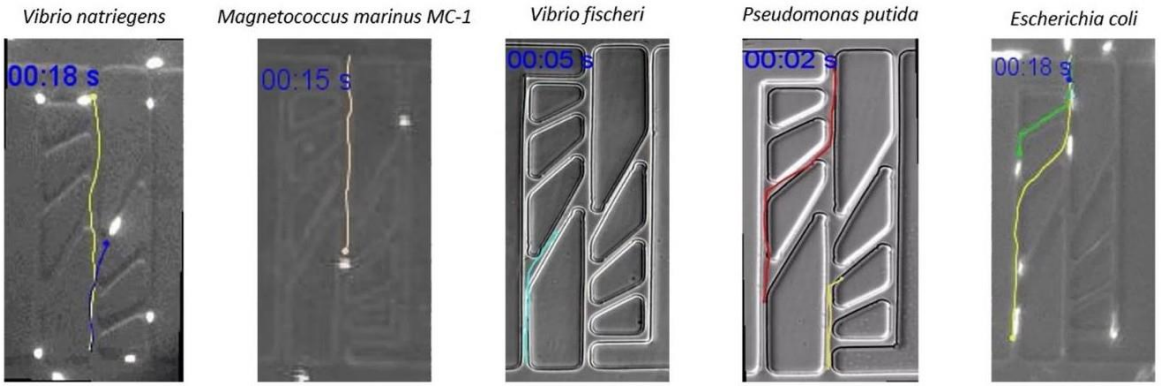

Supporting Movie 3 – Bacterial motility in angled channels

Movie S3. Bacterial motility in angled channels. *V. natriegens:* Preference for moving on straight trajectories along the middle axis channel. *M. marinus:* Trajectories deflected at angles

> 135°. *V. fischeri:* Higher U-turn % and partly wall-accumulating behavior at angled channels. *P. putida:* Trajectories deflected at angles > 135°. *E. coli*: Preference for moving onstraight trajectories along the middle axis channel.

Combed channels

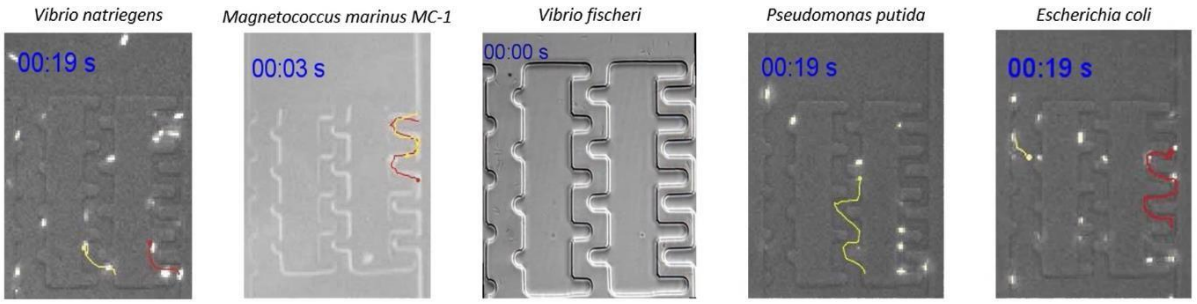

Supporting Movie 4 – Bacterial motility in combed structures

Successful trajectories: Red, Unsuccessful trajectories: Yellow

Movie S4 - Bacterial motility in combed structures. *V. natriegens:* Successfully traversed the combs of lowest and highest tooth length, but not the middle combed-structures due to trapping at the corners. *M. marinus*: Successfully traversed the middle tooth structures compared to the other two combed structures. Least success rate in combs. *V. fischeri:* Possessed a corner–to-corner motility pattern, providing a higher success rates in traversingin all the three comb types. *P. putida:* Exhibited a shifted propensity to follow walls for traversing the combs. Still a second lowest success rate in navigating the complicated comb structures. *E. coli:* 90°: angled corners appear to operate as traps, for *E. coli* very efficientlyin middle sized tooth, while the two other combs were successfully traversed.

References

1. *S. Cheng et al., Microscopical observation of the marine bacterium Vibrio natriegeus growth on metallic corrosion. J Materials, Manufacturing Processes 25, 293-297 (2010).*
2. M. T. Weinstock, E. D. Hesek, C. M. Wilson, D. G. Gibson, Vibrio natriegens as a fast-growing host for molecular biology. *Nature Methods* **13**, 849 (2016).
3. D. A. Bazylinski *et al.*, Magnetococcus marinus gen. nov., sp. nov., a marine, magnetotactic bacterium that represents a novel lineage (Magnetococcaceae fam. nov., Magnetococcales ord. nov.) at the base of the Alphaproteobacteria. *Int J Syst Evol Microbiol* **63**, 801-808 (2013).
4. S. Taherkhani, M. Mohammadi, J. Daoud, S. Martel, M. Tabrizian, Covalent binding of nanoliposomes to the surface of magnetotactic bacteria for the synthesis of self-propelled therapeutic agents. *ACS Nano* **8**, 5049-5060 (2014).
5. M. L. Davis, L. C. Mounteer, L. K. Stevens, C. D. Miller, A. Zhou, 2D motility tracking of Pseudomonas putida KT2440 in growth phases using video microscopy. *J Biosci Bioeng* **111**, 605-611 (2011).
6. J. W. Barton, R. M. Ford, Determination of effective transport coefficients for bacterial migration in sand columns. *Appl Environ Microbiol* **61**, 3329-3335 (1995).
7. M. S. Hendrie, W. Hodgkiss, J. M. Shewan, Proposal that Vibrio marinus (Russell 1891) Ford 1927 be Amalgamated with Vibrio fischeri (Beijerinck 1889) Lehmann and Neumann 1896. *International Journal of Systematic and Evolutionary Microbiology* **21**, 217-221 (1971).
8. D. S. Millikan, E. G. Ruby, Alterations in Vibrio fischeri motility correlate with a delay in symbiosis initiation and are associated with additional symbiotic colonization defects. *Appl Environ Microbiol* **68**, 2519-2528 (2002).
9. M. Binz, A. P. Lee, C. Edwards, D. V. Nicolau, Motility of bacteria in microfluidic structures. *Microelectronic Engineering* **87**, 810-813 (2010).
10. H. C. Berg, *E. coli in Motion* (Springer Science & Business Media, 2008).
11. F. Alejandro Bonilla, N. Kleinfelter, J. H. Cushman, Microfluidic aspects of adhesive microbial dynamics: A numerical exploration of flow-cell geometry, Brownian dynamics, and sticky boundaries. *Advances in Water Resources* **30**, 1680-1695 (2007).
12. J. M. Swiecicki, O. Sliusarenko, D. B. Weibel, From swimming to swarming: Escherichia coli cell motility in two-dimensions. *Integr Biol (Camb)* **5**, 1490-1494

(2013).

13. C. Acikgoz, M. A. Hempenius, J. Huskens, G. J. Vancso, Polymers in conventional and alternative lithography for the fabrication of nanostructures. *European Polymer Journal* **47**, 2033-2052 (2011).
14. D. Qin, Y. Xia, G. M. Whitesides, Soft lithography for micro- and nanoscale patterning. *Nat Protoc* **5**, 491-502 (2010).
15. M. Gan, J. Su, J. Wang, H. Wu, L. Chen, A scalable microfluidic chip for bacterial suspension culture. *Lab on a Chip* **11**, 4087-4092 (2011).
16. R. Watteaux, R. Stocker, J. R. Taylor, Sensitivity of the rate of nutrient uptake by chemotactic bacteria to physical and biological parameters in a turbulent environment. *J Theor Biol* **387**, 120-135 (2015).
17. C. A. Schneider, W. S. Rasband, K. W. Eliceiri, NIH Image to ImageJ: 25 years of image analysis. *Nat Methods* **9**, 671-675 (2012).
18. E. Meijering, O. Dzyubachyk, I. Smal, Methods for cell and particle tracking. *Methods Enzymol* **504**, 183-200 (2012).
19. K. Bente *et al.*, High-speed motility originates from cooperatively pushing and pulling flagella bundles in bilophotrichous bacteria. *eLife* **9** (2020).
20. H. Shum, E. A. Gaffney, D. J. Smith, Modelling bacterial behaviour close to a no-slip plane boundary: The influence of bacterial geometry. *Proceedings of the Royal Society A: Mathematical, Physical and Engineering Sciences* **466**, 1725-1748 (2010).
21. S. E. Spagnolie, E. Lauga, Hydrodynamics of self-propulsion near a boundary: predictions and accuracy of far-field approximations. *Journal of Fluid Mechanics* **700**, 105-147 (2012).
22. H. Shum, E. A. Gaffney, Hydrodynamic analysis of flagellated bacteria swimming in corners of rectangular channels. *Physical Review E - Statistical, Nonlinear, and Soft Matter Physics* **92** (2015).
23. S. Rivas-Lamelo *et al.*, Magnetotactic bacteria as a new model for P sequestration in the ferruginous Lake Pavin. (2017).
24. P. Dean, M. Maresca, S. Schüller, A. D. Phillips, B. J. P. o. t. N. A. o. S. Kenny, Potent diarrheagenic mechanism mediated by the cooperative action of three enteropathogenic Escherichia coli-injected effector proteins. **103**, 1876-1881 (2006).
25. K. Karamanoli *et al.*, Are leaf glandular trichomes of oregano hospitable habitats for bacterial growth? **38**, 476-485 (2012).
26. L. E. B. Baldotto, F. L. J. C. j. o. m. Olivares, Phylloepiphytic interaction between

bacteria and different plant species in a tropical agricultural system. **54**, 918-931 (2008).

27. E. Ringø, R. E. Olsen, T. M. Mayhew, R. J. A. Myklebust, Electron microscopy of the intestinal microflora of fish. **227**, 395-415 (2003).
28. M. M. Baum *et al.*, Characterization of structures in biofilms formed by a Pseudomonas fluorescens isolated from soil. **9**, 103 (2009).
29. I. L. Bagatini *et al.*, Host-specificity and dynamics in bacterial communities associated with bloom-forming freshwater phytoplankton. **9**, e85950 (20